Prediction of *in vivo* metabolite disposition and complex metabolite-dependent drug-drug interactions

Justin D. Lutz

A dissertation

submitted in partial fulfillment of the

requirements for the degree of

Doctor of Philosophy

University of Washington

2013

Reading Committee:

Nina Isoherranen, Chair

Kent L. Kunze

Jashvant D. Unadkat

Program Authorized to Offer Degree:

Pharmaceutics

University of Washington

Abstract

Prediction of *in vivo* metabolite disposition and complex metabolite-dependent drug-drug interactions

Justin D. Lutz

Chair of the Supervisory Committee:
Associate Professor Nina Isoherranen
Department of Pharmaceutics

Metabolites can have pharmacological or toxicological effects, inhibit metabolic enzymes and be used as probes of drug-drug interactions or specific cytochrome P450 phenotypes. Thus better understanding and prediction methods are needed to characterize metabolite exposure and P450 inhibition *in vivo*. This thesis study aimed to test whether *in vitro* data could be used to predict and rationalize *in vivo* metabolite exposures and metabolite-dependent drug-drug interactions (DDIs).

Relative metabolite exposures were predicted using a newly developed model and *in vitro* metabolite formation and elimination clearances for two model systems, dextromethorphan and omeprazole, with their metabolites. Using human liver microsome (HLM) and human hepatocyte kinetic data, dextrorphan/dextromethorphan, 5-hydroxyomeprazole/omeprazole and omeprazole sulfone/omeprazole *in vivo* AUC_m/AUC_p were well predicted. Furthermore, the

importance of understanding *in vivo* metabolite elimination was demonstrated using kinetic modeling.

Fluoxetine with its metabolite, norfluoxetine, was chosen as the model system to evaluate the role of metabolites in DDI prediction because it represents a complex multiple inhibitor system of multiple P450s. In pooled HLMs, the enantiomers of fluoxetine and norfluoxetine were determined to be reversible inhibitors of CYP2D6, time-dependent inhibitors of CYP2C19 and reversible or time-dependent inhibitors of CYP3A4. Fluoxetine administration is predicted to inhibit all three P450s *in vivo* and norfluoxetine enantiomers are predicted to play an important role in this inhibition.

The *in vivo* effect of fluoxetine administration on P450 activity was determined in healthy volunteers following two week dosing of fluoxetine. Strong inhibition of CYP2D6 and CYP2C19 whereas no inhibition of CYP3A4 was observed. Multiple linear regression analysis indicated that (S)-norfluoxetine was solely responsible for *in vivo* CYP2D6 inhibition and undergoes significant hepatic partitioning. The application of (S)-norfluoxetine hepatocyte partitioning afforded accurate predictions of all *in vivo* DDIs.

This thesis study demonstrates that *in vivo* metabolite exposure and metabolite-dependent DDIs can be predicted from *in vitro* data and suggests a major role of metabolites in P450 inhibition. Furthermore, the results of this thesis study advance the ability to predict and rationalize metabolite disposition during new drug development and P450 activity measurement as well as provides insight into analysis of complex metabolite-dependent DDIs.

Table of Contents

List of Figures

List of Tables

List of Abbreviations

alcohol dehydrogenase, ADH

aldehyde dehydrogenase, ALDH

apparent maximum time-dependent inhibition rate, $k_{inact,app}$

area under the plasma concentration versus time curve, AUC

bovine serum albumin, BSA

clearance, Cl

collision energy, CE

cytochrome P450, P450

cytochrome P450 degradation rate constant, k_{deg}

declustering potential, DP

drug-drug interaction, DDI

European Medicines Agency, EMA

extensive metabolizer, EM

extraction ratio, ER

Food and Drug Administration, FDA

fraction of drug that escapes first pass metabolism in the intestine, F_g

fraction of drug that escapes first pass metabolism in the liver, F_h

fraction metabolized, f_m

fraction unbound, f_u

half-life, $t_{1/2}$

hepatic blood flow, Q_h

human liver microsome, HLM

incubation volume, V_{inc}

inhibitor concentration at 50% maximum inhibition, IC_{50}

intrinsic clearance, Cl_i

intravenous, IV

maximum inhibitor plasma concentration, I_{max}

maximum reaction velocity, V_{max}

metabolic-intermediate complex, MIC

metabolite, M

metabolite/parent amount excreted in the urine ratio, U_m/U_p

metabolite/parent area under the plasma concentration versus time curve ratio, AUC_m/AUC_p

metabolite/parent plasma concentration ratio, C_m/C_p

Michaelis-Menten affinity constant, K_m

microsomal protein, MP

multiple reaction monitoring, MRM

nicotinamide adenine dinucleotide phosphate, NADPH

oral, PO

parent drug, P

poor metabolizer, PM

potassium phosphate buffer, KPi

reaction velocity, v

recombinantly expressed cytochrome P450, rP450

recombinantly expressed uridine diphosphate glucuronysltransferase, rUGT

reversible inhibition affinity constant, K_i

selected ion recording, SIR

substrate, S

time, t

time-dependent inhibition affinity constant, K_I

time-dependent inhibition rate, λ

time-dependent inhibitor, TDI

uridine diphosphate glucuronic acid, UDPGA

uridine diphosphate glucuronysltransferase, rUGT

volume of distribution, V_d

Acknowledgements

I am forever indebted to my doctoral advisor, Dr. Nina Isoherranen, for her tireless effort and enthusiasm. I came to her with more arrogance than knowledge, but I now leave with humility and a great appreciation for the hard work that it takes to do something well. I have learned so much from her and she has helped me to be more productive over the course of my training than I ever could have imagined. Both professionally and personally, I could not have had a better mentor.

To my thesis reading and doctoral supervisory committee members, Drs. Baillie, Bloedow, Kunze and Unadkat, I wish to express my gratitude for their guidance, support and scientific curiosity. Their contribution to my growth is beyond measure.

To the faculty of the Pharmaceutics and Medicinal Chemistry departments, I wish to thank you for fostering an environment of collegiality and intense scientific learning, which provides your students endless possibilities to prosper. I am proud to have learned from such talented scientists and teachers.

To the staff and students of the Pharmaceutics and Medicinal Chemistry departments, I wish to thank you for your personal, academic and professional support and encouragement. They have made my time here truly enjoyable and fulfilling.

I wish to sincerely thank all our collaborators who contributed to the clinical study, specifically Dr. Davis, the Staff at the University of Washington Clinical Research Center and the study volunteers. Without their efforts, the clinical study would not have proceeded so smoothly.

Dedication

To Anna.

Always.

Chapter 1

Introduction

The work presented in this chapter was, in part, previously published

in

Expert Opinion in Drug Metabolism and Toxicology 6(9):1095-1109 (2010) and 8(4):449-466 (2012).

1.1. Role of metabolites in drug safety testing

A metabolite can be formed from any enzymatic transformation of a parent drug after the parent is administered *in vivo* or is incubated as substrate *in vitro*. Often, these metabolites prove to have *in vivo* pharmacologic activity (Obach, 2013). Classic examples of metabolites that have pharmacologic activity are metabolites of tricyclic antidepressants and benzodiazepine anxiolytics, where many of the metabolites are also marketed drugs (Akiyoshi *et al.*, 1996; Riss *et al.*, 2008). Metabolites can also possess toxicological activity. Examples of *in vivo* toxic metabolites have been well established for many parent drugs, such as carbamazepine, valproic acid and nefazodone (Rambeck *et al.*, 1990; Ho *et al.*, 2003; Bauman *et al.*, 2008). Due to the realization that metabolites can oftentimes have *in vivo* activity, it is important to understand the disposition of a metabolite after the administration of parent during new drug development.

An FDA guidance on metabolites in safety testing (MIST) has drawn more attention to identifying and predicting human metabolites (<www.fda.gov/downloads/Drugs/GuidanceComplianceRegulatoryInformation/Guidances/ucm079266.pdf>). This guidance states that a metabolite found to circulate at equivalent or greater concentrations in at least one pre-clinical animal species when compared to in human has been adequately evaluated for safety and no further non-clinical testing is warranted. If this cannot be demonstrated, any metabolite with exposure > 10% of the parent at steady-state in humans warrants separate non-clinical toxicological and pharmacokinetic studies. In contrast to the MIST guidance, the European guidance states that separate studies are only warranted when a metabolite exposure is > 10% of the total drug-related material exposure (<www.ema.europa.eu/docs/en_GB/document_library/Scientific_guideline/2009/09/WC500002720.pdf>). More recently, the FDA and the EMA state that *in vivo* circulating metabolites should be characterized for *in vitro* P450

inhibition when present at > 25% of parent exposure or total drug related material exposure, respectively (<www.fda.gov/downloads/Drugs/GuidanceComplianceRegulatoryInformation/Guidances/ucm292362.pdf> and <www.ema.europa.eu/docs/en_GB/document_library/Scientific_guideline/2012/07/WC500129606.pdf>). These guidance pose an important dilemma in new drug development: how to identify and reliably predict potentially important circulating metabolites sufficiently early in new drug development to allow timely synthesis of reference material, development of validated assays and toxicological evaluation.

In vitro metabolism and pre-clinical animal data as well as single dose pharmacokinetic data are often used to predict the *in vivo* steady-state disposition of new drug candidates, as well as the *in vivo* metabolite profile of a candidate drug. However, attempts to predict important circulating metabolites in humans from pre-clinical data are qualitative and have met with variable success (Anderson *et al.*, 2009; Loi *et al.*, 2013). Direct translation of the metabolite profile from animal species to humans may be confounded by species differences in enzyme activity and expression, whereas *in vitro* HLM and hepatocyte studies qualitatively identify metabolites that are likely to be formed *in vivo* but quantitative prediction of metabolite disposition remains challenging. In this chapter, established *in vivo* metabolite kinetic theory will be discussed and a method for quantitatively predicting *in vivo* metabolite disposition from *in vitro* data will be presented.

1.2 Metabolite kinetic theory: *in vivo* aspects

During the late 1960's through to the early 1980's, much interest was paid to the development of pharmacokinetic theory that describes the *in vivo* disposition of a metabolite formed after administration of a parent drug. The metabolite plasma concentration (C_m) versus time (t) curve for a metabolite formed after intravenous (IV) administration will exhibit biphasic kinetics and depend on the dose of parent (D), the fraction of parent that is converted to

metabolite (f_m), the metabolite volume of distribution ($V_{d,m}$) and the formation (k_f) and elimination (k_m) rate constants for the metabolite (Cummings *et al.*, 1967):

$$C_m = \frac{k_f f_m D\left(e^{-k_f t} - e^{-k_m t}\right)}{V_{d,m}\left(k_m - k_f\right)} \qquad (1.1)$$

This expression dictates that the slope of the linear terminal portion of a metabolite concentration versus time profile will either be equal to that of the parent, i.e. formation rate limited (FRL, $k_f < k_m$) kinetics, or less than that of the parent, i.e. elimination rate limited (ERL, $k_f < k_m$) kinetics (Houston, 1981). After oral (PO) administration, the metabolite concentration versus time profile will further depend on the fraction of drug absorbed into the body (F_a) and will be either biphasic or triphasic, depending on the efficiency of metabolite formation during first pass metabolism (Houston and Taylor, 1984).

The AUC_m after either IV or PO administration of the parent was demonstrated to be determined by D, F_a (only after PO administration), f_m and the clearance of the metabolite (Cl_m) (Pang and Gillette, 1978; Pang, 1981). Additionally, the *in vivo* metabolite-to-parent area under the plasma concentration versus time curve ratio (AUC_m/AUC_p) was determined to be dependent only on the *in vivo* formation and elimination clearances for the metabolite (Patel *et al.*, 1978; Levy *et al.*, 1983). Patel et al (1978), demonstrated that after IV administration of a drug the AUC_m/AUC_p is:

$$\frac{AUC_m}{AUC_p} = \frac{f_m Cl_p}{Cl_m} = \frac{Cl_f}{Cl_m} \qquad (1.2)$$

where Cl_p and Cl_m are the total *in vivo* clearances of the parent and the metabolite, respectively, and Cl_f is the formation clearance of the metabolite. The assumptions that are made in this model are that 1) the kinetics of the parent and metabolite are linear with respect to

concentration and time, 2) only one metabolite is formed from the parent (i.e. f_m equals the fraction of drug excreted unchanged subtracted from unity) and 3) all metabolite formed is available to the systemic circulation. It should be noted, that the above expression can be adapted to PO administration if metabolism occurs only in the liver and Cl_p is the apparent oral clearance of parent, i.e. the quotient of the true clearance of parent and the fraction of parent that escapes first pass in the liver (F_h):

$$\frac{AUC_m}{AUC_p} = \frac{f_m Cl_p}{F_h Cl_m} \qquad (1.3)$$

The AUC_m/AUC_p is a primary measure utilized in both the MIST and drug-drug interaction (DDI) guidance and hence, this theory should be examined to address the dilemma posed by the guidance via *in vitro*-to-*in vivo* prediction.

1.3 Prediction of *in vivo* metabolite exposure

There has been a considerable amount of discussion on how to identify important circulating metabolites during pre-clinical phases of development of a new drug candidate (Anderson *et al.*, 2009; Smith and Obach, 2009). Advances in and increased access to analytical technologies have made metabolite identification a routine part of new drug development. Most techniques focus on metabolic incubations of either a radiolabeled (if available) or nonradiolabeled new drug candidate to generate potential metabolites. The products of these incubations are then subjected to ultra performance liquid chromatography, to separate closely chemically related species, and coupled to either accurate mass spectrometry or NMR spectroscopy for structural determination (Espina *et al.*, 2009; Leclercq *et al.*, 2009; Vishwanathan *et al.*, 2009). This procedure results in the identification and quantification of potential metabolites formed from the new drug candidate, but the relative abundance of each

metabolite formed *in vitro* often does not agree with its relative abundance *in vivo* (Anderson *et al.*, 2009).

Intuitively, one would expect that a major metabolite in HLMs or hepatocytes would also be a major metabolite in plasma. However, the clearances of primary metabolites vary, even within closely chemically related species such as two primary metabolites of the same parent. The relative exposure to different metabolites formed from the same parent drug will depend on the rank order of the ratio of formation clearance to elimination clearance for each metabolite (Equation 1.2). Hence, a major metabolite observed in HLMs or hepatocytes will not be dominant *in vivo* unless it has sufficiently low elimination clearance in comparison to other metabolites formed and in comparison to the parent drug. Whether this is clinically important was tested using published literature data of all metabolite/parent pairs for which both *in vivo* AUC_m/AUC_p and *in vitro* metabolite intrinsic formation clearance ($Cl_{i,f}$) data for parent drug with at least two metabolites was available. In total, 31 metabolite/parent pairs from 14 parent drugs were examined. Table 1.1 summarizes the *in vitro* $Cl_{i,f}$ and the observed *in vivo* AUC_m/AUC_p ratios for each metabolite/parent pair examined for a given parent drug. AUC_m/AUC_p ratios for each metabolite/parent pair, for a given parent, were considered to rank correctly with respect to *in vitro* $Cl_{i,f}$ if the metabolite/parent pair with a > 15% higher $Cl_{i,f}$ also had a > 15% AUC_m/AUC_p. Only 7 parent drugs (50%) had AUC_m/AUC_p ratios for their respective metabolites that rank ordered correctly. One of the parent drugs examined in the rank order analysis was clomipramine. Clomipramine has three important metabolites: 8-hydroxyclomipramine, N-desmethylclomipramine and 2-hydroxyclomipramine. Based solely on *in vitro* $Cl_{i,f}$, N-desmethylclomipramine would be predicted to be the major metabolite, followed by equal exposures to 8-hydroxy and 2-hydroxyclomipramine. However, 8-hydroxyclomipramine can be detected *in vivo* in plasma at 40% of the parent whereas 2-hydroxyclomipramine is undetectable in plasma. This can be explained by the greater intrinsic elimination clearance of 2-

hydroxyclomipramine when compared to 8-hydroxyclomipramine, 6.5 versus 1.5 μL/min/mg microsomal protein (Kramer-Nielsen *et al.*, 1996). Incorrect rank ordering of metabolites for a given parent drug for half of the cases examined demonstrates that the consideration of only *in vitro* metabolite formation clearance is not sufficient for predicting the relative importance of a given metabolite *in vivo.*

The *in vivo* metabolite kinetic theory developed in the late 1960s through the 1980s (Cummings *et al.*, 1967; Pang, 1981; Houston and Taylor, 1984) laid the foundation of *in vivo* metabolite pharmacokinetics but these theories have not yet been applied to *in vitro*-to-*in vivo* prediction, a useful tool in anticipating the *in vivo* pharmacokinetics of a parent drug during new drug development. The prediction of *in vivo* clearance of drugs based on *in vitro* metabolism data is well established, although predictions have varying degrees of accuracy (Obach *et al.*, 1997; Carlile *et al.*, 1999). In an extensive analysis of scaling *in vitro* HLM clearance values to *in vivo* clearance using multiple hepatic clearance models and plasma protein binding considerations, 29 drugs with varying physicochemical properties were predicted with a 2.1 to 4.4 average fold error (Obach, 1999). Another study of scaling *in vitro* Cl_i values from human hepatocyte data for 50 drugs, obtained a 2.5 average fold error to the observed *in vivo* clearance, with outliers having up to 15-fold error (McGinnity *et al.*, 2004). Although quantitative *in vitro*-to-*in vivo* clearance prediction for a parent drug is now commonplace, little attention has been paid to the prediction of the *in vivo* disposition of a metabolite from *in vitro* metabolism data.

The MIST guidance requires the evaluation of absolute steady-state AUC_m between pre-clinical animal species and human for major metabolites. If similar exposure is not obtained in animals, additional safety testing of the metabolite may be required. This requirement generates a need to predict, prior to clinical studies, what metabolites will be quantitatively important in humans. Predicting absolute AUC_m values in humans poses a significant challenge because the

result will depend on the dose of the parent, the fraction of the dose absorbed after PO administration, and the overall clearance of the parent drug. In addition, the AUC_m will depend on the metabolite specific parameters, such as the fraction of the dose converted to the metabolite of interest and the metabolite clearance. Within the MIST guidance, the secondary qualification of the *relative* exposure to the metabolite in human, i.e. $AUC_m/AUC_p > 0.1$, appears more conducive to prediction. The AUC_m/AUC_p is independent of the parent dose and fraction absorbed after PO administration and the predicted AUC_m/AUC_p can be utilized as a proportionality constant for anticipating the absolute levels of the metabolite of interest when a desired AUC or steady-state concentration of parent is ascertained. Normalizing the predicted metabolite exposure to that of the parent also provides valuable insight into whether the metabolite will be quantitatively important *in vivo,* regardless of the parent dose.

The prediction of *in vivo* AUC_m/AUC_p from *in vitro* parameters relies on methods for clearance predictions of both parent and metabolite. This is because an important principle of metabolite kinetics is that the *in vivo* disposition of a metabolite is dependent not only on its formation clearance, but also its elimination (Equation 1.2). Based on this principle, predicting relative exposure to human metabolites can only be done if the formation and elimination clearances for the metabolite are predicted. To adapt Equations 1.2 and 1.3 to *in vitro*-to-*in vivo* prediction of AUC_m/AUC_p after IV or oral PO administration, four assumptions were made: 1) the kinetics of both parent and metabolite are linear, 2) all metabolite formed is available to the systemic circulation, 3) parent and metabolite elimination is via metabolism only and 4) metabolism occurs only in the liver which can be represented by the well-stirred model (Wilkinson and Shand, 1975):

$$Cl_h = \frac{Q_h f_u Cl_i}{Q_h + f_u Cl_i} \qquad (1.4)$$

where Cl_h is the hepatic clearance, Q_h is the hepatic blood flow, $f_{u,}$ is the plasma fraction unbound and Cl_i is the hepatic intrinsic metabolic clearance. The well-stirred model was chosen for this analysis because it is the most commonly utilized hepatic clearance model and easiest to adapt for predictions.

In order to develop a model for prediction of AUC_m/AUC_p, a general metabolic scheme based on the scheme of Houston and Taylor (1984) can be considered for both IV and PO administration (Figure 1.1). In this scheme, $D_{g,}$ D_h and D_s are the amounts of drug in the gut lumen, liver during first pass and systemic circulation, respectively. F_a and F_h are the fraction of drug absorbed from the gut lumen into the enterocytes and fraction of drug that escapes first pass elimination in the liver, respectively, and M_h and M_s refer to the amount of metabolite formed from first pass in the liver and from systemic elimination, respectively.

The *in vivo* fraction of parent converted to the metabolite of interest, when the parent is cleared only through hepatic metabolism was previously defined as the fraction of hepatic parent drug clearance that results in the metabolite of interest (Pang and Kwan, 1983). This definition was adapted to *in vitro* parameters and defined as $f_{m,h}$:

$$f_{m,h} = \frac{Cl_{i,f}}{Cl_{i,p}} \qquad (1.5)$$

where $Cl_{i,f}$ and $Cl_{i,p}$ are the intrinsic formation clearance of the metabolite *in vitro* and intrinsic elimination clearance of the parent *in vitro*, respectively. When the parent is cleared entirely via hepatic metabolism, the *in vivo* f_m for the metabolite of interest is equal to the *in vitro* $f_{m,h}$. Utilizing the scheme in Figure 1.1, the AUC_m after PO administration can be defined as:

$$AUC_m = \frac{f_{m,h}F_a(1-F_h)D}{Cl_m} + \frac{f_{m,h}F_aF_hD}{Cl_m} \qquad (1.6)$$

and the AUC_p after PO administration can be defined as:

$$AUC_p = \frac{F_a F_h D}{Cl_p} \qquad (1.7)$$

By definition (Rane *et al.*, 1977), the hepatic bioavailability (F_h) is a function of the extraction ratio of the parent (ER_p):

$$F_h = 1 - ER_p = \frac{Q_h}{Q_h + f_{u,p} Cl_{i,p}} \qquad (1.8)$$

Substituting for F_h and the well-stirred model for Cl_p and Cl_m (as defined by Equations 1.8 and 1.4, respectively) into the quotient of Equations 1.6 and 1.7 yields:

$$\frac{AUC_m}{AUC_p} = \frac{f_{u,p} Cl_{i,f} (Q_h + f_{u,m} Cl_{i,m})}{f_{u,m} Cl_{i,m} Q_h} \qquad (1.9)$$

After IV administration, by substituting $f_{m,h}$ for f_m (Equation 1.5) and the well-stirred model for Cl_m and Cl_p (Equation 1.4), Equation 1.10 can be defined as:

$$\frac{AUC_m}{AUC_p} = \frac{f_{u,p} Cl_{i,f} (Q_h + f_{u,m} Cl_{i,m})}{f_{u,m} Cl_{i,m} (Q_h + f_{u,p} Cl_{i,p})} \qquad (1.10)$$

Utilizing the common technique of evaluating the limits of pharmacokinetic models with respect to high extraction ratio (ER) ($Q_h << f_u Cl_i$) or low ER ($Q_h >> f_u Cl_i$), the above two models presented result in three pharmacokinetic outcomes: 1) the relative exposure to the metabolite (AUC_m/AUC_p) will be different after IV and PO administration when the parent drug has a high ER, but the AUC_m/AUC_p is independent of route of administration when ER_p is low, 2) changes in the intrinsic clearance of a metabolite with a low ER (ER_m) will alter the exposure to the metabolite resulting in changes in the AUC_m/AUC_p and 3) the relative exposure to the metabolite

depends on the ratio between its formation and elimination clearances, not on the absolute value of either of these two terms.

Equations 1.9 and 1.10 allow for the prediction of *in vivo* AUC_m/AUC_p from *in vitro* metabolite formation and elimination data as well as *in vitro* determined protein binding data. This model would be useful in assessing the risk of *in vivo* metabolite pharmacology and toxicity from pre-clinical data, but has yet to be validated using parent/metabolite pairs. One aim of this thesis study is to validate this model using the metabolites of dextromethorphan and omeprazole, two drugs that their AUC_m/AUC_p are commonly used as *in vivo* P450 probe measures, so that the model can be confidently implemented in pre-clinical new drug development.

1.4 The role of metabolites in P450 inhibition

An increasing number of inhibitors are recognized to possess circulating metabolites (Isoherranen *et al.*, 2009) which in many cases also inhibit the same enzyme as the parent drug (He *et al.*, 1995; Greenblatt *et al.*, 1996; Isoherranen *et al.*, 2004). Sulfinpyrazone, along with its two *in vivo* circulating metabolites, are all considered inhibitors of CYP2C9, with most of the *in vivo* interaction attributed to the metabolites (He *et al.*, 1995). As previously stated, the FDA and the EMA state that *in vivo* circulating metabolites (> 25% of parent exposure or total drug related material, respectively) should be characterized for *in vitro* P450 inhibition (<www.fda.gov/downloads/Drugs/GuidanceComplianceRegulatoryInformation/Guidances/ucm292362.pdf> and <www.ema.europa.eu/docs/en_GB/document_library/Scientific_guideline/2012/07/WC500129606.pdf>), but inhibition of a given enzyme by multiple inhibitors (parent and metabolite) *in vivo* has not been fully investigated and there is limited theoretical data on how enzyme inhibition *in vivo* resulting from simultaneous parent and metabolite inhibition of the same enzyme should be predicted or rationalized. Furthermore, these guidance do not

differentiate between metabolites involved in reversible versus time-dependent inhibition, two separate inhibition mechanisms that have significant implications for the role of metabolites in P450 inhibition and the models used to predict *in vivo* DDIs.

1.5 Prediction of *in vivo* P450 inhibition and drug-drug interactions

There are four general mechanisms of reversible P450 inhibition by a single inhibitor (Segel, 1993): competitive, uncompetitive, noncompetitive and mixed-type. In competitive inhibition, the inhibitor cannot bind to the P450 when the probe substrate is bound and vice versa, hence one can compete off the inhibitor from the P450 by increasing probe substrate concentrations. In uncompetitive inhibition, the inhibitor can only bind when probe substrate is already bound to the P450. In noncompetitive inhibition, both probe substrate and inhibitor can bind to the P450, either alone or simultaneously, and the order of binding is irrelevant. Mixed-type inhibition simply allows for a hybrid combination of the above three mechanisms.

The change in *in vivo* P450 intrinsic clearance from before (Cl_i) to after administration of an *in vitro* reversible competitive inhibitor (Cl_i') can be predicted using the expression (Rowland and Matin, 1973):

$$\frac{Cl_i}{Cl_i'} = 1 + \frac{I}{K_i} \qquad (1.11)$$

where I and K_i are the *in vivo* inhibitor plasma concentration and *in vitro* reversible inhibition affinity constant, respectively. This model relies on the assumption that metabolism occurs only in the liver by the inhibited P450, *in vivo* substrate concentrations are well below K_m (linear kinetics) and that hepatocyte concentrations are static and identical to plasma. It should be noted that *in vivo* inhibitor plasma concentrations and *in vitro* inhibition affinity constants should

always be converted to “unbound” values via incorporation of plasma and *in vitro* protein binding constants (Margolis and Obach, 2003).

It is generally accepted that the total inhibition due to multiple competitive inhibitors can be predicted using the summed contribution of each individual inhibitor, n, via the expression (Venkatakrishnan *et al.*, 2003):

$$\frac{Cl_i}{Cl_i'} = 1 + \sum_{c=1}^{n} \frac{I_c}{K_{i,c}} \qquad (1.12)$$

where Cl_i and Cl_i' are the P450 intrinsic clearances without and with inhibitors, respectively, I_c is the *in vivo* concentration of inhibitor c for n number of inhibitors and $K_{i,c}$ is the *in vitro* P450 competitive reversible inhibition constant of inhibitor c for n number of inhibitors. The assumption that inhibitors must act via a common competitive mechanism to apply this equation is widespread in the literature (Venkatakrishnan *et al.*, 2003; Rostami-Hodjegan and Tucker, 2004; Hinton *et al.*, 2008). Whether this approach can be used in the case of multiple inhibitors that have different inhibition mechanisms is not well defined. It was suggested that the expression:

$$\frac{Cl_i}{Cl_i'} = 1 + \prod_{c=1}^{n} \frac{I_c}{K_{i,c}} \qquad (1.13)$$

is required for multiple inhibitor systems with a combination of inhibition mechanisms (Rostami-Hodjegan and Tucker, 2004), but the mathematical development of this method has not been presented nor has the method been applied to existing multiple inhibitor systems. To determine if Equation 1.13 is required for prediction of inhibition by multiple inhibitors of varying reversible inhibition mechanisms, the velocity equations for two competitive, noncompetitive or mixed-type inhibitors were solved according to the method described by Segel *et al.* (1993) and according

to the kinetic scheme shown in Figure 1.2. The general velocity equation describing the combination of two inhibitors with any combination of inhibition mechanisms can be written as:

$$v' = \frac{V_{max}S}{K_d\left(1 + \frac{I_1}{K_{i,1}} + \frac{I_2}{K_{i,2}}\right) + S\left(1 + \frac{I_1}{\alpha_1 K_{i,1}} + \frac{I_2}{\alpha_2 K_{i,2}}\right)} \qquad (1.14)$$

where v' and V_{max} are the inhibited and maximal velocity of product formation, respectively. S, I_1 and I_2 are the molar concentrations of substrate, inhibitor 1 and inhibitor 2, respectively. K_d, $K_{i,1}$ and $K_{i,2}$ represent the affinity constants for the binding of S, I_1 and I_2 to enzyme, respectively. Whenever possible, I, S, K_d and K_i should represent unbound concentrations and affinity constants. The α_1 or α_2 terms represent the effect of the presence of the specific inhibitor, already bound to enzyme, on the affinity of substrate for enzyme. Conversely, α_1 and α_2 are also coefficients that represent the effect of substrate, already bound to the enzyme, on the affinity of the relevant inhibitor for the enzyme.

Similarly, the method of deriving these velocity equations can be applied to any combination of inhibition mechanisms and hence, Equation 1.14 can be expanded to a general expression of the velocity of product formation in the presence of any number of inhibitors acting by any combination of inhibition mechanisms resulting in Equation 1.15:

$$v' = \frac{V_{max}S}{K_d\left(1 + \sum_{c=1}^{n}\frac{I_c}{K_{i,c}} + \sum_{m=1}^{p}\frac{I_m}{K_{i,m}}\right) + S\left(1 + \sum_{m=1}^{p}\frac{I_m}{\alpha_m K_{i,m}}\right)} \qquad (1.15)$$

where the first summation represents the summation of the I/K_i values of each competitive inhibitor, c, for n competitive inhibitors. The second and third summations represent the summation of I/K, and $I/\alpha{*}K_i$ values, respectively, of each mixed-type or noncompetitive inhibitor, m, for p mixed-type or noncompetitive inhibitors. The α represents the relevant α coefficient, as previously defined, for each mixed-type or noncompetitive inhibitor, i.e. $\alpha \neq 1$ for mixed-type inhibitors and $\alpha = 1$ for noncompetitive inhibitors.

A key assumption in Michaelis-Menten enzyme kinetics is that the catalytic rate constant is negligible in comparison to the dissociation rate constant and so K_m approximates K_d (Rowland and Tozer, 1995). This assumption is generally appropriate for classic slow turnover enzymes such as mammalian P450s. Rearranging Equation 1.15 and substituting v/S with clearance and K_m for K_d yields the clearance of the substrate in the presence of the inhibitors (Cl'):

$$Cl' = \frac{V_{max}}{K_m\left(1 + \sum_{c=1}^{n}\frac{I_c}{K_{i,c}} + \sum_{m=1}^{p}\frac{I_m}{K_{i,m}}\right) + S\left(1 + \sum_{m=1}^{p}\frac{I_m}{\alpha_m K_{i,m}}\right)} \qquad (1.16)$$

Equation 1.16 can be simplified assuming S << K_m and the K_m multiplier term is not significantly less than the multiplier term for S. When these qualifications are met, Cl_i' can be defined as:

$$Cl_i' = \frac{V_{max}}{K_m\left(1 + \sum_{c=1}^{n}\frac{I_c}{K_{i,c}} + \sum_{m=1}^{p}\frac{I_m}{K_{i,m}}\right)} \qquad (1.17)$$

The only situation when the latter qualification would not be met is when one or more of the inhibitors is of mixed-type inhibition and the α-value associated with each mixed-type inhibitor is significantly lower than 1.

By substituting Cl_i for V_{max}/K_m and rearranging, Equation 1.17 yields:

$$\frac{Cl_i}{Cl_i'} = 1 + \sum_{c=1}^{n}\frac{I_c}{K_{i,c}} + \sum_{m=1}^{p}\frac{I_m}{K_{i,m}} \qquad (1.18)$$

which represents the fold-decrease in clearance resulting from multiple inhibitors. Equation 1.18 can be further simplified to:

$$\frac{Cl_i}{Cl_i'} = 1 + \sum_{z=1}^{q}\frac{I_z}{K_{i,z}} \qquad (1.19)$$

which denotes the summation of I/K_i ratios of inhibitor, z, for q inhibitors of any combination of competitive, noncompetitive or mixed-type inhibitors when $S << K_m$ and the α-value for any relevant mixed-type inhibitor is not significantly less than 1. Equation 1.19 is identical to Equation 1.12, except that it does not require the assumption that the inhibition mechanism is the same for all inhibitors within the system. Equation 1.19 does not account for uncompetitive reversible mechanisms. No inhibition by an uncompetitive inhibitor is possible when $S << K_m$ (derivation not shown) and this type of reversible P450 inhibition mechanism is uncommon. The above derivation demonstrates from first principle that parent and metabolite inhibition, regardless of reversible inhibition mechanism, can be simultaneously predicted using the following expression as long as *in vivo* substrate concentrations are well below the substrate K_m. This allows for simplification of *in vitro* inhibition determination and eliminates the need for the assumption that inhibitors must act via a common reversible inhibition mechanism.

Time-dependent inhibitors (TDIs) act by irreversibly or quasi-irreversibly binding to the P450, decreasing P450 activity by decreasing *in vivo* active P450 steady-state concentrations from before (E_{ss}) to after inhibitor administration (E_{ss}'). The resulting change in E_{ss} is a function of the *in vivo* P450 degradation rate constant (k_{deg}) and the predicted *in vivo* time-dependent inhibition rate (λ) (Mayhew *et al.*, 2000):

$$\frac{E_{ss}}{E_{ss}'} = \frac{k_{deg} + \lambda}{k_{deg}} \qquad (1.20)$$

where λ is a function of the *in vitro* time-dependent inhibition affinity constant (K_I) and maximum apparent time-dependent inhibition rate constant ($k_{inact,app}$) (Mayhew *et al.*, 2000):

$$\lambda = \frac{k_{inact,app} I}{K_I + I} \qquad (1.21)$$

When employing the same assumptions necessary to obtain Equation 1.11, the change in *in vivo* P450 intrinsic clearance from before (Cl_i) to after administration of an *in vitro* TDI (Cl_i') can be predicted using the expression (Mayhew *et al.*, 2000):

$$\frac{Cl_i}{Cl_i'} = 1 + \frac{k_{inact,app} I}{k_{deg}(K_I + I)} \qquad (1.22)$$

One additional assumption of this model is that inhibitor dosing length was sufficient to allow for active *in vivo* P450 concentrations (E_{ss}) to reach a new decreased steady-state.

It has been suggested that simultaneous P450 time-dependent inhibition by parent and metabolite can be predicted by simple addition of the *in vivo* predicted inhibition by each inhibitor independently (Rowland Yeo *et al.*, 2010):

$$\frac{Cl_i}{Cl_i'} = 1 + \sum_{a=1}^{n} \frac{k_{inact,app,a} I_a}{k_{deg}\left(K_{I,a} + I_a\right)} \qquad (1.23)$$

Zhang *et al.* suggested that attenuation of time-dependent inhibition due to mutual reversible inhibition must be accounted for according to (2009b):

$$\frac{Cl_i}{Cl_i'} = 1 + \sum_{a=1}^{n} \frac{k_{inact,app,a} I_a}{k_{deg}\left(K_{I,a}\left(1 + \sum_{b\neq a}^{n-1} \frac{I_b}{K_{i,b}}\right) + I_a\right)} \qquad (1.24)$$

Regardless of inhibition mechanism, the predicted change in Cl_i has to be attenuated by *in vivo* probe drug specific factors in order to predict the *in vivo* observable change in probe drug AUC before and after inhibitor administration (AUC'). When the affected P450 is not CYP3A4 and hence inhibition of intestinal CYP3A4 activity is not expected to play a role in increasing probe drug bioavailability, the AUC'/AUC can be predicted using the predicted Cl_i/Cl_i' and the expression (Ito *et al.*, 2005):

$$\frac{AUC'}{AUC} = \frac{1}{\frac{f_m}{Cl_i/Cl_i'} + (1 - f_m)} \qquad (1.25)$$

where f_m is the *in vivo* fraction of probe drug eliminated by the P450 when uninhibited. This model assumes that substrate metabolism occurs solely in the liver. Equation 1.25 describes change in probe drug exposure due to systemic P450 inhibition. If changes in probe drug intestinal bioavailability (F_g) are expected due to intestinal P450 inhibition, the change in F_g can be predicted using the expression (Wang *et al.*, 2004):

$$\frac{F_g'}{F_g} = \frac{1}{\frac{(1 - F_g)}{Cl_i/Cl_i'} + F_g} \qquad (1.26)$$

The ultimate change in probe AUC can be predicted by combining Equations 1.25 and 1.26 (Wang *et al.*, 2004):

$$\frac{AUC'}{AUC} = \frac{1}{\frac{(1 - F_g)}{Cl_i/Cl_i'} + F_g} * \frac{1}{\frac{f_m}{Cl_i/Cl_i'} + (1 - f_m)} \qquad (1.27)$$

1.6 Prediction of parent and metabolite reversible P450 inhibition

Although parent and metabolite inhibition can be due to either reversible or time-dependent inhibition, much of the available literature pertaining to metabolite inhibition has centered on predicting *in vivo* inhibition after administration of an *in vitro* reversible P450 inhibitor that possesses a circulating metabolite with *in vitro* reversible inhibitory potency towards the same P450 as the parent. Two notable examples are that of bupropion and itraconazole. Bupropion is metabolized to three major circulating metabolites: hydroxybupropion, threohydrobupropion and erythrohydrobupropion. The above three metabolites are more potent *in vitro* CYP2D6 reversible inhibitors compared to the parent (K_i =

21 μM for bupropion versus K_i = 13.3, 5.4 and 1.7 μM for the metabolites, respectively) (Reese *et al.*, 2008). Additionally, the estimated *in vivo* hepatocyte concentrations for the metabolites are at least 2-fold higher than that of the parent. When predicting the *in vivo* CYP2D6 interaction of bupropion with desipramine, bupropion alone predicts no significant *in vivo* interaction, but when all four inhibitory species (parent and metabolites) are incorporated, the *in vivo* interaction predicts within 2-fold accuracy (Reese *et al.*, 2008). Itraconazole also has three circulating metabolites: hydroxyitraconazole, keto-itraconazole and N-desalkyl itraconazole. All four species are potent reversible CYP3A4 inhibitors, with K_i values in the nanomolar range (Isoherranen *et al.*, 2004). After co-administration of midazolam with either a single dose of 200 mg or 400 mg itraconazole, the midazolam AUC'/AUC was more accurately predicted after accounting for all 4 inhibitory species, as opposed to itraconazole alone (observed/predicted AUC'/AUC value of 2.2 versus 1.5 for the 200 mg itraconazole dose and 1.7 versus 1.3 for the 400 mg itraconazole dose) (Templeton *et al.*, 2007; Templeton *et al.*, 2010). These studies indicate that, when predicting interactions arising from multiple inhibitor systems, all relevant inhibitory species (parent and metabolite) must be accounted for.

In contrast, a recent study reviewed the abundance of circulating reversible inhibitory metabolites of P450 reversible inhibitors and used literature K_i and plasma concentration values for both parent and metabolite(s) to predict the AUC'/AUC for 10 parent/metabolite pairs (Yeung *et al.*, 2011). When using either maximum or average inhibitor plasma concentrations, the *in vivo* inhibition of 7 out of the 10 metabolite/parent systems were more accurately predicted when incorporating both parent and metabolite(s) into the prediction, but improvement for many of the metabolite/parent pairs was modest. This result indicates that inclusion of metabolite reversible inhibition in *in vivo* DDI prediction may only provide minimal increase in prediction accuracy compared to parent alone. In this thesis study, fluoxetine, a reversible CYP2D6

inhibitor, and metabolite P450 inhibition will be characterized *in vitro* and used to predict *in vivo* observed DDIs to investigate the role of metabolite reversible inhibition in *in vivo* DDI prediction.

1.7 Prediction of parent and metabolite time-dependent P450 inhibition

Out of the 129 marketed *in vivo* P450 inhibitors, 24 % are TDIs (Isoherranen *et al.*, 2009). TDIs can be categorized into 2 general groups: P450 protein alkylators and P450 heme-metabolic-intermediate complex (MIC) formers (Kalgutkar *et al.*, 2007). Of the 31 marketed TDIs in 2009, 45 % are MIC-formers (VandenBrink and Isoherranen, 2010). The most common mechanism of MIC-formation involves an alkylamine moiety that undergoes several metabolic transformations to the MIC-forming nitrosoalkane (Mansuy *et al.*, 1977; Jonsson and Lindeke, 1992; Ortiz de Montellano, 2005) (Figure 1.3). All marketed alkylamine MIC-forming TDIs possess an *in vivo* circulating N-dealkylated metabolite that is considered “on pathway” to MIC-formation (VandenBrink and Isoherranen, 2010). The FDA and the EMA state that *in vivo* circulating metabolites should be characterized for *in vitro* P450 inhibition (<www.fda.gov/downloads/Drugs/GuidanceComplianceRegulatoryInformation/Guidances/ucm292362.pdf> and <www.ema.europa.eu/docs/en_GB/document_library/Scientific_guideline/2012/07/WC500129606.pdf>), but little guidance exists on exactly how to predict the *in vivo* effects of multiple TDI systems (parent and metabolite) from *in vitro* data. Several groups have examined this problem, using two different *in vitro*-to-*in vivo* prediction methodologies. First, the N-dealkylated secondary alkylamine metabolites of diltiazem and verapamil were incorporated into a model that simply summed up the predicted *in vivo* time-dependent inhibition rate contants (λ) for both parent and metabolite to improve the under prediction of *in vivo* CYP3A4 inhibition (Equation 1.23) (Wang *et al.*, 2004; Rowland Yeo *et al.*, 2010). An additional study applied this additive model to the diltiazem-CYP3A4 interaction, but incorporated mutual *in vivo* reversible inhibition interplay between the two TDIs to attenuate λ (Equation 1.24) (Zhang *et al.*,

2009b). Both models demonstrated improved *in vitro*-to-*in vivo* prediction accuracy with the inclusion of metabolite TDI, but there appears to be no consensus as to which model is correct. Additionally, diltiazem and verapamil are tertiary alkylamines that must be first N-dealkylated prior to MIC-formation (Murray and Murray, 2003) and hence, considering both tertiary and secondary alkylamine species as independent TDIs may not be appropriate. In this thesis study, Equations 1.23 and 1.24 will be examined using both *in vitro*-to-*in vitro* and *in vitro*-to-*in vivo* prediction methodology to determine which model, if any, correctly assesses *in vivo* DDI liability due to multiple (parent and metabolite) *in vitro* TDI systems.

MIC-formation from a secondary alkylamine is a complex process that requires, at minimum, an additional N-dealkylation and hydroxylation prior to nitrosoalkane formation (Mansuy *et al.*, 1977; Jonsson and Lindeke, 1992; Ortiz de Montellano, 2005) (Figure 1.3). The overall kinetic flux through the secondary alkylamine to the nitrosoalkane could be via formation of primary alkylamine, secondary hydroxylamine or both, and this flux is inhibitor specific (Hanson *et al.*, 2010). In practice, TDI characterization is performed by coincubating enzyme with the alkylamine (tertiary, secondary and/or primary) using the “two-step” methodology (Grimm *et al.*, 2009) as a function of time and inhibitor concentration and *in vitro* TDI constants are determined for *in vitro*-to-*in vivo* prediction. When multiple alkylamine species circulate *in vivo*, it is unclear which alkylamine species should be used to drive the *in vitro*-to-*in vivo* prediction calculations, or if all *in vivo* quantifiable species should be accounted for. In this thesis study, parent and metabolite time-dependent P450 inhibition will be characterized *in vitro* and used to predict *in vivo* observed DDIs to further understand DDI prediction of multiple TDI systems.

1.8 Hypothesis and specific aims

Hypothesis 1: The *in vivo* AUC_m/AUC_p of dextrorphan, 5-hydroxyomeprazole and omeprazole sulfone can be accurately predicted from *in vitro* metabolite formation and elimination data.

Aim 1.1: Determine the *in vitro* formation and elimination clearance of dextromethorphan and omeprazole metabolites in human liver microsomes (HLMs) and cryopreserved human hepatocytes (Chapter 2).

Aim 1.2: Predict the AUC_m/AUC_p of dextromethorphan and omeprazole metabolites from *in vitro* data and determine prediction accuracy via comparison to literature *in vivo* AUC_m/AUC_p (Chapter 2).

Hypothesis 2: Incorporation of *in vitro* inhibition by both fluoxetine and norfluoxetine is required for accurate prediction of the *in vivo* DDIs observed after multiple-dose fluoxetine administration

Aim 2.1: Determine the stereoselective *in vitro* time-dependent inhibition of CYP2C19 and CYP3A4 by fluoxetine and norfluoxetine in HLMs and assess the risk of *in vivo* DDI due to multiple *in vitro* TDI systems (Chapter 3).

Aim 2.2: Determine the stereoselective reversible inhibition of CYP2D6 by fluoxetine and norfluoxetine in HLMs and predict the magnitude of *in vivo* CYP2D6, CYP2C19 and CYP3A4 inhibition (Chapter 4).

Aim 2.3: Determine the effects of multiple dose fluoxetine on the *in vivo* activity of CYP2D6, CYP2C19, and CYP3A4 via an *in vivo* probe cocktail DDI study in healthy volunteers to assess prediction accuracy (Chapter 4).

1.9 Rational for using dextromethorphan, omeprazole and fluoxetine as parent drug models to study prediction of metabolite disposition and P450 inhibition

To test the developed *in vitro*-to-*in vivo* AUC_m/AUC_p prediction model (Equation 1.9), the AUC_m/AUC_p for two model drugs was predicted: dextromethorphan and omeprazole. Dextromethorphan is a cough suppressant that has two major *in vivo* metabolites, the CYP2D6-formed dextrorphan and the CYP3A4-formed 3-methoxymorphinan (Kerry *et al.*, 1994). Omeprazole is a medication for gastroesophageal reflux disease that also has two major *in vivo* metabolites, the CYP2C19-formed 5-hydroxyomeprazole and the CYP3A4-formed omeprazole sulfone (Andersson *et al.*, 1993). These two parent drugs were chosen as the model systems to study relative metabolite disposition because they 1) are commonly administered over-the-counter medications, 2) both have circulating metabolites and 3) the *in vivo* dextrorphan/dextromethorphan and 5-hydroxyomeprazole/omeprazole AUC_m/AUC_p ratios are often used as *in vivo* probe measures for CYP2D6 and CYP2C19 activity, respectively, in drug-drug interaction and genetic polymorphism studies (Furuta *et al.*, 1999; Abduljalil *et al.*, 2010).

Fluoxetine is a commonly prescribed antidepressant secondary alkylamine medication and a multiple P450 inhibitor. Fluoxetine is administered as a racemic mixture, demonstrates dose-dependent nonlinear pharmacokinetics and has a circulating N-dealkylating metabolite, norfluoxetine (Jannuzzi *et al.*, 2002). The (S)-enantiomers of fluoxetine and norfluoxetine circulate at 2- to 3-fold higher concentrations than the (R)-enantiomers *in vivo* (Jannuzzi *et al.*, 2002). After multiple-dose oral administration, fluoxetine is a strong inhibitor (AUC'/AUC > 5) of CYP2D6 (Bergstrom *et al.*, 1992) and moderate inhibitor (2 < AUC'/AUC < 5) of CYP2C19 (Vlase *et al.*, 2011), but *in vivo* CYP3A4 inhibition is controversial (Grimsley *et al.*, 1991; Greenblatt *et al.*, 1992; Lam *et al.*, 2003). *In vitro*, the (R)- and (S)-enantiomers of fluoxetine and

norfluoxetine are reversible inhibitors of CYP2D6 (Stevens and Wrighton, 1993). Fluoxetine is an *in vitro* stereoselective TDI of CYP2C19 and *rac*-norfluoxetine may be a TDI of CYP2C19, although the metabolite has never been studied stereoselectively and there is only cursory information pertaining to *in vitro* time-dependent inhibition by norfluoxetine (Kobayashi *et al.*, 1995; Stresser *et al.*, 2009). Finally, *rac*-fluoxetine is a TDI and *rac*-norfluoxetine is a reversible inhibitor of CYP3A4 *in vitro* (von Moltke *et al.*, 1996; Mayhew *et al.*, 2000). Based on what is known of fluoxetine and norfluoxetine *in vitro* inhibition, complete stereoselective characterization and *in vivo* CYP2D6, CYP2C19 and CYP3A4 inhibition prediction incorporating all four inhibitory species and accounting for both *in vitro* and *in vivo* protein binding is warranted. Additionally, retrospective *in vivo* DDI rank order analysis from literature studies may not be appropriate due to fluoxetine dose-dependent disposition (Jannuzzi *et al.*, 2002) and P450 genetic polymorphisms (Scordo *et al.*, 2005). Fluoxetine was chosen as the model inhibitor system for studying multiple P450 inhibitor systems because 1) fluoxetine is a secondary alkylamine MIC-forming TDI, 2) possesses an *in vivo* circulating inhibitory metabolite and 3) inhibits multiple P450s *in vivo* via both *in vitro* reversible and time-dependent inhibition.

Due to the possibility of drug metabolites eliciting pharmacologic/toxicologic effects and/or P450 inhibition, FDA and EMA regulation has emphasized the importance of understanding the *in vivo* disposition of and P450 inhibition by metabolites of newly developed drugs. Considerable theory exists on how to predict parent drug exposure or P450 inhibition, but little work has been performed in adapting these prediction methodologies to metabolite exposure or P450 inhibition. By examining the ability to predict *in vivo* dextromethorphan and omeprazole metabolite disposition as well as *in vivo* fluoxetine metabolite P450 inhibition, better understanding of the *in vivo* role of metabolites can be obtained. This understanding will translate to better risk assessment of metabolite liability during new drug development and ultimately improve patient safety.

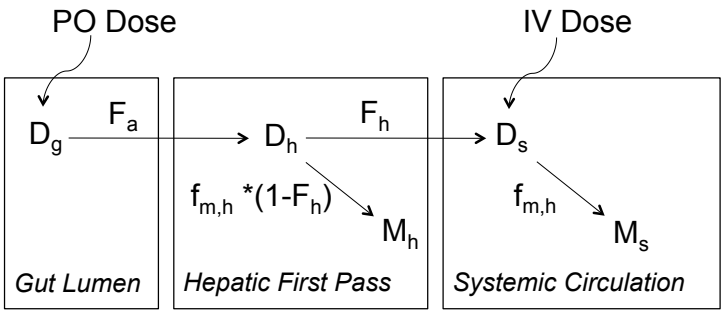

Figure 1.1. Schematic representation of the metabolic fate of a parent drug after PO or IV administration. This figure was previously published in Lutz *et al.* (2010).

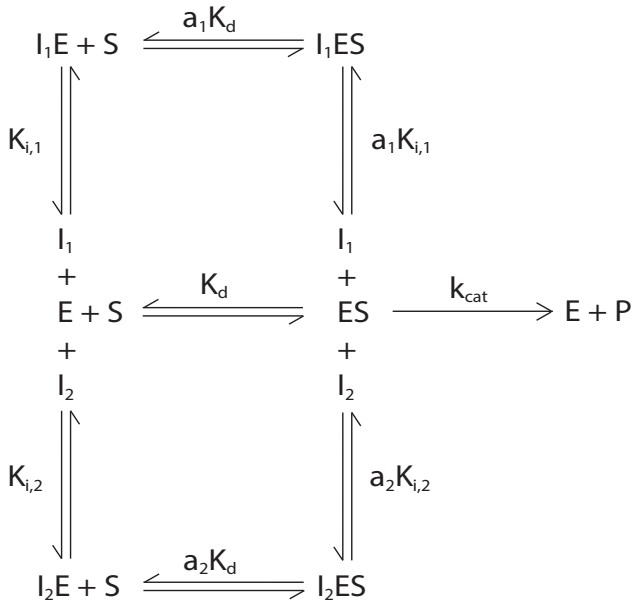

Figure 1.2. Kinetic scheme of two inhibitors with any combination of competitive, noncompetitive, mixed-type or uncompetitive reversible inhibition mechanism. An α_1 or α_2 value approaching infinity, approaching zero or equal to unity would indicate a reversible inhibition mechanism of competitive, uncompetitive or noncompetitive, respectively, for the given inhibitor. An α_1 or α_2 value of any other value indicates mixed-type reversible inhibition for the given inhibitor.

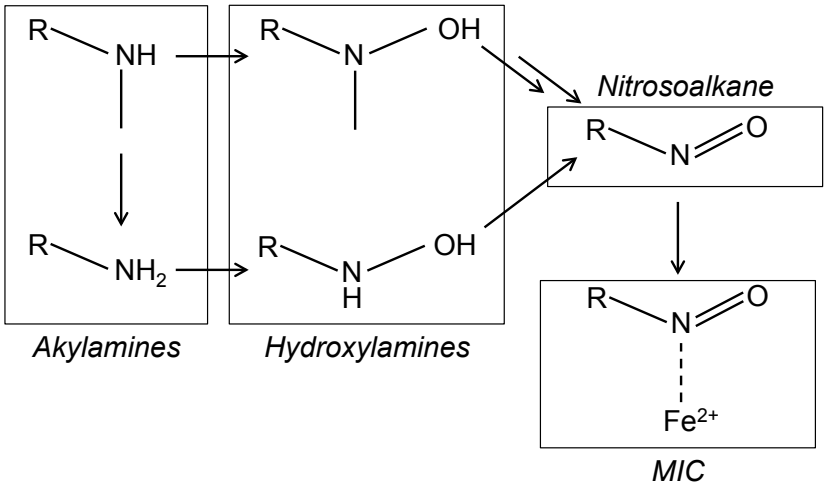

Figure 1.3. Schematic representation of the metabolic transformation of alkylamine TDIs to the ultimate formation of a metabolic-intermediate complex (MIC) with the P450 heme. Shown are the secondary and primary alkylamines (parent drug and *in vivo* circulating metabolite, respectively), secondary and primary hydroxylamines, nitrosoalkane and MIC.

Table 1.1. Rank order analysis of the *in vitro* $CL_{i,f}$ and the *in vivo* AUC_m/AUC_p for metabolite/parent pairs of a given parent drug. The *in vitro* $CL_{i,f}$ and *in vivo* AUC_m/AUC_p values are provided. Additionally, whether or not the metabolites of a given parent rank ordered correctly with respect to these two values is provided. All *in vivo* AUC_m/AUC_p values were determined under steady-state conditions except for those parent drugs marked with an asterisk, which were determined after single dose administration. Superscript 'a' indicates a value not determined because the observed *in vivo* metabolite concentrations were not detectable. Superscript 'b' indicates a set of metabolite/parent pairs for a given parent drug that were considered to not rank order correctly because the *in vitro* $CL_{i,f}$ values exhibited a > 15% difference but the AUC_m/AUC_p values did not or the AUC_m/AUC_p values exhibited a > 15% difference but the *in vitro* $CL_{i,f}$ values did not.

Parent	Metabolite	*In vitro* $CL_{i,f}$ (µL/min/mg)	*In vivo* AUC_m/AUC_p	Rank Order Correctly?	References
Iprazolam	1-hydroxyalprazolam	0.51	0.11	No	(Buch *et al.*, 1993; Greene *et al.*, 1995; Hirota *et al.*, 2001)
	4-hydroxyalprazolam	4.1	0.034		
Atorvastatin	2-hydroxyatorvastatin	20	0.87	No[b]	(Novartis, 2007; Park *et al.*, 2008)
	4-hydroxyatorvastatin	9.1	0.88		
Caffeine*	Theophylline	0.072	0.14	Yes	(Akinyinka *et al.*, 2000; Labedzki *et al.*, 2002)
	Paraxanthine	1.4	0.48		
	Theobromine	0.019	0.080		
Clomipramine	2-hydroxyclomipramine	0.98	ND[a]	No[b]	(Linnoila *et al.*, 1982; Kramer-Nielsen *et al.*, 1996)
	8-hydroxyclomipramine	0.94	0.36		
	N-desmethylclomipramine	16	2.2		
Codeine*	Morphine	0.23	0.029	No	(Yue *et al.*, 1991a; Yue *et al.*, 1991b; Soars *et al.*, 2001)
	Norcodeine	1.1	0.25		
	Codeine-6-glucuronide	0.45	9.2		
Imipramine*	Desipramine	8.3	0.54	Yes	(Skelbo and Brosen, 1992; Koyama *et al.*, 1994)
	2-hydroxyimipramine	2.8	0.37		
Lansoprazole	5-hydroxylansoprazole	19	0.085	No	(Ieiri *et al.*, 2001; Kim *et al.*, 2003)
	Lansoprazole sulfone	10	0.61		
Morphine*	Morphine-3-glucuronide	8.4	23	Yes	(Eliot *et al.*, 2002; Morrish *et al.*, 2006)
	Morphine-6-glucuronide	1.8	2.8		
Nefazodone	Hydroxynefazodone	240	0.36	Yes	(Greene *et al.*, 1995; Von Moltke *et al.*, 1999)
	Meta-chlorophenylpiperazine	190	0.090		
Omeprazole	5-hydroxyomeprazole	24	0.92	Yes	(Shu *et al.*, 2000; Shirai *et al.*, 2001)
	Omeprazole sulfone	20	0.54		
Propafenone	5-hydroxypropafenone	530	0.50	Yes	(Dilger *et al.*, 1999; Hemeryck *et al.*, 2000)
	N-desalkylpropafenone	3.5	0.064		
Quinidine	3-hydroxyquinidine	15	0.24	No	(Schellens *et al.*, 1991; Nielsen *et al.*, 1999)
	Quinidine N-oxide	2.9	0.37		
Tamoxifen	4-hydroxytamoxifen	2.3	0.034	Yes	(Lien *et al.*, 1990; Desta *et al.*, 2004)
	N-desmethyltamoxifen	31	2.1		
Theophylline*	3-methylxanthine	0.012	0.035	No[b]	(Rodopoulos and Norman, 1996; Tjia *et al.*, 1996)
	1,3-dimethyluric acid	0.16	0.032		

Chapter 2

Prediction of relative *in vivo* metabolite exposure from *in vitro* data using two model drugs: dextromethorphan and omeprazole

The work presented in this chapter was previously published

in

Drug Metabolism and Disposition 40(1):159–168, 2012.

2.1 Abstract

Metabolites can have pharmacological or toxicological effects, inhibit metabolic enzymes and be used as probes of drug-drug interactions or specific P450 phenotypes. Thus better understanding and prediction methods are needed to characterize metabolite exposures *in vivo*. This study aimed to test whether *in vitro* data could be used to predict and rationalize *in vivo* metabolite exposures using two model drugs and P450 probes: dextromethorphan and omeprazole with their primary metabolites dextrorphan, 5-hydroxyomeprazole and omeprazole sulfone. Relative metabolite exposures were predicted using metabolite formation and elimination clearances. For dextrorphan, the formation clearances of dextrorphan glucuronide and 3-hydroxymorphinan in human liver microsomes (HLMs) were used to predict metabolite (dextrorphan) clearance. For 5-hydroxyomeprazole and omeprazole sulfone the depletion rates of the metabolites in human hepatocytes were used to predict metabolite clearance. Dextrorphan/dextromethorphan *in vivo* AUC_m/AUC_p was over-predicted by 2.1-fold whereas 5-hydroxyomeprazole/omeprazole and omeprazole sulfone/omeprazole were predicted within 0.75 and 1.1-fold, respectively. The effect of inhibition or induction of the formation and elimination of the probe metabolite on the AUC_m/AUC_p ratio was simulated and showed that, unless metabolite clearance pathways are characterized, interpretation of the metabolic ratios is exceedingly difficult. This study shows that relative *in vivo* metabolite exposure can be predicted from *in vitro* data, and characterization of secondary metabolism of probe metabolites is critical for interpretation of phenotypic data.

2.2 Introduction

Metabolites of drugs can possess *in vivo* pharmacologic, toxicologic or enzyme inhibitory activity and contribute to the clinical effects of the drug (Ho *et al.*, 2003; Riss *et al.*, 2008). For example, the secondary metabolite of clopidogrel, R-130964, is the primary active species that

is responsible for the anti-coagulant effect *in vivo*, and decreasing its abundance *in vivo* leads to decreased pharmacological effect (Angiolillo *et al.*, 2010). The role of metabolites in drug toxicity is illustrated by the removal of fenfluramine from the US market due to its association with valvular heart disease. This cardiovascular toxicity was proposed to be 5-HT_{2B} receptor-mediated and norfenfluramine, the N-deethylated metabolite of fenfluramine, was demonstrated to be a significantly more potent agonist of human 5-HT_{2B} receptors than fenfluramine (Fitzgerald *et al.*, 2000). The inhibition of cytochrome P450 2D6 following bupropion administration appears to be mainly due to the primary metabolites of bupropion rather than bupropion itself, demonstrating the potential role of metabolites in inhibitory drug-drug interactions (Reese *et al.*, 2008; Yeung *et al.*, 2011). Due to the concern of exposures to metabolites in humans that are not covered by preclinical safety testing, the US Food and Drug Administration (FDA) and the European Medicines Agency (EMA) recently published guidance documents for the safety testing of metabolites (<www.fda.gov/downloads/Drugs/GuidanceComplianceRegulatoryInformation/Guidances/ucm079266.pdf> and <www.ema.europa.eu/pdfs/human/ich/028695en.pdf>) and the EMA included recommendations for *in vitro* P450 enzyme inhibition testing of new drug metabolites (<www.ema.europa.eu/docs/en_GB/document_library/Scientific_guideline/2012/07/WC500129606.pdf>). These recent guidances have drawn attention to the development of methods for early identification of metabolites and prediction of metabolite exposures (Anderson *et al.*, 2009; Leclercq *et al.*, 2009).

Metabolic ratios such as the metabolite/parent area under the plasma concentration versus time curve ratio (AUC_m/AUC_p), plasma concentration of the metabolite/parent (C_m/C_p) or urinary concentration ratios are commonly used in drug-drug interaction and pharmacogenetic studies as *in vivo* activity measures of the P450 mediating the formation of the metabolite. Use of metabolite formation or a metabolic ratio instead of an area under the plasma concentration versus time curve (AUC) of the parent drug is necessary when the parent drug is only partially

cleared by the P450 isoform of interest. Commonly used metabolic ratios include the hydroxybupropion/bupropion ratio for CYP2B6, the paraxanthine/caffeine ratio for CYP1A2, the dextrorphan/dextromethorphan ratio for CYP2D6 and the 5-hydroxyomeprazole/omeprazole ratio for CYP2C19 (Jones *et al.*, 1996; Streetman *et al.*, 2000; Yu and Haining, 2001; Abduljalil *et al.*, 2010). The 3-methoxymorphinan/dextromethorphan and omeprazole sulfone/omeprazole ratios have also been proposed as CYP3A4 probes (Jones *et al.*, 1996; Bertilsson *et al.*, 1997; Böttiger *et al.*, 1997; Tu *et al.*, 2010). In general, a decrease in the metabolic ratio is interpreted as inhibition of the P450 forming the metabolite or a poor metabolizer phenotype, whereas an increase suggests induction of the specific metabolic pathway. All metabolite/parent ratios are dependent on the formation and elimination clearances of the metabolite and their interpretation relies on the assumption that the clearance of the metabolite is not affected by the treatment or the genotype studied (Levy *et al.*, 1983). However, the clearance of the metabolite may be inadequately characterized in terms of quantitative importance by a specific enzyme. When the contribution of a specific enzyme is unknown, interpretation of the metabolic ratio may be confounded by changes in metabolite clearance. Hence the effect of interacting drug on the probe metabolite clearance is rarely determined.

A method for predicting the *in vivo* metabolite/parent AUC_m/AUC_p using clearance scaling from *in vitro* metabolite formation and elimination data was proposed (Chapter 1). The proposed method could be useful for *a priori* prediction of the relative metabolite exposure *in vivo* before clinical testing, or for identification of important secondary metabolism of metabolites whose AUC_m/AUC_p are greatly over-predicted after clinical administration. To test the method, published *in vitro* data for the formation of 3-hydroxymorphinan from dextrorphan (Figure 2.1) (Kerry *et al.*, 1994) and 5-hydroxyomeprazole sulfone from 5-hydroxyomeprazole (Figure 2.2) (Andersson *et al.*, 1993; Andersson *et al.*, 1994), was used to predict *in vivo* AUC_m/AUC_p ratios for dextrorphan/dextromethorphan and 5-hydroxyomeprazole/omeprazole. The

metabolite/parent AUC ratios were over-predicted by 160- and 20-fold, for dextrorphan/dextromethorphan and for 5-hydroxyomeprazole/omeprazole, respectively, indicating that significant uncharacterized metabolic pathways exist for dextrorphan and 5-hydroxyomeprazole. The aim of this study was to determine whether these elimination pathways do exist, and whether the dextrorphan/dextromethorphan, 5-hydroxyomeprazole/omeprazole and omeprazole sulfone/omeprazole *in vivo* AUC_m/AUC_p could be accurately predicted using *in vitro* metabolism data. Additionally, the effect of altered secondary metabolism on *in vivo* AUC_m/AUC_p was tested via pharmacokinetic simulation.

2.3 Materials and Methods

2.3.1 Chemicals and reagents

Dextromethorphan, dextrorphan, 3-hydroxymorphinan, omeprazole, 5-hydroxyomeprazole, omeprazole sulfone, nicotinamide adenine dinucleotide phosphate (NADPH), uridine diphosphate glucuronic acid (UDPGA), alamethicin and saccharolactone were purchased from Sigma-Aldrich (St. Louis, MO, USA). Dextrorphan-O-glucuronide and omeprazole-d_3 were purchased from Toronto Research Chemicals (North York, ON, CA). HPLC/MS grade water, acetonitrile and methanol were purchased from Sigma-Aldrich (St. Louis, MO, USA).

2.3.2 Human liver microsome (HLM) and recombinantly expressed UDP-glucuronysltransferase (rUGT) incubations

All HLM incubations were performed using HLMs pooled from seven different donors obtained from the University of Washington Human Liver Bank (Seattle, WA, USA). All seven donors were both phenotyped and genotyped to confirm that they were CYP2C19 and CYP2D6

extensive metabolizers as well as CYP3A5 non-expressors to avoid potential confounding effects of CYP3A5 expression in metabolite formation and elimination. Recombinantly expressed UDP-glucuronsyltransferase (rUGT) enzymes were obtained from BD Biosciences (Sparks, MD, USA). For all pooled HLM incubations, 0.1 mg microsomal protein (mg MP)/mL was utilized. All CYP-mediated incubations were performed in 100 mM potassium phosphate (KPi) buffer at 37˚ C, after a 10 minute pre-incubation with substrate at 37˚ C to achieve binding equilibrium. The incubations were then initiated with 1 mM final concentration of NADPH cofactor. For pooled HLM and rUGT dextrorphan-O-glucuronide formation, the incubations were first pre-incubated with 50 µg/mg MP alamethicin and 5 mM saccharolactone on ice in 100 mM KPi buffer for 30 minutes to allow insertion of the alamethicin pore former into the microsomal membrane, then further pre-incubated at 37˚ C for 10 minutes to achieve binding equilibrium. The incubations were then initiated with 5 mM final concentration of UDPGA cofactor. Pooled HLM dextrorphan-O-glucuronide formation was performed with and without the presence of 2% bovine serum albumin (BSA). Except for the substrate depletion experiments, all pooled HLM incubations were performed in 96-well plates in triplicate under determined time and HLM protein linearity conditions. The formation of dextrorphan-O-glucuronide by rUGT was measured with 10 µM dextrorphan as substrate in duplicate. Depletion of 5-hydroxyomeprazole in pooled HLMs was determined both in the absence and presence of NADPH. The initial concentration of either 5-hydroxyomeprazole or omeprazole sulfone in the substrate depletion experiments was 0.1 µM. All incubations were quenched with equivolume methanol (for dextromethorphan or dextrorphan as substrate) or acetonitrile (for omeprazole, 5-hydroxyomeprazole or omeprazole sulfone as substrate), centrifuged at 2,000 x *g* for 15 minutes and an aliquot was transferred to a clean 96-well plate for analysis.

2.3.3 Human hepatocyte incubations

The cryopreserved plated human hepatocyte incubations were performed utilizing a single donor (hu4199) obtained from Invitrogen (Carlsbad, CA, USA). Donor hu4199 was confirmed to exhibit adequate CYP2D6, CYP2C19 and CYP3A4/5 metabolic activity. Hepatocytes were first thawed at 37˚ C, centrifuged at 100 x *g* in Cryopreserved Hepatocyte Recovery Media (Invitrogen) and re-suspended in plating media (DMEM containing Plating Supplements with fetal bovine serum, Invitrogen). Viability and density were measured by trypan blue exclusion and 52,000 viable cells/well were plated onto 96-well collagen-coated plates. Hepatocytes were allowed to attach for 4 - 6 hours, plating media was removed and replaced with protein-free maintenance media (William's E medium plus maintenance supplements) containing 0.25 mg/mL Matrigel (BD Biosciences). All hepatocyte incubations were performed in quadruplicate in 96-well plates, utilizing identical protein-free hepatocyte maintenance media, within 3 days of initial plating. Metabolite formation clearance was determined at 37˚ C under confirmed time linearity conditions. When determining the hepatocyte formation clearance of either 5-hydroxyomeprazole or omeprazole sulfone, the initial concentration of omeprazole was 1 μM. In the hepatocyte substrate depletion experiments, the initial concentration of either 5-hydroxyomeprazole or omeprazole sulfone was 0.1 μM. All hepatocyte incubations were quenched by the addition of an aliquot of media into an equal volume of acetonitrile, centrifuged at 2,000 x *g* for 15 minutes and then aliquot was transferred to a clean 96-well plate for analysis. The intrinsic formation clearance ($Cl_{i,f}$) of 5-hydroxyomeprazole and omeprazole sulfone from omeprazole was determined over 6 hours and the intrinsic depletion clearance ($Cl_{i,dep}$) of 5-hydroxyomeprazole or omeprazole sulfone was determined over 24 hours.

2.3.4 Determination of *in vitro* and plasma fraction unbound ($f_{u,HLM}$ and f_u, respectively)

0.1 μM of dextromethorphan, dextrorphan, omeprazole, 5-hydroxyomeprazole or omeprazole sulfone was spiked into either human plasma or HLMs at 0.1 mg MP/mL in 100 mM KPi buffer in triplicate. The sample was then divided and either centrifuged at 800,000 x *g* for 90 minutes at 37˚ C or held at 37˚ C for 90 minutes without centrifugation, adapted from the method of Templeton et al (2007). An aliquot was then transferred from both samples to a clean 96-well plate for analysis.

2.3.5 Sample analysis

Except for dextrorphan-O-glucuronide analysis, all pooled HLM incubations were analyzed using a Shimadzu HPLC with a CTC autosampler coupled to an AB Sciex API4000 Q/Q mass spectrometer (Foster City, CA, USA) operating in positive ion electrospray mode. Separation of dextromethorphan and dextromethorphan metabolites was achieved using an Agilent Zorbax Eclipse C-18, 5μm, 2.1 x 50 mm column (Santa Clara, CA, USA) with a solvent gradient (water:methanol) of 80:20 isocratic for 3.5 minutes, then a linear increase to 45:55 over 2.5 minutes then rapidly increased to and held at 5:95 for 1.5 minutes. The injection volume was 10 μL. Separation of omeprazole, omeprazole metabolites and omeprazole-d_3 (internal standard) was achieved using an identical column with a solvent gradient (10 mM ammonium formate in water:acetonitrile) consisting of a linear increase from 95:5 to 65:35 over 6 minutes then held at 10:90 for 1.5 minutes. The multiple reaction monitoring (MRM) mass transition, Declustering Potential (DP) (V) and Collision Energy (CE) (V) values for each analyte are as follows (MRM, DP, CE): dextromethorphan (272→171, 60, 50), dextrorphan (258→157, 60, 50), 3-hydroxymorphinan (244→157, 70, 50), omeprazole (346→198, 45, 20), omeprazole-d_3 (349→198, 45, 20), 5-hydroxyomeprazole (362→214, 55, 20) and omeprazole sulfone (362→214, 45, 80). All analyte channels were confirmed to be free of co-eluting contaminants, either from the matrix or from other analytes within the assay. The injection volume for both

assays was 10 µL. The day-to-day % CV for all analytes were < 15% and the limits of quantification for all analytes were ≤ 100 pM.

The formation of dextrorphan-O-glucuronide in pooled HLMs and rUGTs was analyzed utilizing an Agilent 1100 HPLC and autosampler coupled to an Agilent MSD Q mass spectrometer operated in negative ion electrospray mode. An identical column to that described above and a solvent gradient (water:methanol) was utilized with a linear increase from 90:10 to 5:95 over 3 minutes, then held at 5:95 for an additional 3 minutes. The selected ion recording (SIR) mass for dextrorphan-O-glucuronide was $[M - H]^-$ = 432 m/z and Fragmentor Voltage was -5000 V. The injection volume was 10 µL.

The hepatocyte incubations were analyzed utilizing an Agilent Infinity 1290 UPLC coupled to an AB Sciex API 5500 Q/LIT mass spectrometer operated in positive ion electrospray mode. The separation and detection settings for omeprazole and its metabolites were identical to those described above. The injection volume was 10 µL.

2.3.6 Data analysis

All data was fit via linear or nonlinear regression numerical analysis utilizing GraphPad Prism v.5 (LaJolla, CA, USA). Unless otherwise noted, all parameter estimates are given as mean ± standard deviation. The maximum primary or secondary metabolite formation velocity (V_{max}) and total Michaelis-Menten affinity constant (K_m) in pooled HLMs was determined by the equation:

$$v = \frac{V_{max}[S]_0}{K_m + [S]_0} \qquad (2.1)$$

where v and $[S]_0$ are the metabolite formation velocity and initial substrate concentration, respectively. The primary or secondary metabolite total intrinsic formation clearance ($Cl_{i,f}$) was determined by the equation:

$$Cl_{i,f} = \frac{V_{max}}{K_m} \qquad (2.2)$$

The primary metabolite total intrinsic depletion clearance ($Cl_{i,dep}$) was determined utilizing the equation:

$$[S]_t = [S]_0 e^{-\frac{Cl_{i,dep}}{V_{inc}}t} \qquad (2.3)$$

where $[S]_t$ and V_{inc} are the concentration of substrate at a specific time point (t) and the incubation volume, respectively. In hepatocytes, the primary metabolite total intrinsic formation clearance ($Cl_{i,f}$) was determined by the equation:

$$[M]_t = \frac{Cl_{i,f}[S]_0 t}{V_{inc}} \qquad (2.4)$$

where $[M]_t$ is the concentration of metabolite at a specific time point. When either $Cl_{i,dep}$ (in pooled HLMs and hepatocytes) or $Cl_{i,f}$ (in hepatocytes only) was determined, it was assumed that $[S]_0 << K_m$. The pooled HLM fraction unbound ($f_{u,HLM}$) or plasma fraction unbound (f_u) for either parent or metabolite was determined by the equation:

$$f_u = \frac{[A]'}{[A]} \qquad (2.5)$$

where [A]' and [A] are the concentrations of analyte (metabolite or parent) with and without centrifugation, respectively.

2.3.7 Prediction of AUC_m/AUC_p

The *in vivo* AUC_m/AUC_p for a specific metabolite/parent pair after oral administration was predicted from *in vitro* data using Equations 2.6 and 2.7. Equation 2.6 can be described as:

$$\frac{AUC_m}{AUC_p} = \frac{f_{u,p} Cl_{f,u} \left(Q_h + f_{u,m} Cl_{m,u}\right)}{Q_h f_{u,m} Cl_{m,u}} \qquad (2.6)$$

This equation assumes that all metabolite formed in the liver is available to the systemic circulation (Chapter 1). The $f_{u,p}$ and $f_{u,m}$ are the plasma fraction unbound of the parent and metabolite, respectively. The $Cl_{f,u}$ and $Cl_{m,u}$ are the scaled unbound formation and elimination clearances of the metabolite, respectively and hepatic plasma flow is denoted as Q_h. A value of 49.5 L/hr was used for Q_h (product of the hepatic blood flow and the proportion of blood that is plasma).

To accommodate likely sequential metabolism of the metabolites within the liver before they reach systemic circulation, Equation 2.7 was derived. For Equation 2.7, the formation of the metabolite within the liver is considered analogous to portal vein dosing of the metabolite. Equation 2.7 is obtained from Equation 2.6 by adding an additional bioavailability term for the metabolite (F_h equaling unity minus the hepatic extraction ratio of the metabolite) that represents the fraction of metabolite formed in the liver that is not sequentially metabolized prior to reaching the systemic circulation (Pang and Gillette, 1979). Incorporation of this metabolite bioavailability term yields Equation 2.7:

$$\frac{AUC_m}{AUC_p} = \frac{f_{u,p} Cl_{i,f}}{f_{u,m} Cl_{i,m}} \qquad (2.7)$$

For predictions, all *in vitro* determined total Cl or Cl_i values were divided by the corresponding $f_{u,HLM}$ value to obtain the unbound clearance (Cl_u or $Cl_{i,u}$) values. For all

hepatocyte data, the $f_{u,HLM}$ was assumed to equal unity, due to the use of protein-free hepatocyte maintenance media during the incubations. The accuracy of the prediction was determined by the ratio of the predicted value over the observed value, extracted from the literature for *in vivo* studies that determined both parent and metabolite AUC in plasma. Only *in vivo* studies in CYP2D6 and CYP2C19 extensive metabolizers as determined by dextromethorphan phenotype or CYP2C19 genotype were used.

2.3.8 Simulations of the effect of secondary metabolism on AUC_m/AUC_p

Using a generic scheme of one enzyme (E1) forming a single metabolite (M) from parent drug (P) and two enzymes (E1 and E2) eliminating the metabolite, the AUC_m/AUC_p, was simulated using SAAM II (University of Washington, Seattle, WA, USA). It was assumed that the metabolite formed can be sequentially metabolized prior to reaching the systemic circulation (Equation 2.7). This simple metabolic scheme is presented as:

$$FD \overset{k_a}{\rightarrow} [P] \xrightarrow{f_{u,p}Cl_{f,u}^{E1}} [M] \xrightarrow{f_{u,m}\left(Cl_{m,u}^{E1}+Cl_{m,u}^{E2}\right)}$$

where F, D and k_a are the bioavailabilty, dose and absorption rate constant of the parent after oral administration, respectively. All other variables are as previously defined. Equations 2.8 and 2.9 are the differential equation describing the change in parent (d[P]/dt) and metabolite concentrations over time (d[M]/dt):

$$\frac{d[P]}{dt} = \frac{FDk_a - [P]f_{u,p}X_f^{E1}Cl_{f,u}^{E1}}{V_p} \qquad (2.8)$$

$$\frac{d[M]}{dt} = \frac{[P]f_{u,p}X_f^{E1}Cl_{f,u}^{E1} - [M]f_{u,m}\left(X_m^{E1}Cl_{m,u}^{E1} + X_m^{E2}Cl_{m,u}^{E2}\right)}{V_m} \qquad (2.9)$$

where V_p and V_m are the volumes of distribution for the parent and metabolite, respectively. X_f and X_m were incorporated to represent the coefficients describing the effect of induction (> 1) or inhibition (< 1) on $Cl_{f,u}$ or $Cl_{m,u}$, respectively. All other variables are as previously defined. The second integral of Equations 2.8 and 2.9 describe the AUC_p and AUC_m, respectively. The quotient of AUC_m and AUC_p can be described by Equation 2.10:

$$\frac{AUC_m}{AUC_p} = \frac{f_{u,p} X_f^{E1} Cl_{f,u}^{E1}}{f_{u,m}\left(X_m^{E1} Cl_{m,u}^{E1} + X_m^{E2} Cl_{m,u}^{E2}\right)} \qquad (2.10)$$

The values in Equation 2.10 were set so that when X_f and X_m were 1 the AUC_m/AUC_p = 1. The value for AUC_m/AUC_p was simulated for a range of interactions ($1 \leq X \leq 10$ for induction and $1 \geq X \geq 0.1$ for inhibition). Several different enzymatic scenarios were considered in which the fraction of metabolite clearance by E1 varied from 0 to 1.

2.4 Results

2.4.1 *In vitro* formation and elimination of dextrorphan

The formation kinetics of dextrorphan from dextromethorphan was determined in pooled HLMs (Figure 2.3A). Pooled HLMs were also used to characterize 3-hydroxymorphinan and dextrorphan-O-glucuronide formation from dextrorphan (Figure 2.3B and 3C). The kinetic parameters for dextrorphan, 3-hydroxymorphinan and dextrorphan-O-glucuronide formation as well as the $f_{u,HLM}$ and plasma f_u values are summarized in Table 2.1. The resulting intrinsic clearance for dextrorphan formation from dextromethorphan was 13 µL/min/mg MP and for 3-hydroxymorphinan formation from dextrorphan was 0.88 µL/min/mg MP. Dextrorphan-O-glucuronide was formed in a time, UDPGA cofactor and dextrorphan concentration dependent manner in the presence and absence of 2% BSA. The K_m for dextrorphan glucuronidation determined from total dextrorphan concentration decreased by 70% from 690 ± 140 µM to 210 ±

110 μM as a result of adding 2% BSA. The $f_{u,HLM}$ value for dextrorphan decreased from 1.0 ± 0.04 to 0.88 ± 0.05 in the presence of 2% BSA and hence the unbound K_m decreased from 690 ± 140 μM to 190 ± 100 μM after addition of 2% BSA. The V_{max} for dextrorphan glucuronidation was unchanged by adding BSA, 2.0 ± 0.2 nmol/min/mg MP in the absence of BSA and 2.3 ± 0.4 nmol/min/mg MP in the presence of BSA. The unbound intrinsic clearance ($Cl_{i,u}$) for dextrorphan-O-glucuronide formation was 2.9 μL/min/mg MP in the absence of BSA and 12 μL/min/mg MP in the presence of BSA (Table 2.1). To identify the UGT isoforms responsible for dextrorphan glucuronidation, dextrorphan was incubated with a panel of 12 recombinant UGT isoforms (Figure 2.3D). All four UGT2B isoforms studied (2B4, 2B7, 2B15 and 2B17), but none of the eight UGT1A isoforms studied (1A1, 1A3, 1A4, 1A6, 1A7, 1A8, 1A9 and 1A10) formed dextrorphan-O-glucuronide suggesting that dextrorphan glucuronidation is catalyzed mainly by the UGT2B subfamily *in vivo*.

2.4.2 Prediction of *in vivo* dextrorphan/dextromethorphan AUC_m/AUC_p

The $Cl_{i,u}$ (V_{max}/ $K_{m,u}$) values determined in pooled HLMs were scaled to obtain total *in vivo* formation and elimination clearances (Cl_f and Cl_m, respectively) for dextrorphan. The *in vivo* AUC_m/AUC_p was predicted using these values and dextromethorphan and dextrorphan plasma f_u values, and then compared to *in vivo* literature values. Utilizing 3-hydroxymorphinan Cl_f from dextrorphan as the only secondary metabolic pathway of dextrorphan yielded a predicted AUC_m/AUC_p of 22 using Equation 2.6 (all metabolite available for systemic circulation). Since the average observed dextrorphan/dextromethorphan *in vivo* AUC_m/AUC_p is 0.61 (range = 0.52 - 0.70) this resulted in an average 36-fold over-prediction when compared to published exposure data (Abdul-Manap *et al.*, 1999; Yeh *et al.*, 2003; Nakashima *et al.*, 2007). Incorporation of the UGT pathway (characterized *in vitro* in the presence of 2% BSA) decreased the predicted AUC_m/AUC_p to 2.3 and decreased the extent of over-prediction to a 3.8-fold average (range =

3.3 – 4.4) (Table 2.2). When the glucuronidation pathway of dextrorphan is accounted for, dextrorphan is predicted to be a high extraction ratio metabolite and hence it is likely that only a fraction of the formed metabolite is available to systemic circulation. Therefore Equation 2.7 was also used for predicting the AUC_m/AUC_p of dextrorphan (Table 2.2). Indeed, when the glucuronidation characterized *in vitro* in the presence of 2% BSA and the methoxymorphinan formation were included in the predictions a predicted AUC_m/AUC_p of 1.3 was obtained resulting in an approximately 2-fold over-prediction.

2.4.3 *In vitro* formation and elimination kinetics of 5-hydroxyomeprazole and omeprazole sulfone

The total intrinsic formation ($Cl_{i,f}$) and elimination ($Cl_{i,dep}$) clearances for 5-hydroxyomeprazole and omeprazole sulfone were determined in pooled HLMs and in cryopreserved plated human hepatocytes. Since comprehensive characterization of the secondary metabolites of omeprazole sulfone and 5-hydroxyomeprazole is not available, the depletion clearances of these metabolites were measured instead of specific secondary metabolite formation clearance. The K_m and V_{max} for the formation of 5-hydroxyomeprazole and omeprazole sulfone from omeprazole, as well as the depletion of these two metabolites in HLMs, is shown in Figure 2.4. The kinetic parameters for 5-hydroxyomeprazole and omeprazole sulfone formation and depletion in HLMs and human hepatocytes are summarized in Table 2.3. In pooled HLMs, the unbound formation and depletion clearances for omeprazole sulfone were 7.7 µL/min/mg MP and 35 µL/min/mg MP, respectively, demonstrating that the clearance of omeprazole sulfone is 5 times faster than its formation. Similarly, in human hepatocytes (Figure 2.5) the elimination clearance of omeprazole sulfone ($Cl_{i,dep}$ = 48 ± 6 µL/hr/10^6 cells) was approximately 13 times faster than the formation of omeprazole sulfone ($Cl_{i,f}$ = 3.6 ± 0.5 µL/hr/10^6 cells).

The unbound formation clearance for 5-hydroxyomeprazole in HLMs was 8.2 µL/min/mg MP but no depletion of 5-hydroxyomeprazole was observed in pooled HLMs (Figure 2.4) and the percent remaining of 5-hydroxyomeprazole at 30 and 60 minutes when incubated with and without NADPH was similar. Since the *in vitro*-to-*in vivo* predictions of 5-hydroxyomeprazole exposure suggested that 5-hydroxyomeprazole is metabolically cleared, but no depletion of 5-hydroxyomeprazole could be observed in pooled HLMs, the depletion of 5-hydroxyomeprazole was studied in cultured human hepatocytes (Figure 2.5). Unlike in HLMs, depletion of 5-hydroxyomeprazole was detected in plated human hepatocytes. The $Cl_{i,f}$ for 5-hydroxyomeprazole was 55 ± 2 µL/hr/10^6 cells and the $Cl_{i,dep}$ for 5-hydroxyomeprazole was 100 ± 20 µL/hr/10^6 cells.

2.4.4 Prediction of *in vivo* 5-hydroxyomeprazole/omeprazole and omeprazole sulfone/omeprazole AUC_m/AUC_p

The *in vivo* AUC_m/AUC_p was predicted from only hepatocyte data for the 5-hydroxyomeprazole/omeprazole pair and from both *in vitro* pooled HLM and hepatocyte data for the omeprazole sulfone/omeprazole pair. The AUC_m/AUC_p was predicted using Equations 2.6 and 2.7 and compared to *in vivo* reported literature values. The predicted AUC_m/AUC_p values are summarized in Table 2.2 together with the average reported *in vivo* AUC_m/AUC_p values. Similar predicted AUC_m/AUC_p values were obtained using Equation 2.6 and Equation 2.7. Based on hepatocyte data, both the omeprazole sulfone/omeprazole and the 5-hydroxyomeprazole/omeprazole AUC_m/AUC_p were predicted within 25% of the observed average AUC ratio and the predicted ratio was within the observed range of the AUC ratios reported in different studies. Using HLM data, the AUC_m/AUC_p for omeprazole sulfone/omeprazole was over-predicted by 3-fold on average.

2.4.5 Simulation of the effect of altered formation or elimination clearance on *in vivo* AUC_m/AUC_p

To determine whether altered metabolism of the probe metabolite affects the interpretation of *in vivo* AUC_m/AUC_p, the changes in a generic metabolite/parent AUC_m/AUC_p as a result of induction or inhibition of the formation and/or elimination of the metabolite were simulated. The simulations were conducted assuming sequential metabolism of the metabolite prior to reaching the systemic circulation is possible. Induction or inhibition of the formation of the metabolite resulted in an increase or decrease in AUC_m/AUC_p, respectively, when the elimination of the metabolite was not entirely mediated by the same enzyme which forms the metabolite ($f_{m,E1} < 1$). This effect was attenuated when the metabolite was cleared partly by the same enzyme that forms it and no change in the AUC_m/AUC_p was observed when the metabolite was entirely eliminated by the same enzyme that forms it. Induction or inhibition of the elimination of the metabolite by E2 resulted in a decrease or increase in AUC_m/AUC_p, respectively. This effect was most pronounced when $f_{m,E2}$ approached unity. The simulations show that based on observed *in vivo* AUC_m/AUC_p data it is extremely difficult to determine whether metabolite formation or elimination pathways are affected unless the elimination pathways of the metabolite are characterize and measured.

2.5 Discussion

The data obtained in this study shows that *in vivo* AUC_m/AUC_p can be accurately predicted form *in vitro* data using only primary metabolite formation and depletion kinetics. Comparison of the predicted and observed AUC_m/AUC_p for a given metabolite allows determination of the importance of hepatic metabolic clearance in the elimination of that metabolite as shown for omeprazole and dextromethorphan metabolite AUC_m/AUC_p. On the

other hand, the over-prediction of AUC_m/AUC_p can be used as an indication of missing/unidentified elimination pathways. Such information could be useful during drug development for compounds whose elimination has not been completely characterized but preliminary *in vivo* concentration data is available, as can be the case when a candidate compound is tested for a new target.

Although the dextrorphan/dextromethorphan AUC_m/AUC_p was predicted within 2.1-fold using HLM data alone, based on the predictions with 5-hydroxyomeprazole and omeprazole sulfone, using hepatocytes instead of HLMs for metabolite depletion studies is more reliable. Based on the *in vitro* formation clearances, glucuronidation is the major elimination pathway for dextrorphan. In this study, dextrorphan-O-glucuronide formation measured in the presence of 2% BSA was 12-fold more efficient than the formation of 3-hydroxymorphinan. The overall prediction accuracy suggests that the major elimination pathways of dextrorphan are accounted for via glucuronidation and 3-hydroxymorphinan formation. UGT2B isoforms were found to be responsible for dextrorphan glucuronidation, similar to related opioids morphine and codeine (Court *et al.*, 2003). Dextrorphan glucuronidation has been previously reported *in vitro* and *in vivo* (Duché *et al.*, 1993; Takashima *et al.*, 2005; Abduljalil *et al.*, 2010), but formation kinetics have not been characterized. Overall the kinetic values determined for dextrorphan and 3-hydroxymorphinan formation were similar to those previously reported (Kerry *et al.*, 1994). The values determined for glucuronidation in the presence of 2% BSA are likely appropriate for clearance predictions since BSA increases glucuronidation efficiency in HLMs by binding fatty acids that inhibit UGTs (Kilford *et al.*, 2009). The difference in the prediction accuracy between Equation 2.6 and 2.7 (3.8 and 2.1 fold, respectively) reflects the fact that dextrorphan extraction ratio is predicted to be high and hence, sequential metabolism of dextrorphan in the liver is likely. The remaining 2.1 fold over-prediction in the AUC_m/AUC_p is likely due to extra-hepatic glucuronidation of dextrorphan rather than unaccounted renal clearance. UGT2B enzymes are

expressed in many extra-hepatic tissues (Nakamura *et al.*, 2008) and dextrorphan undergoes only minor renal elimination relative to predicted total metabolic clearance (4.5 L/hr vs 38.7 L/hr) (Duché *et al.*, 1993).

The fact that *in vivo* AUC_m/AUC_p for 5-hydroxyomeprazole/omeprazole and omeprazole sulfone/omeprazole could be accurately predicted from hepatocyte primary metabolite $Cl_{i,dep}$ suggests that, to predict the exposure of primary metabolites, secondary metabolic pathways do not need to be identified. This is useful for metabolites such as 5-hydroxyomeprazole and omeprazole sulfone that appear to undergo metabolism to multiple sequential species. The measured $Cl_{i,f}$ for 5-hydroxyomeprazole and omeprazole sulfone are in agreement with previously determined values in HLMs (Andersson *et al.*, 1993). The $Cl_{i,dep}$ of omeprazole sulfone (32 µL/min/mg MP) was greater than the previously measured $Cl_{i,f}$ of 5-hydroxyomeprazole sulfone from omeprazole sulfone (9.7 µL/min/mg MP) suggesting a contribution of additional pathways to omeprazole sulfone elimination. The reason for a better prediction of the *in vivo* omeprazole sulfone/omeprazole AUC_m/AUC_p from hepatocyte data than from HLM data could be due to more accurate prediction of both the formation and elimination clearance of omeprazole sulfone from hepatocytes than from HLMs, but *in vivo* data of clearance of omeprazole sulfone would be needed to determine this. It is noteworthy that since omeprazole sulfone is 12.7-fold more bound in plasma than omeprazole (Table 2.3), the unbound AUC_m/AUC_p of omeprazole sulfone/omeprazole is 0.067 while the observed total AUC_m/AUC_p is 0.85 (Table 2.2). This shows that when AUC_m/AUC_p ratios are used to predict the importance of metabolites in pharmacologic activity, the difference between the plasma f_u for the metabolite and parent should be considered together with the AUC_m/AUC_p. The AUC_m/AUC_p for 5-hydroxyomeprazole/omeprazole could not be predicted from HLM data due to the lack of measurable depletion of 5-hydroxyomeprazole. Based on the reported formation kinetics of 5-hydroxyomeprazole sulfone from 5-hydroxyomeprazole (Andersson *et al.*, 1994), 0.5% depletion

is expected in HLMs after a 60 min incubation. This is not sufficient to obtain depletion kinetic estimates. 5-hydroxyomeprazole and carboxyomeprazole are the major metabolites detected in urine after omeprazole administration (Renberg *et al.*, 1989) and sequential formation of carboxyomeprazole from omeprazole aldehyde is likely responsible for the majority of 5-hydroxyomeprazole depletion in hepatocytes. It is likely that alcohol and aldehyde dehydrogenases (ADHs and ALDHs, respectively) form omeprazole aldehyde and carboxylic acid in human hepatocytes since the ADH isoforms that metabolize xenobiotics are localized in the cytosol and expressed the liver (Crabb *et al.*, 2004). Since ADH enzymes are induced by ethanol (Kawashima *et al.*, 1996; Crabb *et al.*, 2004) their activity is expected to vary between individuals. This may explain the considerable variability (up to 10-fold) observed in the AUC_m/AUC_p of 5-hydroxyomeprazole/omeprazole between reported *in vivo* studies even after controlling for CYP2C19 genotype (Tassaneeyakul *et al.*, 2000; Shirai *et al.*, 2001).

Metabolite ratios or specific metabolite formation measures are usually considered more sensitive measures than the AUC_p to determine inhibition or induction of specific P450 enzymes. This is especially the case for probe drugs that undergo metabolism by multiple CYPs, for which use of a specific metabolite measure rather than AUC_p is necessary. Thus, altered AUC_m/AUC_p (or C_m/C_p) of the probe metabolite will usually be considered as indication of an interaction even in the absence of effect on AUC_p. For example, an increase in AUC_m/AUC_p could be interpreted as weak *in vivo* induction of Cl_f when the drug-drug interaction was in fact due to inhibition of Cl_m as shown by the simulations. In practice, this is illustrated when CYP2C19 poor metabolizer genotype, likely decreasing the CYP2C19-mediated elimination of omeprazole sulfone, causes an increased omeprazole sulfone/omeprazole AUC_m/AUC_p, the probe measure for CYP3A4 (Yang *et al.*, 2009; Tu *et al.*, 2010). For the dextrorphan/dextromethorphan and 5-hydroxyomeprazole/omeprazole ratios, it is unlikely that major changes in secondary pathways would be misinterpreted if AUC_p is measured in the

study. However, if the change in the metabolic ratio is weak (suggesting that no effect in the less sensitive AUC_p measure would be expected) or only a single time point ratio is measured, the likelihood of misinterpretation is high. The challenge of identifying the correct interpretation of AUC_m/AUC_p ratios is emphasized by the simulations that show that induction of metabolite clearance has an identical effect on the AUC_m/AUC_p as inhibition of the formation of the metabolite. In addition, the simulations show that the sensitivity of the metabolic ratio is greatly dampened if the metabolite clearance is partially mediated by the same enzyme as the formation, with no effect on the ratio if the same enzyme forms and eliminates the metabolite. These results warrant more thorough characterization of the complete formation and elimination clearances of the metabolites (including sequential metabolites) in drug-drug interaction studies. For dextrorphan, treatment of samples with β-glucuronidase or measurement of the dextrorphan glucuronide should be considered when CYP2D6 activity is measured.

In this study, *in vitro*-to-*in vivo* predictions of AUC_m/AUC_p were used to determine the importance of secondary metabolism in 5-hydroxyomeprazole and dextrorphan clearance, and the major *in vivo* metabolic pathways were predicted. The results show that *in vitro*-to-*in vivo* predictions of metabolite exposure are a valuable tool for improving our understanding of P450 probes and metabolite clearance pathways and for predicting relative metabolite exposures after administration of parent drug. Kinetic characterization of the metabolism of dextrorphan and 5-hydroxyomeprazole afforded accurate prediction of AUC_m/AUC_p, demonstrating that *in vivo* metabolite disposition (relative to parent) can be predicted from *in vitro* data. The results obtained in this study emphasize the significance of understanding the secondary metabolic processes involved in elimination of metabolites utilized as *in vivo* P450 activity measures.

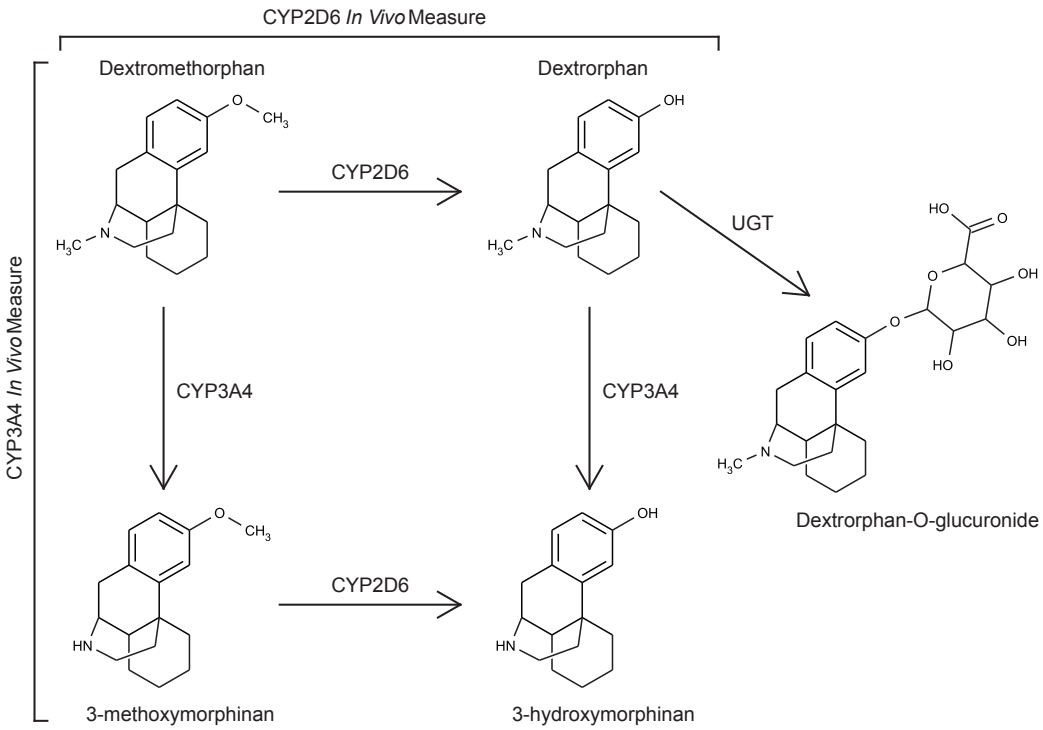

Figure 2.1. Metabolic scheme of dextromethorphan. The enzyme responsible for the formation of each metabolite as well as the metabolite/parent pair utilized as an *in vivo* activity measure for the specified P450 isoform is indicated. UGT indicates proposed UDP-glucuronysltransferase metabolism. This figure was previously published in Lutz and Isoherranen (2012b).

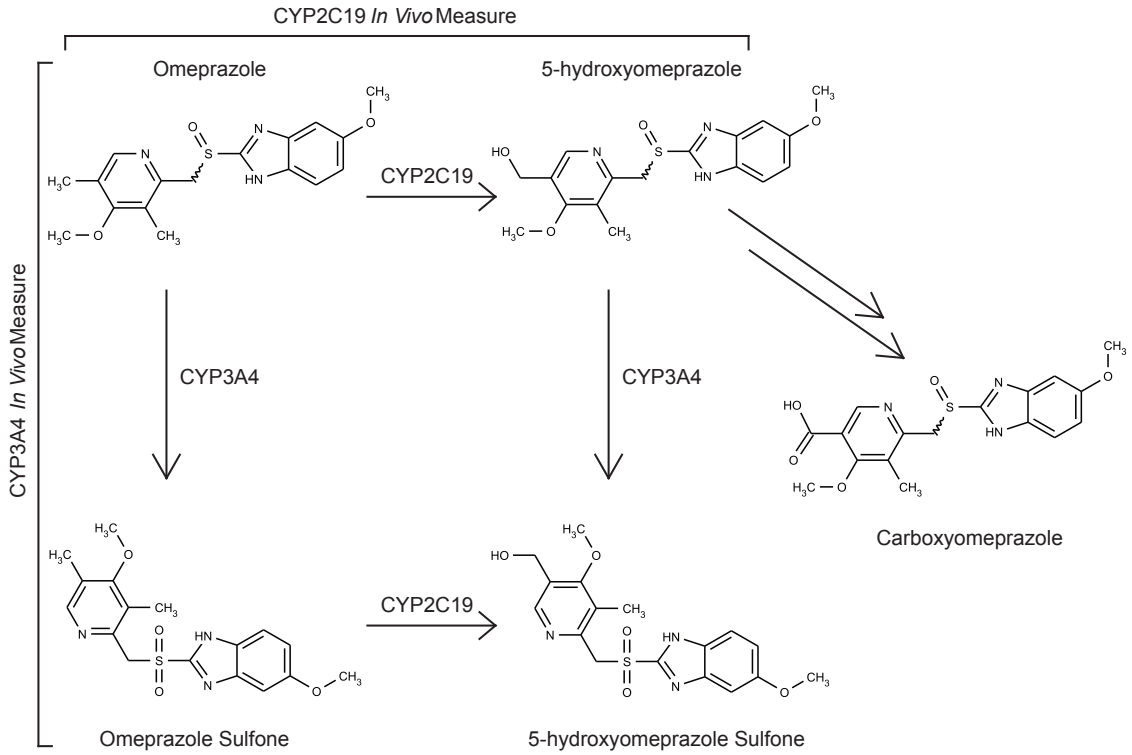

Figure 2.2. Metabolic scheme of omeprazole. The enzyme responsible for the formation of each metabolite as well as the metabolite/parent pair utilized as an *in vivo* activity measure for the specified P450 isoform is indicated. This figure was previously published in Lutz and Isoherranen (2012b).

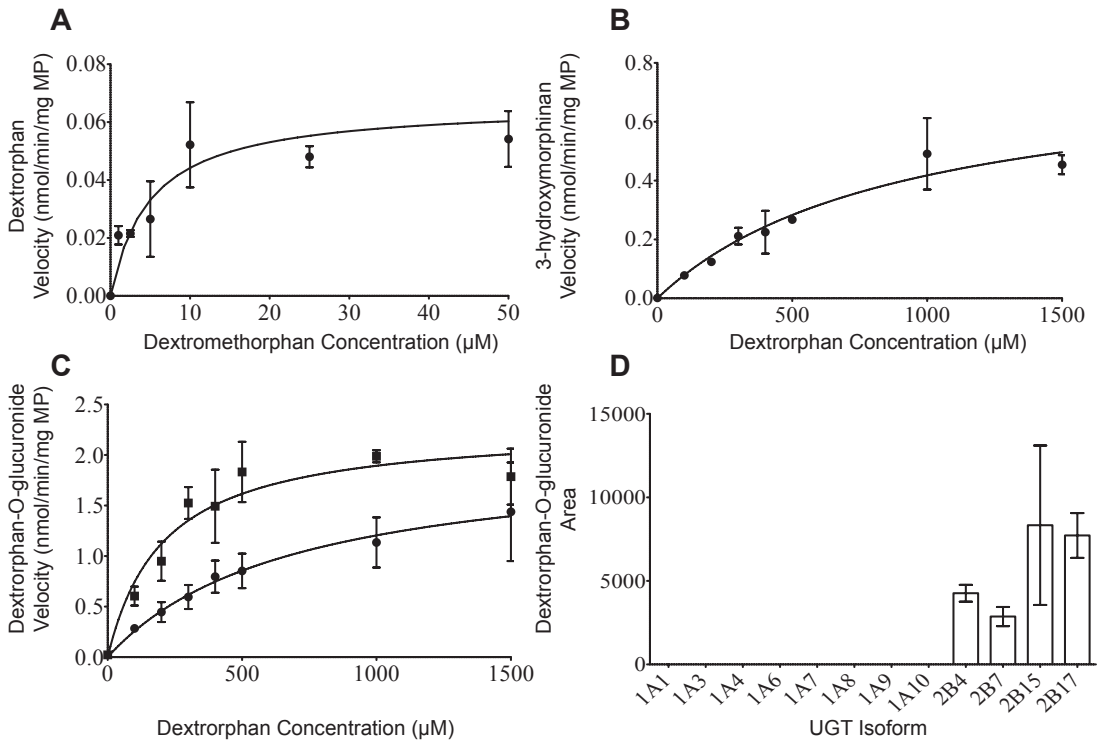

Figure 2.3. *In vitro* formation and metabolism of dextrorphan. The formation of dextrorphan from dextromethorphan (A), 3-hydroxymorphinan from dextrorphan (B) and dextrorphan-O-glucuronide from dextrorphan (C) in pooled HLMs are shown. Dextrorphan-O-glucuronide is shown both with (■) and without (●) the presence of 2% BSA. Panel D displays the formation of dextrorphan-O-glucuronide after incubation of dextrorphan with 12 rUGT isoforms. Error bars for Panels A – C represent the standard deviation of three measurements. Error bars for Panel D represent the range of 2 measurements. This figure was previously published in Lutz and Isoherranen (2012b).

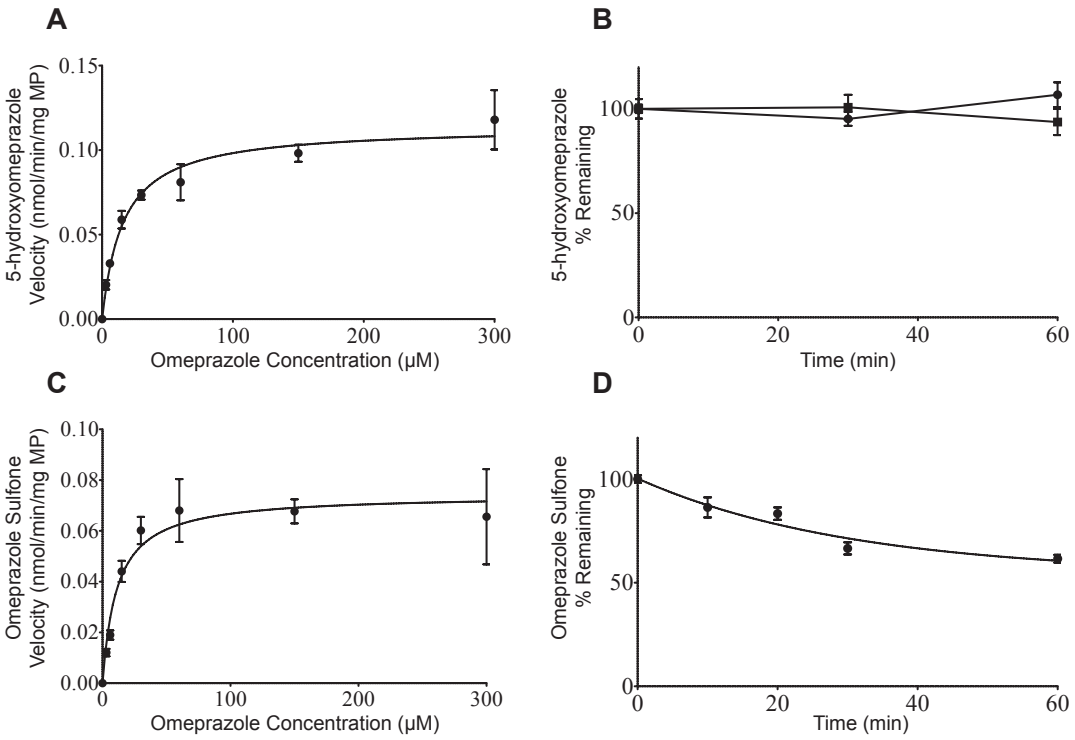

Figure 2.4. *In vitro* formation and depletion of 5-hydroxyomeprazole and omeprazole sulfone in pooled HLMs. The formation (A) and depletion (B) of 5-hydroxyomeprazole from omeprazole and the formation (C) and depletion (D) of omeprazole sulfone from omeprazole are shown. In Panel B, the % Remaining of 5-hydroxyomeprazole over time is provided as both with (■) and without NADPH (●). Error bars represent the standard deviation of three measurements. This figure was previously published in Lutz and Isoherranen (2012b).

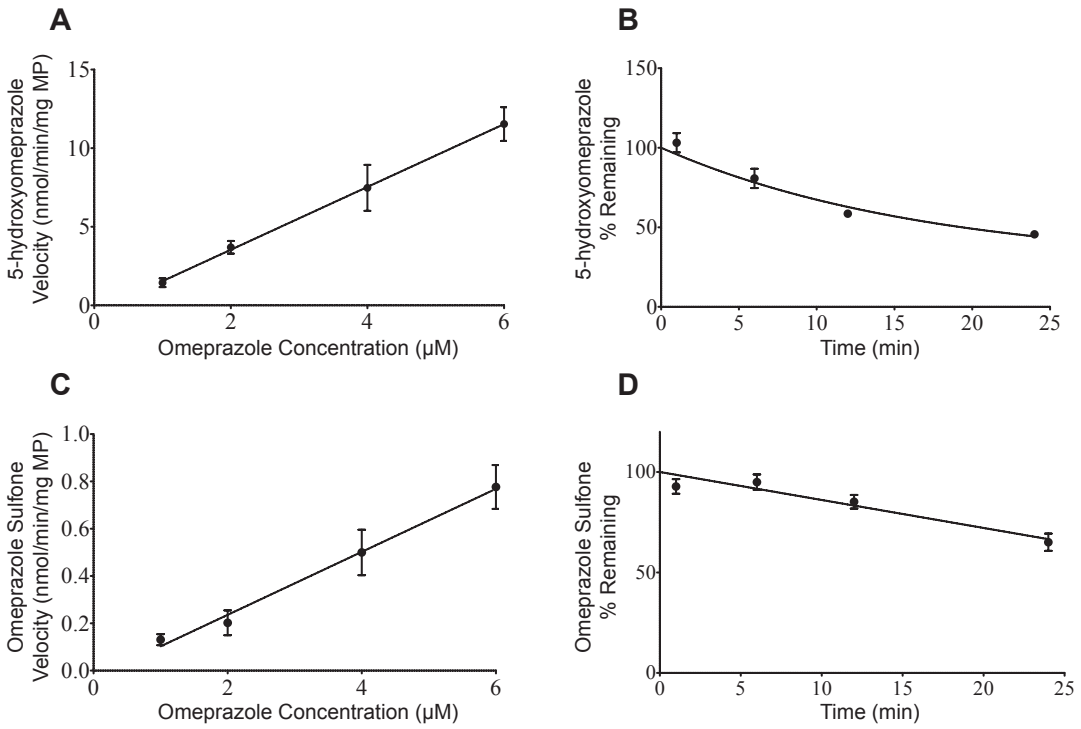

Figure 2.5. *In vitro* formation and depletion of 5-hydroxyomeprazole and omeprazole sulfone in hepatocytes. Panels A and C display the formation of 5-hydroxyomeprazole and omeprazole sulfone from omeprazole, respectively. Panels B and D display the % Remaining of 5-hydroxyomeprazole and omeprazole sulfone, respectively. Error bars represent the standard deviation of four measurements. This figure was previously published in Lutz and Isoherranen (2012b).

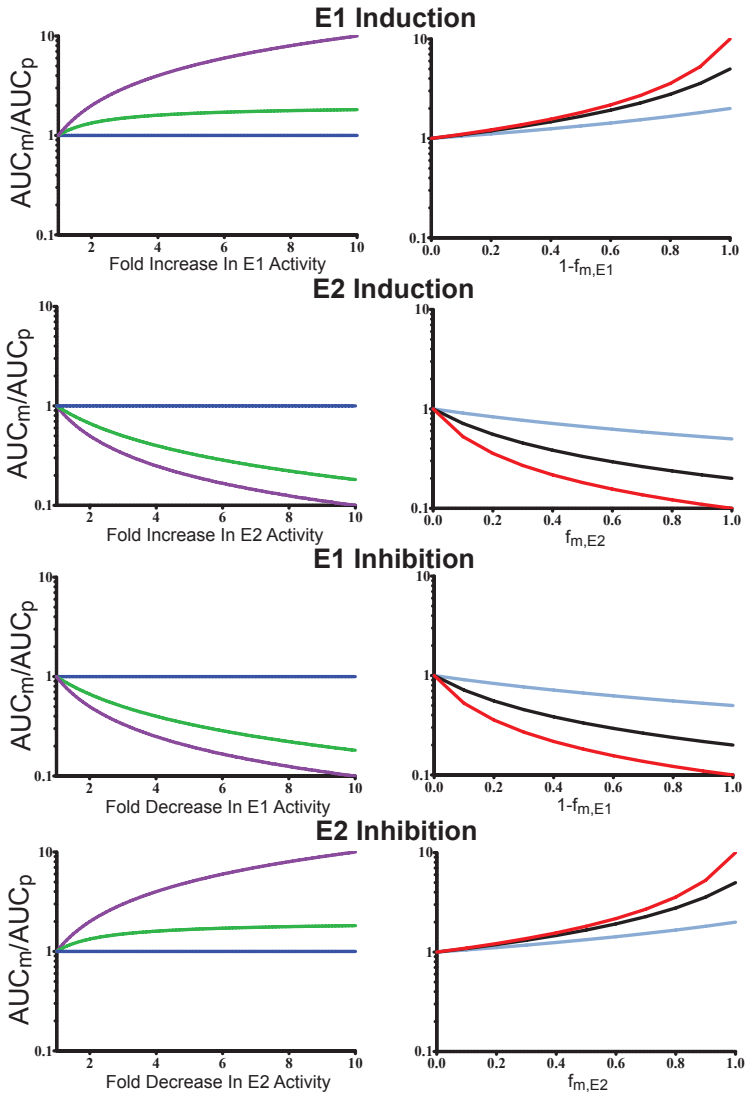

Figure 2.6. *In vivo* effects of secondary metabolism inhibition or induction on *in vivo* AUC_m/AUC_p activity measures. The effects on AUC_m/AUC_p for a generic metabolite/parent pair are displayed under the conditions of E1 induction (Panels A and B), E2 induction (Panels C and D), E1 inhibition (Panels E and F) and E2 inhibition (Panels G and H). The independent variable for Panels A, C, E and F is the fold increase (Panels A and C) or decrease (Panels E and F) in enzyme activity. The blue, green and orange lines indicates the simulated scenario of when the affected enzyme is the only enzyme that clears the metabolite (f_m = 1), both E1 and E2 have equal responsibility for clearing the metabolite (f_m = 0.5) or the unaffected enzyme is the only enzyme that clears the metabolite (f_m = 0), respectively. The independent variable in Panels B, D, F and G is unity minus the fraction metabolized by E1 ($1-f_{m,E1}$). The red, purple and brown lines indicate a 2-fold, 5-fold and 10-fold increase (B and D) or decrease (F and H) in enzyme activity. This figure was previously published in Lutz and Isoherranen (2012b).

Table 2.1. The Michaelis-Menten constants for the formation of dextrorphan from dextromethorphan as well as 3-hydroxymorphinan and dextrorphan-O-glucuronide from dextrorphan in HLMs. The pooled HLM and plasma unbound fraction values are also listed. The formation of dextrorphan-O-glucuronide was determined both in the presence and absence of 2% bovine serum albumin (BSA).

	Dextromethorphan → Dextrorphan	Dextrorphan → 3-hydroxymorphinan	Dextrorphan → Dextrorphan-O-glucuronide (Without 2% BSA)	Dextrorphan → Dextrorphan-O-glucuronide (With 2% BSA)
V_{max} (nmol/min/mg MP)	0.066 ± 0.001	0.80 ± 0.24	2.0 ± 0.2	2.3 ± 0.4
K_m (μM)	5.0 ± 3.1	910 ± 500	690 ± 140	210 ± 110
Substrate $f_{u,HLM}$	0.93 ± 0.10	1.0 ± 0.04	1.0 ± 0.04	0.88 ± 0.05
Cl_i (μl/min/mg MP)	13	0.88	2.9	11
$Cl_{i,u}$ (μl/min/mg MP)	14	0.95	2.9	12
Substrate Plasma f_u	0.72 ± 0.07	0.55 ± 0.03	0.55 ± 0.03	0.55 ± 0.03

Table 2.2. The observed and predicted AUC_m/AUC_p values for the dextrorphan/dextromethorphan, 5-hydroxyomeprazole/omeprazole and omeprazole sulfone/omeprazole metabolite/parent pairs. Included is the *in vitro* system used to determine the values and the AUC_m/AUC_p Predicted/Observed ratio. The AUC_m/AUC_p for each pair was predicted using both Equations 2.6 and 2.7.

Parent	Metabolite	Observed AUC_m/AUC_p (Range)	*In vitro* System	Equation Used	Predicted AUC_m/AUC_p	Pred/Obs (Range)
Dextromethorphan	**Dextrorphan**	0.61 (0.52-0.70)	Pooled HLMs	2.6	2.3	3.8 (3.3-4.4)
				2.7	1.3	2.1 (1.9-2.5)
Omeprazole	**5-hydroxy omeprazole**	0.48 (0.24-0.74)	Hepatocytes	2.6	0.37	0.78 (0.50-1.5)
				2.7	0.36	0.75 (0.49-1.5)
Omeprazole	**Omeprazole Sulfone**	0.85 (0.79-0.94))	Pooled HLMs	2.6	2.8	3.3 (3.0-3.5)
				2.7	2.6	3.1 (2.8-3.3)
			Hepatocytes	2.6	0.90	1.1 (0.96-1.2)
				2.7	0.90	1.1 (0.96-1.2)

Table 2.3. The Michaelis-Menten constants for the formation of 5-hydroxyomeprazole and omeprazole sulfone from omeparazole in HLMs. The depletion clearance of 5-hydroxyomeprazole and omeprazole sulfone in HLMs and the formation and depletion clearances of 5-hydroxyomeprazole and omeprazole sulfone in hepatocytes and HLMs are also listed. The pooled HLM and plasma unbound fraction values for each substrate are listed as well. ND indicates that the value was not determined.

	Omeprazole → 5-hydroxyomeprazole	Omeprazole → Omeprazole sulfone	5-hydroxyomeprazole Depletion	Omeprazole sulfone Depletion
V_{max} (nmol/min/mg MP)	0.11 ± 0.01	0.074 ± 0.007	ND	ND
K_m (μM)	16 ± 5	11 ± 5	ND	ND
Substrate $f_{u,HLM}$	0.86 ± 0.04	0.86 ± 0.04	0.84 ± 0.04	0.92 ± 0.03
Cl_i (μl/min/mg MP)	7.1	6.6	No Depletion	32 ± 4
$Cl_{i,u}$ (μl/min/mg MP)	8.2	7.7	No Depletion	35
Hepatocyte $Cl_{i,u}$ (μl/hr/10^6 Cells)	55 ± 2	3.6 ± 0.5	100 ± 20	48 ± 6
Substrate Plasma f_u	0.061 ± 0.014	0.061 ± 0.014	0.092 ± 0.033	0.0048 ± 0.029

Chapter 3

Stereoselective inhibition of CYP2C19 and CYP3A4 by fluoxetine and its metabolite: implications for prediction of multiple time-dependent inhibitor systems

The work presented in this chapter was submitted for publication

to

Drug Metabolism and Disposition (submitted June, 2013)

3.1 Abstract

Recent guidance on drug-drug interaction (DDI) testing recommends evaluation of circulating metabolites. However, there is little consensus on how to quantitatively predict and/or assess the risk of *in vivo* DDIs by multiple time-dependent inhibitors (TDIs), including metabolites from *in vitro* data. Fluoxetine was chosen as the model drug to evaluate the role of TDI metabolites in DDI prediction because it is a TDI of both CYP3A4 and CYP2C19 with a circulating N-dealkylated inhibitory metabolite, norfluoxetine. In pooled HLMs, both enantiomers of fluoxetine and norfluoxetine were TDIs of CYP2C19, with (S)-norfluoxetine being the most potent (K_I = 7 μM and $k_{inact,app}$ = 0.059 min^{-1}). Only (S)-fluoxetine and (R)-norfluoxetine were TDIs of CYP3A4, with (R)-norfluoxetine being the most potent (K_I = 8 μM and $k_{inact,app}$ = 0.011 min^{-1}). Based on *in vitro*-to-*in vivo* predictions, (S)-norfluoxetine plays the most important role in *in vivo* CYP2C19 DDIs, whereas (R)-norfluoxetine is most important in CYP3A4 DDIs. Comparison of two multiple TDI prediction models demonstrated significant differences between them in *in vitro*-to-*in vitro* predictions but not in *in vitro*-to-*in vivo* predictions. Inclusion of all four inhibitors predicted an *in vivo* decrease in CYP2C19 (95%) and CYP3A4 (60 – 62%) activity. The results of this study suggest that adequate worst-case risk assessment for *in vivo* DDIs by multiple TDI systems can be achieved by incorporating time-dependent inhibition by both parent and metabolite via simple addition of *in vivo* λ/k_{deg} values, but quantitative DDI predictions will require more thorough understanding of TDI mechanisms.

3.2 Introduction

A multiple inhibitor system is any drug-drug interaction (DDI) where multiple inhibitors of the same enzyme coexist. Such systems can arise from co-administration of multiple independent inhibitors (Kharasch *et al.*, 2009; Schmitt *et al.*, 2009), administration of an inhibitor that has a circulating inhibitory metabolite (Reese *et al.*, 2008; Templeton *et al.*, 2010) or

administration of a racemic inhibitor that exhibits stereoselective inhibition and *in vivo* disposition (Liu *et al.*, 2005). Of the possible multiple inhibitor systems, inhibitors with inhibitory metabolites are well recognized. An analysis of 129 marketed *in vivo* P450 inhibitors showed that 80% of these inhibitors possess circulating metabolites (Isoherranen *et al.*, 2009), with a subset that have confirmed inhibitory metabolites (Yeung *et al.*, 2011). Of the same 129 inhibitors, 20% are chiral drugs administered as racemic mixtures. Hence, a total of 90% of *in vivo* P450 inhibitors are potential multiple inhibitor systems, highlighting the need for increased attention to development of risk assessment methods for multiple inhibitor systems.

Studies of *in vitro*-to-*in vivo* prediction of DDIs resulting from reversible P450 inhibition have demonstrated that incorporation of metabolites (Reese *et al.*, 2008; Templeton *et al.*, 2010) and stereoselective inhibition by both parent and metabolite enantiomers (Lutz and Isoherranen, 2012a) increases the accuracy of the predictions. Despite increased prediction accuracy, for most of the known reversible P450 inhibitors, incorporation of metabolite inhibition did not alter DDI risk assessment (Yeung *et al.*, 2011). The effect of metabolites in risk assessment of time-dependent inhibitors (TDIs) has not been systematically evaluated. However, it has been suggested that circulating metabolites are important in P450 time-dependent inhibition, and circulating metabolites should be characterized for time-dependent inhibition to improve *in vivo* DDI predictions and understanding (VandenBrink and Isoherranen, 2010). The FDA and EMA recommend that *in vivo* circulating metabolites be characterized for *in vitro* P450 inhibition, but little guidance exists on how to incorporate the contribution of TDI metabolites to prediction of DDIs. While models have been established for prediction of single inhibitors with multiple interaction mechanisms (Fahmi *et al.*, 2009), there is limited data on predictions for multiple inhibitors with multiple inhibition mechanisms.

By definition, metabolism is required for time-dependent inhibition by mechanism-based inhibitors. TDIs were estimated to constitute approximately 25% of *in vivo* P450 inhibitors in

2009 (Isoherranen *et al.*, 2009). Since then, several new P450 TDIs have been approved, including boceprevir (Victrelis© Prescribing Information, 2011), telaprevir (Incivek© Prescribing Information, 2011), crizotinib (Mao *et al.*, 2013), erlotinib and everolimus (Kenny *et al.*, 2012), demonstrating the continued clinical significance of TDIs. Almost half of *in vitro* TDIs are alkylamine drugs (VandenBrink and Isoherranen, 2010) that undergo initial N-dealkylation and subsequent metabolism to result in P450 time-dependent inhibition via a quasi-irreversible heme coordinated metabolic-intermediate complex (MIC) (Kalgutkar *et al.*, 2007). All alkylamine TDIs possess an *in vivo* circulating N-dealkylated metabolite that can also inactivate P450s (VandenBrink and Isoherranen, 2010), but only a few studies have examined the role of these metabolites in *in vivo* DDIs. Two models have been evaluated to improve upon the under-prediction of *in vivo* CYP3A4 inhibition using diltiazem and verapamil and their N-dealkylated metabolites as models. In these models the TDI kinetics of the parent and metabolite were either summed to predict total time-dependent inhibition (Wang *et al.*, 2004; Rowland Yeo *et al.*, 2010) or a mutual *in vivo* inhibitor-inhibitor interaction component was incorporated to predict *in vivo* interaction (Zhang *et al.*, 2009b). Both models demonstrated improved prediction accuracy with the inclusion of metabolite time-dependent inhibition when compared to parent alone suggesting that incorporation of multiple inhibitors into TDI predictions and risk assessment is necessary.

The aim of this study was to establish how multiple inhibitor systems, that include time-dependent inhibition, can be incorporated into DDI risk assessment. The secondary alkylamine fluoxetine was used as a model because it is a complex multiple P450 inhibitor. Fluoxetine provides both a model of a metabolite-parent pair and enantiomer mixture that incorporates combinations of time-dependent and reversible inhibition with multiple P450s. Fluoxetine, and its circulating metabolite, norfluoxetine, are present as mixtures of stereoisomers *in vivo* (Jannuzzi *et al.*, 2002). *In vitro*, fluoxetine is a TDI of CYP2C19 and CYP3A4 and norfluoxetine

causes an IC_{50} shift with CYP2C19, suggesting that it is a TDI of CYP2C19 (Mayhew *et al.*, 2000; Stresser *et al.*, 2009). Norfluoxetine appears to be a reversible inhibitor of CYP3A4 (von Moltke *et al.*, 1996). In this study, fluoxetine and norfluoxetine were stereoselectively characterized as CYP2C19 and CYP3A4 TDIs. The contribution of norfluoxetine to the predicted DDI was determined for each P450 and the prediction of multiple TDIs between CYP2C19 and CYP3A4 was compared.

3.3 Materials and Methods

3.3.1 Chemical and reagents

(R)-Fluoxetine, (S)-fluoxetine, *rac*-fluoxetine, *rac*-norfluoxetine, MS grade acetonitrile and MS grade water were purchased from Sigma-Aldrich (St. Louis, MO, USA). Midazolam, 1-hydroxymidazolam and 1-hydroxymidazolam-d_4 were purchased from Cerilliant (Round Rock, TX, USA). 4-Hydroxymephenytoin-d_3 was purchased from Toronto Research Chemicals (Toronto, ON, CA). (S)-Mephenytoin and 4-hydroxymephenytoin were synthesized in Dr. William Trager's laboratory (University of Washington, Seattle, WA). The (R)- and (S)-enantiomers of norfluoxetine were synthesized as previously described (Hanson *et al.*, 2010).

3.3.2 Determination of reversible and time-dependent inhibition constants

For all metabolic incubations, 6 different human liver microsome (HLM) donors were pooled. All donors were confirmed to be CYP2D6*1/*1, CYP2D6*1/*2 or CYP2D6*2/*2 genotype, CYP2C19*1/*1 and CYP3A5*3/*3 genotypes to limit confounding effects of genetic polymorphisms and CYP3A substrate overlap in inhibition characterization. All pooled HLM experiments were performed in triplicate at either 0.1 mg/mL (reversible inhibition) or 1.0 mg/mL (time-dependent inhibition) microsomal protein concentration in 100 mM potassium phosphate

(KPi) buffer at pH = 7.4. All reversible and time-dependent inhibition was determined using 7 and 11 inhibitor concentrations (2-fold serial dilutions), respectively. Maximum inhibitor concentrations were 100 μM, except for when determining time-dependent CYP2C19 inhibition of (R)- and (S)-fluoxetine (50 μM and 250 μM, respectively) and reversible CYP3A4 inhibition of (R)- and (S)-fluoxetine (1000 μM for both). For reversible inhibition, the substrate concentrations were approximately 5-fold below K_m: 6 μM (S)-mephenytoin (CYP2C19) and 1 μM midazolam (CYP3A4). For time-dependent inhibition, the substrate concentrations were 5-fold above K_m: 150 μM (S)-mephenytoin and 25 μM midazolam. After a 5 min preincubation at 37 °C, all metabolic incubations were initiated with 1 mM final concentration of nicotinamide adenine dinucleotide phosphate (NADPH) and allowed to proceed at 37 °C. For time dependent inhibition determination, no substrate was initially present but aliquots were diluted 10-fold into wells containing 1 mM NADPH and substrate after 0.25, 10, 20 and 30 minutes. In the fluoxetine incubation experiments, negligible accumulation of norfluoxetine product (< 6% of fluoxetine initial concentration) under the incubation conditions was confirmed. All incubations with substrate proceeded for 3 min (midazolam), and 15 min ((S)-mephenytoin) before quenching with an equal volume acetonitrile containing 100 nM internal standard. The inhibitor concentration at 50% maximum inhibition (IC_{50}) was determined by the equation:

$$v_I = v_0\left(1 - \frac{I}{IC_{50} + I}\right) \qquad (3.1)$$

where v_I and v_0 are the velocity of product formation at a given inhibitor concentration (I) or without the presence of inhibitor, respectively. The time-dependent inhibition affinity (K_I) and apparent maximum time-dependent inhibition rate ($k_{inact,app}$) were determined by the equation:

$$v_I = v_0 e^{-\lambda t} \qquad (3.2)$$

where λ is:

$$\lambda = \frac{k_{inact,app} I}{K_I + I} \qquad (3.3)$$

All velocity data was transformed to percent of maximum velocity (no inhibitor control). All inhibition constants are presented as mean and standard error. All *in vitro* constants were determined via nonlinear regression using GraphPad Prism v.5 (La Jolla, CA, USA). Two-sided t-tests were used to evaluate the significance of change in time-dependent inhibition rate between 100 μM inhibitor and control during initial time-dependent inhibition screening. A p-value of < 0.05 was considered significant.

3.3.3 Determination of fluoxetine protein binding

Using the same pooled HLMs as above (at 1 mg/mL and 0.1 mg/mL microsomal protein in KPi buffer) or blank human plasma, (R)-fluoxetine, (S)-fluoxetine, (R)-norfluoxetine or (S)-norfluoxetine were added to triplicate samples to make a 1 μM final concentration. The samples were split to two ultra-centrifuge tubes at equal volumes and either centrifuged at 440,000 x g for 90 min at 37 °C or incubated for 90 min at 37 °C as previously described (Templeton *et al.*, 2010). An aliquot was removed from both tubes and an equal volume of acetonitrile was added, the samples were centrifuged at 3000 x g for 15 min and the supernatant was used for analysis. The $f_{u,HLM}$ or $f_{u,plasma}$ was determined as the quotient of determined inhibitor concentration with and without centrifugation.

3.3.4 Quantitation of analytes

Concentrations of 1-hydroxymidazolam, (S)-4-hydroxymephenytoin, (R)-fluoxetine, (S)-fluoxetine, (R)-norfluoxetine and (S)-norfluoxetine were analyzed using a Shimadzu Prominence UHPLC (Tokyo, Japan) coupled to an AB Sciex API 3200 MS/MS (Framingham, MA, USA). All analytes were separated using an Agilent Zorbax Eclipse XDB 2.1 x 50 mm, 5 μm column

(Santa Clara, CA, USA) with a linear gradient elution from 95% water with 0.1% formic acid:5% acetonitrile to 50% acetonitrile over 3 minutes, 95% acetonitrile for 2 minutes, then allowed to re-equilibrate to initial conditions for 2 minutes. All analytes were detected using positive electrospray ionization with a source temperature of 500 °C, Ionization voltage of 5500 V and curtain gas, collisionally activated dissociation gas, source gas 1 and source gas 2 of 10, 5, 80 and 60 respectively. The multiple reaction monitoring transitions (m/z) used were 342→324 (1-hydroxymidazolam), 235→150 (4-hydroxymephenytoin), 310→44 ((R)- or (S)-fluoxetine), 296→134 ((R)- or (S)-norfluoxetine). The injection volume for all assays was 10 µL. The lower limit of quantitation was less than 5 nM for all analytes. Inter-day percent coefficient of variation for all analytes at 5 nM was less than 15%. Analyst software version 1.4 (AB Sciex, Foster City, CA) was used for data analysis. All samples were protein precipitated with an equal volume acetonitrile, centrifuged at 3000 x g for 15 min, and the supernatant was used for analysis. The organic solvent contained either 100 nM of 1-hydroxymidazolam-d_4 or 4-hydroxymephenytoin-d_3 internal standards.

3.3.5 Simulations and predictions using *in vitro* data

The apparent time-dependent inhibition rate (λ_{app}) versus inhibitor concentration curve for *rac*-fluoxetine, *rac*-norfluoxetine, 1:1 (R)-fluoxetine:(R)-norfluoxetine and 1:1 (S)-fluoxetine:(S)-norfluoxetine were simulated using the determined component enantiomer time-dependent inhibition rate constants and the equation (additive model):

$$\lambda_{app} = \frac{k_{inact,app,1} I_1}{K_{I,1} + I_1} + \frac{k_{inact,app,2} I_2}{K_{I,2} + I_2} \qquad (3.4)$$

Additionally, the same data were simulated using an equation that incorporates competitive reversible inhibitor-inhibitor interaction (inhibitor-inhibitor interaction model):

$$\lambda_{app} = \frac{k_{inact,app,1} I_1}{K_{I,1}\left(1 + \frac{I_2}{K_{i,2}}\right) + I_1} + \frac{k_{inact,app,2} I_2}{K_{I,2}\left(1 + \frac{I_1}{K_{i,1}}\right) + I_2} \qquad (3.5)$$

The unbound FDA R-value for assessing *in vivo* CYP2C19 and CYP3A4 DDI risk due to reversible (Equation 3.6) or time-dependent inhibition (Equation 3.7) was predicted:

$$R = \frac{I_{max}}{K_i} \qquad (3.6)$$

$$R = \frac{\lambda}{k_{deg}} = \frac{k_{inact,app} I_{max}}{k_{deg}(K_I + I_{max})} \qquad (3.7)$$

where I_{max}, K_i, K_I and $k_{inact,app}$ are the unbound *in vivo* maximum plasma concentration of the inhibitor, *in vitro* unbound reversible inhibition affinity constant, *in vitro* unbound time-dependent inhibition affinity constant and *in vitro* time-dependent inhibition maximum time-dependent inhibition rate constant, respectively. For Equation 3.6 the unbound IC_{50} values were used instead of K_i because substrate concentrations were less than K_m for the inhibition experiments (Lutz and Isoherranen, 2012a). The *in vivo* P450 degradation rate constants (k_{deg}) for CYP2C19 and CYP3A4 were 4.5 x 10^{-4} min^{-1} and 4.8 x 10^{-4} min^{-1}, respectively (Ghanbari *et al.*, 2006; Obach *et al.*, 2007). The change in the concentration of active enzyme *in vivo* in the presence of multiple TDIs was predicted using two models, additive and inhibitor-inhibitor interaction models (Zhang *et al.*, 2009b; Rowland Yeo *et al.*, 2010):

$$\frac{Cl_i}{Cl_i'} = 1 + \sum_{a=1}^{n} \frac{k_{inact,app,a} I_{max,a}}{k_{deg}\left(K_{I,a} + I_{max,a}\right)} \qquad (3.8)$$

$$\frac{Cl_i}{Cl_i'} = 1 + \sum_{a=1}^{n} \frac{k_{inact,app,a} I_{max,a}}{k_{deg}\left(K_{I,a}\left(1 + \sum_{b\neq a}^{n-1} \frac{I_{max,b}}{K_{i,b}}\right) + I_{max,a}\right)} \qquad (3.9)$$

The Cl_i/Cl_i' ratio is the ratio of the active P450 concentrations in the presence and absence of the inhibitor, respectively. The I_{max} values used for (R)-fluoxetine, (S)-fluoxetine, (R)-norfluoxetine and (S)-norfluoxetine after 8 days of daily oral 60 mg fluoxetine were 130 nM, 360 nM, 130 nM and 280 nM, respectively (Bergstrom *et al.*, 1992; Jannuzzi *et al.*, 2002). To obtain unbound affinity constants and concentrations, all inhibitor I_{max} values were multiplied by the fraction unbound in plasma ($f_{u,p}$) and all IC_{50} and K_I values were multiplied by the fraction unbound in pooled HLMs ($f_{u,HLM}$) determined at 0.1 mg/mL and 1.0 mg/mL microsomal protein, respectively.

To determine the over-prediction that would occur when predicting the *in vivo* Cl_i/Cl_i' using the additive model compared to the inhibitor-inhibitor interaction model, the fold prediction difference in Cl_i/Cl_i' was simulated using the quotient of Equations 3.8 and 3.9 over a range of possible I_{max}/IC_{50} values from 0.01 to 100 for a two-inhibitor system. The two-inhibitor systems simulated were (R)-fluoxetine with (R)-norfluoxetine and (S)-fluoxetine with (S)-norfluoxetine. The *in vitro* reversible and time-dependent inhibition constants used for the simulation were as determined for each enantiomer. Additionally, one generic parent-metabolite inhibitor pair was simulated, with IC_{50} and K_I values for both parent and metabolite set at 10 μM and the $k_{inact,app}$ values for parent and metabolite set at 0.1 min^{-1} and 0.01 min^{-1}, respectively.

3.4 Results

3.4.1 Stereoselective time-dependent inhibition of CYP2C19 and CYP3A4 by fluoxetine and norfluoxetine

To determine which of the fluoxetine and norfluoxetine enantiomers are *in vitro* TDIs of CYP2C19 and CYP3A4, time-dependent decrease in enzyme activity was first determined with 100 μM of each inhibitor using pooled HLMs (data not shown). Both fluoxetine and norfluoxetine enantiomers decreased CYP2C19 activity as a function of time ($p < 0.05$). In contrast, only (S)-fluoxetine and (R)-norfluoxetine decreased CYP3A4 activity with time ($p < 0.05$). Reversible and time-dependent *in vitro* inhibition parameters were then determined in pooled HLMs based on the data on which of the compounds demonstrated time-dependent inhibition of CYP3A4 or CYP2C19 in the initial screen.

In pooled HLMs, all fluoxetine and norfluoxetine enantiomers were characterized for time-dependent CYP2C19 inhibition. (R)-Fluoxetine (K_I = 2 ± 1 μM and $k_{inact,app}$ = 0.017 ± 0.001 min^{-1}) and (S)-norfluoxetine (K_I = 7 ± 1 μM and $k_{inact,app}$ = 0.059 ± 0.002 min^{-1}) were the most efficient TDIs against CYP2C19, with $k_{inact,app}/K_I$ values of 9.4 L/min/μmol and 8.4 L/min/μmol, respectively (Figure 3.1 and Table 3.1). The K_I value for (R)-fluoxetine was 75% lower than any of the other three compounds studied. Reversible IC_{50} values against CYP2C19 were also determined in pooled HLMs (Table 3.1 and Figure 3.2). (R)-Fluoxetine was also the most potent reversible inhibitor (IC_{50} = 2 ± 1 μM) of CYP2C19. The IC_{50} values were in agreement with the K_I values (Table 3.1).

In vitro time-dependent inhibition constants were determined for (S)-fluoxetine and (R)-norfluoxetine against CYP3A4 in pooled HLMs based on the initial time-dependent inhibition screen. (R)-norfluoxetine (K_I = 8 ± 3 μM and $k_{inact,app}$ = 0.011 ± 0.001 min^{-1}) was a more efficient TDI ($k_{inact,app}/K_I$ value of 1.4 L/min/μmol) of CYP3A4 than (S)-fluoxetine (K_I = 21 ± 19 μM, $k_{inact,app}$ = 0.009 ± 0.003 min^{-1} and $k_{inact,app}/K_I$ of 0.5 L/min/μmol). Overall, the fluoxetine and norfluoxetine enantiomers studied were less efficient at inactivating CYP3A4 than CYP2C19. Interestingly, the most efficient TDIs of CYP2C19 in HLMs were (R)-fluoxetine and (S)-norfluoxetine, whereas these two compounds were the ones that did not inactivate CYP3A4.

The reversible IC_{50} values for each enantiomer against CYP3A4 in pooled HLMs were also determined (Table 3.1, Figures 3.3 and 3.4). (R)- and (S)-norfluoxetine were determined to be the most potent *in vitro* reversible inhibitors, with IC_{50} values of 5 ± 1 μM and 11 ± 1 μM, respectively. The *in vitro* CYP3A4 IC_{50} values for (S)-fluoxetine and (R)-norfluoxetine were in agreement with their determined K_I values (Table 3.1).

3.4.2 Risk assessment of CYP3A4 and CYP2C19 inhibition by fluoxetine and norfluoxetine enantiomers

Fraction unbound (f_u) values for both enantiomers of fluoxetine and norfluoxetine were determined in plasma and HLMs (Table 3.2). Protein binding between (R)-fluoxetine, (S)-fluoxetine, (R)-norfluoxetine and (S)-norfluoxetine was similar in HLMs ($f_{u,HLM}$ 0.42-0.52 at 1.0 mg/mL and $f_{u,HLM}$ 0.07-0.10 at 0.1 mg/mL microsomal protein) and in plasma ($f_{u,p}$ from 0.13 to 0.22). Using the determined *in vitro* parameters, the risk of *in vivo* inhibition (FDA unbound R-value) of CYP2C19 and CYP3A4 was predicted using I_{max}/IC_{50} (Equation 3.5) for reversible inhibition and λ/k_{deg} (Equation 3.6) for time-dependent inhibition (Table 3.3). The I_{max} value used was the maximum unbound plasma concentration ($f_{u,p}*I_{max}$) for each of the four compounds after 8 daily oral doses of 60 mg *rac*-fluoxetine (Bergstrom *et al.*, 1992; Jannuzzi *et al.*, 2002). For both CYP2C19 and CYP3A4, reversible inhibition was predicted to be unlikely *in vivo* (I_{max}/IC_{50} < 0.1), with the maximum predicted I_{max}/IC_{50} value of 0.03 for (R)-fluoxetine against CYP2C19 (Table 3.3). Both fluoxetine and norfluoxetine enantiomers are predicted to result in *in vivo* time-dependent inhibition of CYP2C19 (λ/k_{deg} > 0.1), with (S)-norfluoxetine predicted to result in the greatest magnitude of *in vivo* inhibition between the four inhibitors (λ/k_{deg} = 9.4) (Table 3.3). Overall, (S)-norfluoxetine and (R)-fluoxetine are predicted to play the most important roles in *in vivo* inhibition of CYP2C19. Based on λ/k_{deg} values, CYP3A4 is predicted to be inhibited *in vivo* (λ/k_{deg} > 0.1) by both (S)-fluoxetine and (R)-norfluoxetine, with (R)-norfluoxetine predicted to

cause a greater *in vivo* DDI than (S)-fluoxetine (λ/k_{deg} values of 1.1 and 0.5, respectively). The overall role of norfluoxetine enantiomers (approximately 60% with CYP2C19 and 70% with CYP3A4 predicted contribution) indicates a significant contribution of the metabolites to *in vivo* P450 inhibition.

3.4.3 Evaluation of inhibitor-inhibitor interactions in *in vitro*-to-*in vitro* predictions of multiple CYP2C19 TDI systems

Mixtures of inhibitor enantiomers represent multiple independent inhibitor systems. Since both norfluoxetine and fluoxetine enantiomers are predicted to play a significant role in *in vivo* CYP2C19 inhibition, time-dependent inhibition by enantiomer mixtures of fluoxetine and norfluoxetine and mixture of fluoxetine with norfluoxetine were determine to evaluate different models for the prediction of multiple independent TDI systems. The *in vitro* time-dependent inhibition of CYP2C19 after *rac*-fluoxetine or *rac*-norfluoxetine incubation was predicted using the time-dependent inhibition data by individual enantiomers and the accuracy of these predictions was tested. In pooled HLMs, time-dependent inhibition of CYP2C19 was similar with *rac*-fluoxetine and *rac*-norfluoxetine (Figure 3.5). Using the individual enantiomer K_I and $k_{inact,app}$ values, CYP2C19 time-dependent inhibition versus total inhibitor ((R)- plus (S)-enantiomer) concentration curves were simulated using the additive (Equation 3.4) and inhibitor-inhibitor interaction (Equation 3.5) models. Greater time-dependent inhibition was predicted with the additive model (red curve) than was observed for both *rac*-fluoxetine and *rac*-norfluoxetine (Figure 3.5). The inhibitor-inhibitor interaction model under-predicted (green curve) *rac*-fluoxetine time-dependent inhibition but predicted the time-dependent inhibition by *rac*-norfluoxetine well.

To evaluate whether time-dependent inhibition by parent plus *in vivo* formed metabolite can be rationalized using *in vitro* data, the *in vitro* time-dependent inhibition of CYP2C19 by a

1:1 mixture of fluoxetine:norfluoxetine individual enantiomers was predicted based on the parameters determined for each compound as independent inhibitors, and the accuracy of each prediction was evaluated. Although it is unlikely that in *in vitro* incubations, norfluoxetine will accumulate to a 1:1 ratio with fluoxetine under normal experimental conditions, this ratio was chosen to mimic *in vivo* plasma ratios (Jannuzzi *et al.*, 2002). Both the additive and inhibitor-inhibitor interaction models over-predicted time-dependent inhibition after co-incubating 1:1 (R)-fluoxetine:(R)-norfluoxetine or 1:1 (S)-fluoxetine:(S)-norfluoxetine (Figure 3.6). The inhibitor-inhibitor interaction model was the closest to capturing the λ versus total inhibitor concentration (fluoxetine plus norfluoxetine) profiles in both experiments. Overall, *in vitro*-to-*in vitro* prediction results suggest that significant inhibitor-inhibitor interaction occurs between multiple co-incubated TDIs *in vitro*, but this model does not fully capture the complexity of the examined multiple TDI systems.

3.4.4 Evaluation of the additive versus inhibitor-inhibitor interaction model in risk assessment of multiple TDI systems

Because inhibitor-inhibitor interaction can play a significant role in *in vitro* multiple TDI systems, it was examined whether this phenomenon is likely to play a significant role in predicting *in vivo* multiple TDI DDIs. Both the additive (Equation 3.8) and inhibitor-inhibitor interaction (Equation 3.9) models were used to predict *in vivo* inhibition risk after *rac*-fluoxetine administration. The models were used to predict *in vivo* inhibition risk under different combinations of fluoxetine and norfluoxetine enantiomers and the *in vivo* relevant combination of all four inhibitors (Table 3.4). For both CYP2C19 and CYP3A4, the predicted inhibition was not different between the additive and the inhibitor-inhibitor interaction models. This similarity can be explained by the fact that *in vivo* unbound plasma I_{max} concentrations are at least 30-fold below the *in vitro* determined unbound IC_{50} values ($I_{max}/IC_{50} \leq 0.03$) (Table 3.3). Summation of

effects of all four inhibitors yields a λ/k_{deg} of 20 and 2.5 – 2.6 for CYP2C19 and CYP3A4, respectively (Table 3.4). Since the use of the additive or inhibitor-inhibitor interaction models had little consequence in risk assessment of inhibition by fluoxetine, the overall differences in these two models were further explored via simulation of different concentrations of fluoxetine and norfluoxetine (Figure 3.7). The aim was to determine what inhibitor conditions would differentiate the two models *in vivo* and indicate which model is more prudent to use for risk assessment of multiple TDI systems. In both multiple TDI systems, the fold prediction difference increased as either inhibitor in the system increased in I_{max}/IC_{50}. This discrepancy between the additive and inhibitor-inhibitor interaction models was more pronounced with the combination of (R)-fluoxetine with (R)-norfluoxetine than with the combination of (S)-fluoxetine and (S)-norfluoxetine (maximum fold prediction difference under the simulated conditions of 3.2-fold versus 2.6-fold). Sensitivity analysis revealed that this difference between systems is not due to the overall magnitude of predicted interaction, but is directly proportional to the differences in magnitude of $k_{inact,app}$ between parent and metabolite: the quotient of (R)-norfluoxetine and (R)-fluoxetine or (S)-norfluoxetine and (S)-fluoxetine $k_{inact,app}$ values is 2.9 and 1.1, respectively. To demonstrate this relationship, a generic metabolite and parent inhibitor pair was simulated where the parent $k_{inact,app}$ was 10-fold larger than the metabolite $k_{inact,app}$ (Figure 3.7, Panel C). In this generic example, prediction differences up to 6.8-fold between the additive and inhibitor-inhibitor interaction models were calculated, indicating the possibility of significant differences in *in vivo* risk assessment between the two models when $I_{max} > IC_{50}$ for both inhibitors and the inhibitor $k_{inact,app}$ values are very different. This difference in the prediction accuracy between the models illustrates the importance in determining TDI parameters for both the metabolites and the parent drug as independent inhibitors to refine the *in vitro*-to-*in vivo* prediction models.

3.5 Discussion

Prediction of *in vivo* DDIs due to *in vitro* TDI is challenging (Venkatakrishnan and Obach, 2007; Grimm *et al.*, 2009). In 2009, a survey by the Pharmaceutical Research and Manufacturers of America (PhRMA) group found that over 75% of the researchers believe that *in vivo* DDIs due to *in vitro* TDIs cannot be accurately predicted (Grimm *et al.*, 2009). Pertaining to TDIs that inhibit P450s via formation of an MI complex, one challenge to DDI prediction is that the parent drug must undergo a series of metabolic transformations to ultimately inactivate the P450 (Mansuy *et al.*, 1977; Jonsson and Lindeke, 1992; Ortiz de Montellano, 2005). Hence, it is unclear whether the concentration of the parent TDI can be used as a surrogate for the concentration of the metabolite that ultimately complexes with the P450 heme. In addition, MIC-formation from alkylamine TDIs may arise from two competing pathways: initial N-dealkylation or N-hydroxylation (Hanson *et al.*, 2010; Barbara *et al.*, 2013). Thus, it is not clear whether inclusion of parent drug and circulating metabolites should be considered as independent *in vivo* inhibitors. The aim of this study was to evaluate, using fluoxetine and norfluoxetine enantiomers as a model, whether risk assessment of *in vivo* DDIs can be done using static models of time-dependent inhibition for multiple independent inhibitors.

Fluoxetine is a racemic secondary alkylamine, MIC-forming TDI of both CYP2C19 and CYP3A4 (Mayhew *et al.*, 2000; Hanson *et al.*, 2010). It also has an *in vivo* circulating N-dealkylated metabolite, norfluoxetine (Jannuzzi *et al.*, 2002) that is formed by CYP2D6 and other P450s (Margolis *et al.*, 2000). *In vivo*, fluoxetine can be classified as a moderate CYP2C19 inhibitor based on the 2.9-fold increase in lansoprazole AUC (Vlase *et al.*, 2011) after fluoxetine administration, yet *in vivo* CYP3A4 inhibition by fluoxetine is controversial. Multiple-dose fluoxetine increases alprazolam (40 mg/day fluoxetine for 9 days) and carbamazepine (20 mg/day fluoxetine for 7 days) AUC by 1.3-fold (Grimsley *et al.*, 1991; Greenblatt *et al.*, 1992) but

administration of 60 mg/day for 5 days then 20 mg/day fluoxetine for 7 days resulted in no change in midazolam AUC (Lam *et al.*, 2003). The current study demonstrated that the (R)- and (S)-fluoxetine isomers as well as (R)- and (S)-norfluoxetine metabolites, are TDIs of CYP2C19 while only (S)-fluoxetine and (R)-norfluoxetine are TDIs of CYP3A4. *In vivo*, norfluoxetine is formed by multiple P450 enzymes and its formation is not dependent on CYP2C19 and CYP3A4 (Jannuzzi *et al.*, 2002). As such, it is expected that inhibition of CYP2C19 and CYP3A4 *in vivo* by norfluoxetine enantiomers can be predicted based on norfluoxetine plasma concentrations, independent of fluoxetine exposure. When each of the four inhibitors is considered independently, (S)-norfluoxetine was predicted to contribute the most to CYP2C19 inhibition and (R)-norfluoxetine to CYP3A4 inhibition. (S)-fluoxetine was also predicted to cause CYP3A4 inhibition *in vivo* but its projected contribution was less (30%) than that of (R)-norfluoxetine enantiomer. Norfluoxetine enantiomers were predicted to be responsible for about 60% of the *in vivo* CYP2C19 inhibition. The importance of both norfluoxetine enantiomers in overall predicted CYP2C19 inhibition highlights the need to evaluate models for risk prediction of multiple TDIs simultaneously.

Two models for *in vitro*-to-*in vivo* prediction of DDIs due to multiple TDIs have been proposed (Zhang *et al.*, 2009b; Rowland Yeo *et al.*, 2010). *In vitro*-to-*in vitro* predictions were done to evaluate the applicability of the additive (Equation 3.4) and inhibitor-inhibitor interaction (Equation 3.5) models in describing the effect of multiple TDIs in P450 activity. The comparison of the models showed that at low inhibitor concentrations there were no differences between the two models but significant differences were observed at inhibitor concentrations above K_I. Both models predicted the observed decrease in CYP2C19 activity well at low concentrations of the enantiomer mixtures, but did not predict the combination of the metabolite and parent. At high inhibitor concentrations only the inhibition of CYP2C19 by norfluoxetine enantiomers could be predicted and only using the inhibitor-inhibitor interaction model. Overall, the additive model

over-predicted the observed inhibition at inhibitor concentrations above the K_I while the inhibitor-inhibitor interaction model better reflected the observed CYP2C19 time-dependent inhibition. These results are in agreement with previous results of *in vitro*-to-*in vitro* prediction using both models with the tertiary alkylamine TDIs, erythromycin and diltiazem (with their respective N-dealkylated metabolites) (Zhang *et al.*, 2009a). Collectively the results suggest that the multiple TDI system is more complex than either model can account for and demonstrate the challenges of incorporating mechanistic complexity into mathematical models of these types of TDIs.

Despite uncertainty in how to predict the *in vivo* decrease in P450 activity due to both parent and metabolite TDIs, risk assessment of *in vivo* DDI liability due to multiple TDI systems is imperative at some stage during new drug development. The results of this study demonstrate that the DDI risk following fluoxetine administration could be identified for CYP2C19 using either the additive or inhibitor-inhibitor interaction model. The simplest and most practical risk assessment scenario for multiple TDIs is to use the additive model (Equation 3.8), however, independent inhibitors are expected to interact with each other according to Equation 3.9. For fluoxetine, there were no differences in *in vitro*-to-*in vivo* predictions between the two models (Table 3.4). The lack of differences between the models is due to the fact that none of the inhibitors circulate at concentrations *in vivo* that are required to cause significant reversible inhibition of the P450 of interest since Equation 3.9 simplifies to Equation 3.8 at low inhibitor concentrations. For example, with fluoxetine and norfluoxetine the I_{max}/IC_{50} values against CYP2C19 or CYP3A4 are close to zero (Table 3.3). Simulations of the two models with fluoxetine and norfluoxetine (Figure 3.7) further supported this, indicating that minimal model discrimination (< 2-fold) occurs when $I_{max}/IC_{50} < 1$ for both fluoxetine and norfluoxetine enantiomers.

The additive model is likely to be sufficient for *in vitro*-to-*in vivo* risk assessment for majority of *in vivo* multiple TDI systems. Based on literature data, approximately 90% of

marketed TDIs circulate at *in vivo* unbound concentrations less than their *in vitro* unbound inhibition affinity constants (Fujioka *et al.*, 2012). For example, both diltiazem and N-desalkyldiltiazem circulate at concentrations below their K_i values. The simulations of *in vitro*-to-*in vivo* predictions using the two models demonstrate why time-dependent *in vitro* inhibition of CYP3A4 by diltiazem and N-desalkyldiltiazem independently yield similar predicted *in vivo* DDIs when using the additive (Rowland Yeo *et al.*, 2010) and inhibitor-inhibitor interaction (Zhang *et al.*, 2009b) models. Extrapolation of this simulation to any system with two TDIs indicates that less than 2-fold difference between models will be observed when $I_{max}/IC_{50} < 1$ for both inhibitors. Some TDIs, such as ritonavir (Luo *et al.*, 2003) and amprenavir (Ernest *et al.*, 2005), circulate at concentrations above their *in vitro* inhibition affinity constants (Hsu *et al.*, 1998; Polk *et al.*, 2001) and hence, significant differences in risk assessment between the two models would be expected, but only if the $k_{inact,app}$ values are significantly different for the independent inhibitors. In this situation, use of the inhibitor-inhibitor interaction model may be more accurate, but the additive model will always predict a larger *in vivo* DDI (i.e. a worst-case scenario) and hence, may be more appropriate for *in vivo* DDI risk assessment of multiple TDI systems.

In conclusion, the results of this study show that *in vitro*, both fluoxetine and norfluoxetine are stereoselective TDIs of CYP2C19 and CYP3A4 and that norfluoxetine is predicted to play an equal or greater role in *in vivo* CYP2C19 and CYP3A4 DDIs than fluoxetine. Worst-case scenario risk assessment for *in vivo* DDI liability of multiple TDI systems can be achieved by incorporating *in vitro* time-dependent inhibition information for both parent and metabolite (determined independently and stereoselectively when applicable) and predicted using a simple additive model of $\lambda/k_{deg,}$ but this methodology will likely quantitatively over-predict the magnitude of *in vivo* DDIs. The results of this study provide insight into how circulating metabolites could be accounted for in *in vivo* DDI risk assessment for TDIs during new drug

development, but emphasize the need for further research to determine the most appropriate methodology and models to use for prediction of multiple TDI systems.

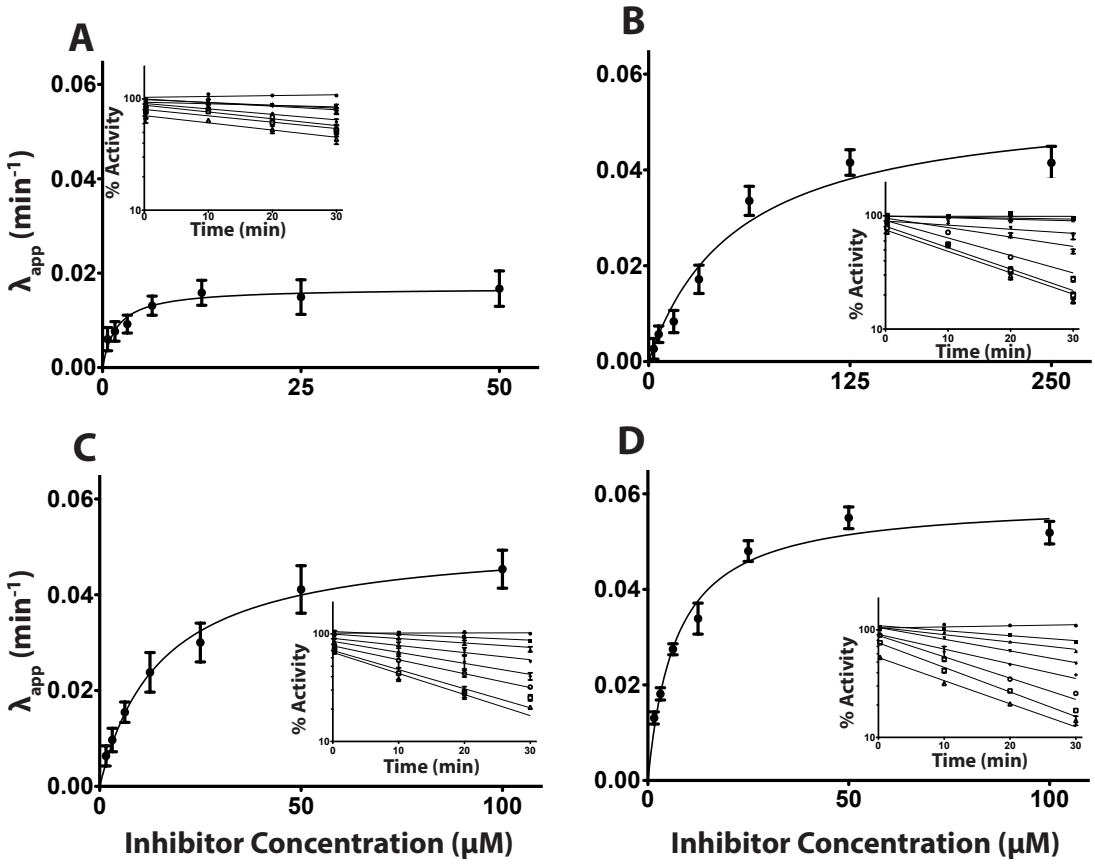

Figure 3.1. Inhibitor concentration- and time-dependent inhibition of CYP2C19 in pooled HLMs. The panels depict time-dependent inhibition by (R)-fluoxetine (Panel A), (S)-fluoxetine (Panel B), (R)-norfluoxetine (Panel C) and (S)-norfluoxetine (Panel D). The insets show the percent of CYP2C19 activity versus time at each inhibitor concentration. The error bars are the standard deviation of three replicate experiments.

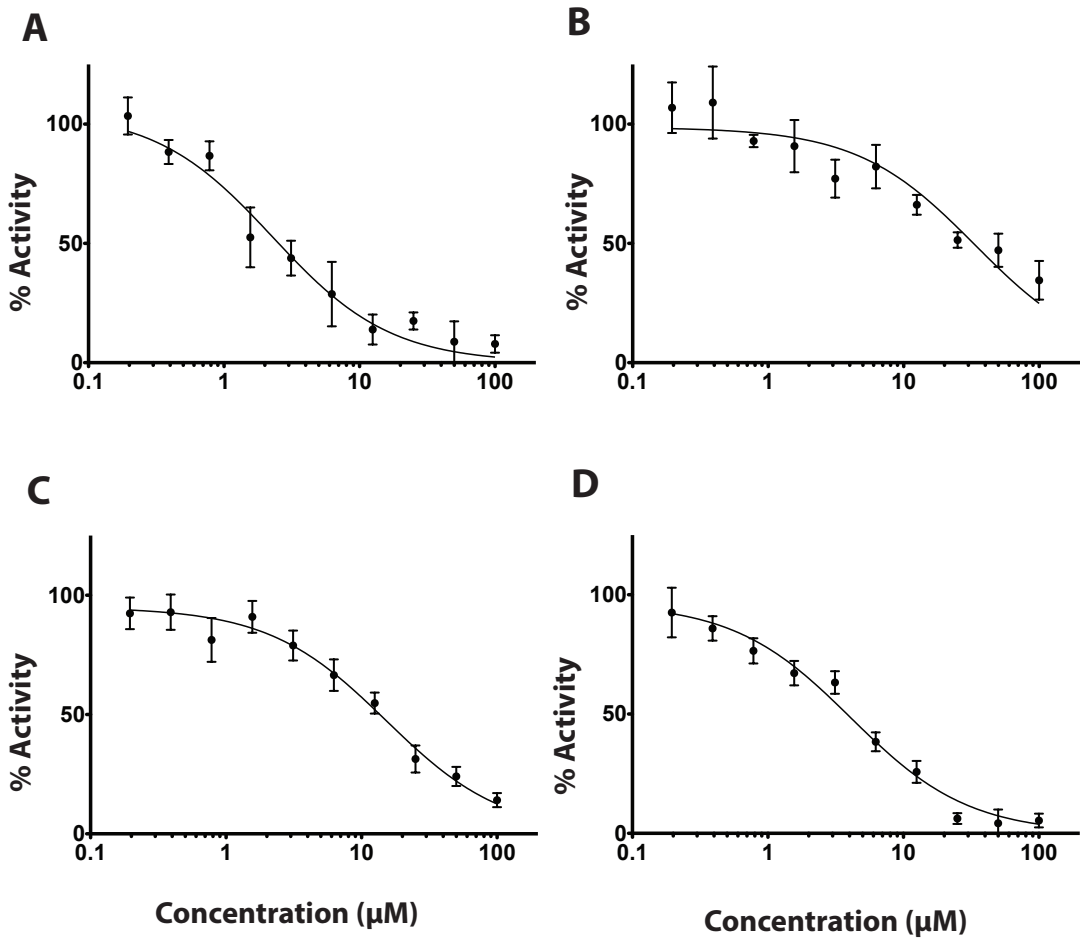

Figure 3.2. Percent of CYP2C19 activity versus inhibitor concentration in pooled HLMs. The inhibitors shown are (R)-fluoxetine (Panel A), (S)-fluoxetine (Panel B), (R)-norfluoxetine (Panel C) and (S)-norfluoxetine (Panel D). The error bars are the standard deviation of three values.

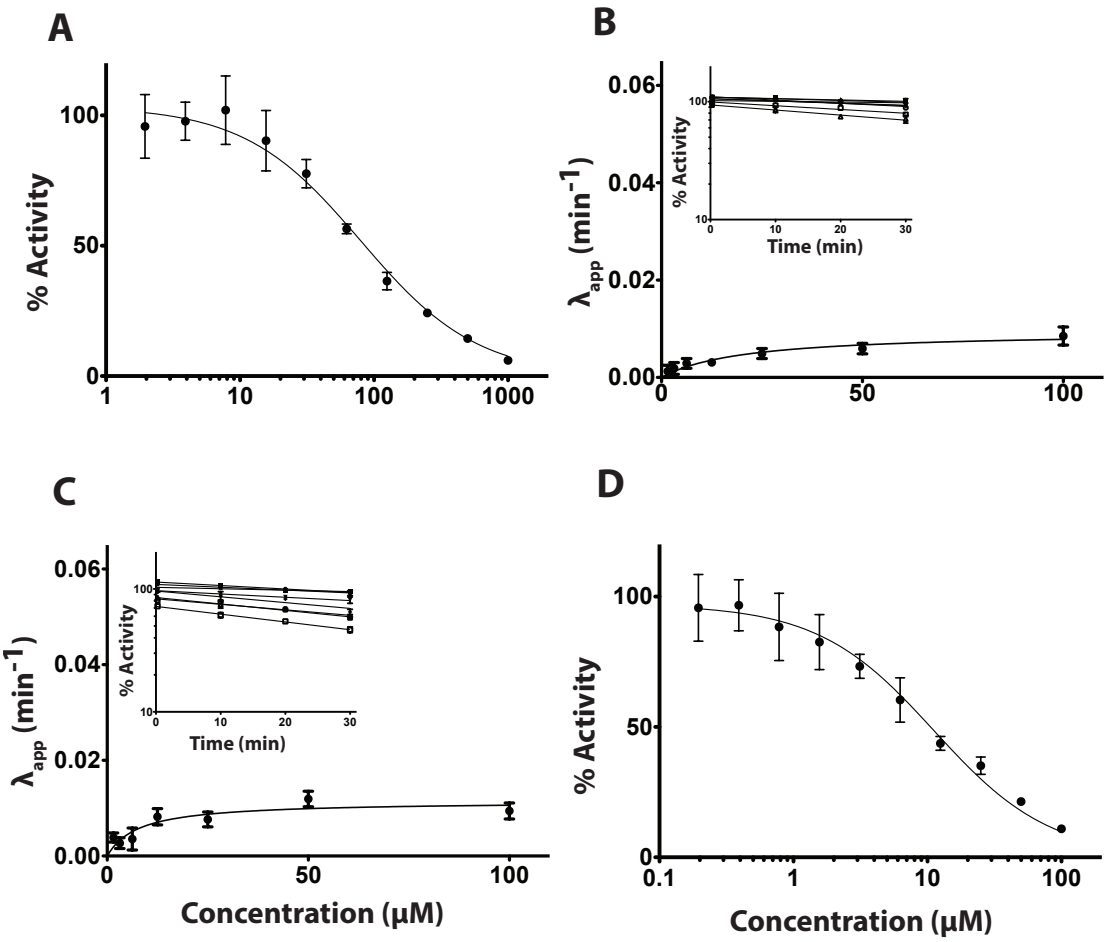

Figure 3.3. Inhibitor concentration-dependent CYP3A4 percent activity or CYP3A4 time-dependent inhibition in pooled HLMs. The panels depict CYP3A4 inhibition by (R)-fluoxetine (Panel A), (S)-fluoxetine (Panel B), (R)-norfluoxetine (Panel C) and (S)-norfluoxetine (Panel D). The insets show the percent of CYP3A4 activity versus time at each inhibitor concentration. The error bars are the standard deviation of three replicate experiments.

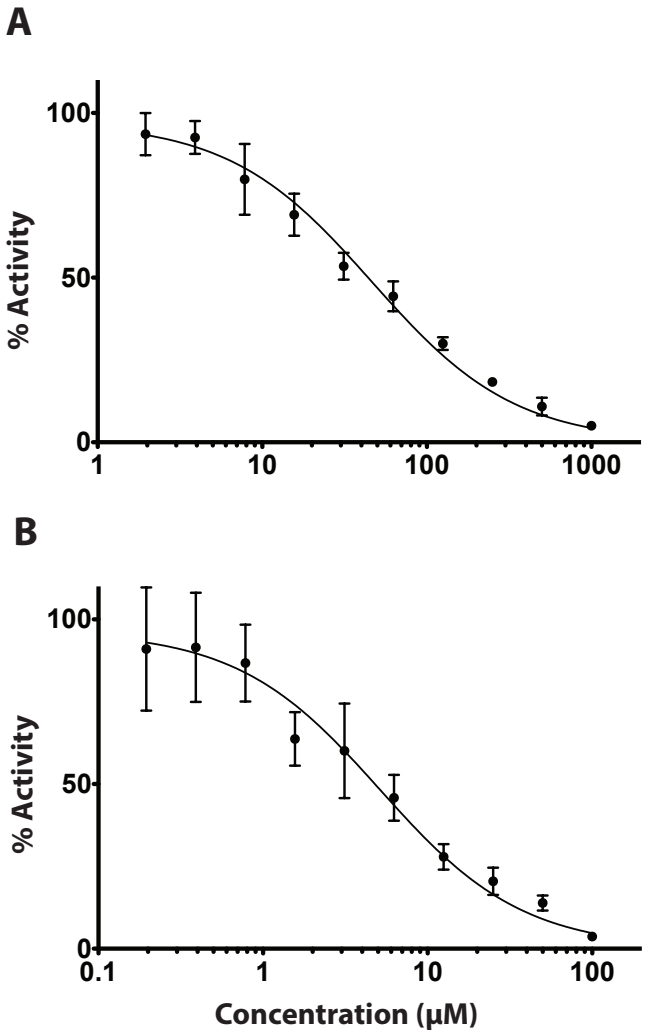

Figure 3.4. Percent of CYP3A4 activity versus inhibitor concentration in pooled HLMs. The inhibitors shown are (R)-fluoxetine (Panel A) and (S)-norfluoxetine (Panel B). The error bars are the standard deviation of three values.

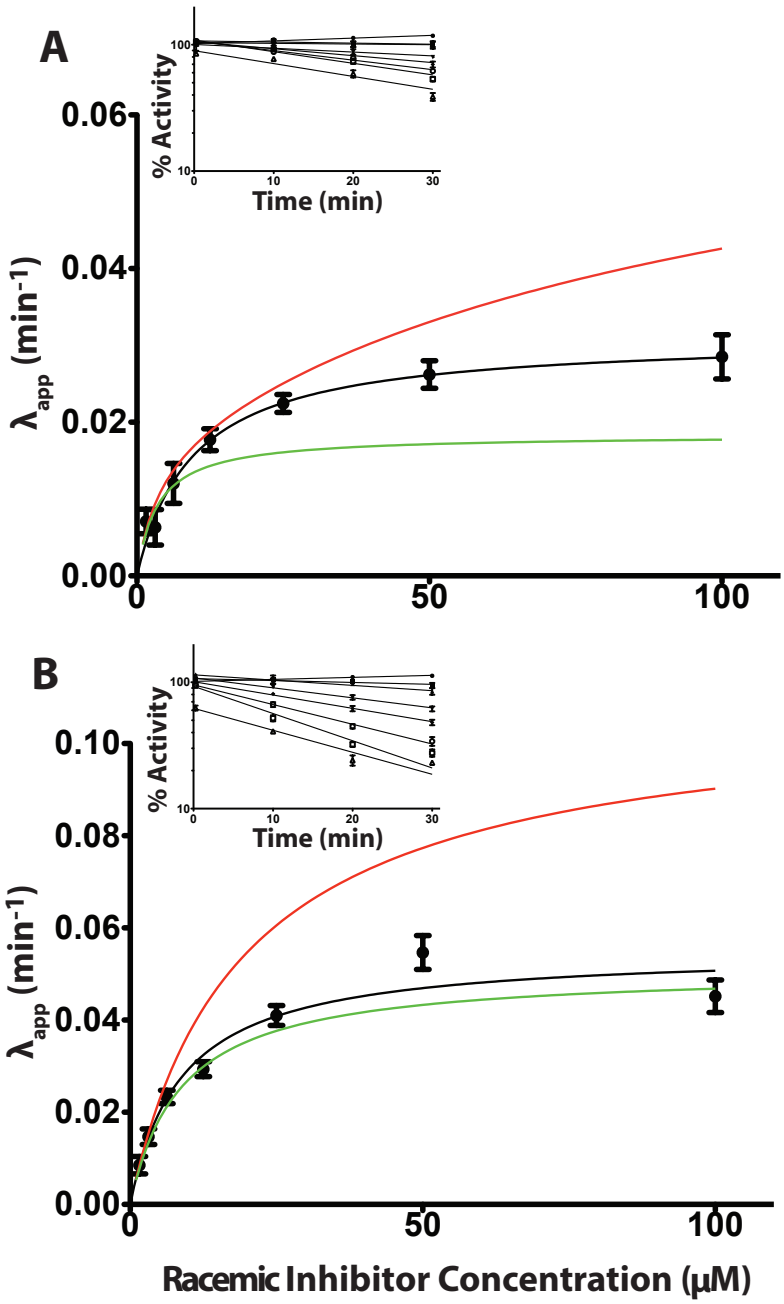

Figure 3.5. Comparison of simulated and experimentally determined time-dependent inhibition rates of CYP2C19 by a racemic mixture of fluoxetine or norfluoxetine in pooled HLMs. The time-dependent inhibition of CYP2C19 by a racemic mixture of fluoxetine (panel A) and norfluoxetine (Panel B) are depicted. The insets show the percent of CYP2C19 activity versus time at each total inhibitor concentration. The error bars are the standard deviation of three replicate experiments. The black lines show the best fit to the experimentally determined time-dependent inhibition data, the red lines show the simulated time-dependent inhibition curve using the additive model (Equation 3.4) and the green lines show the simulated time-dependent inhibition curve using the inhibitor-inhibitor interaction model (Equation 3.5). Simulations were performed by predicting racemic mixture time-dependent inhibition from the individual enantiomer values.

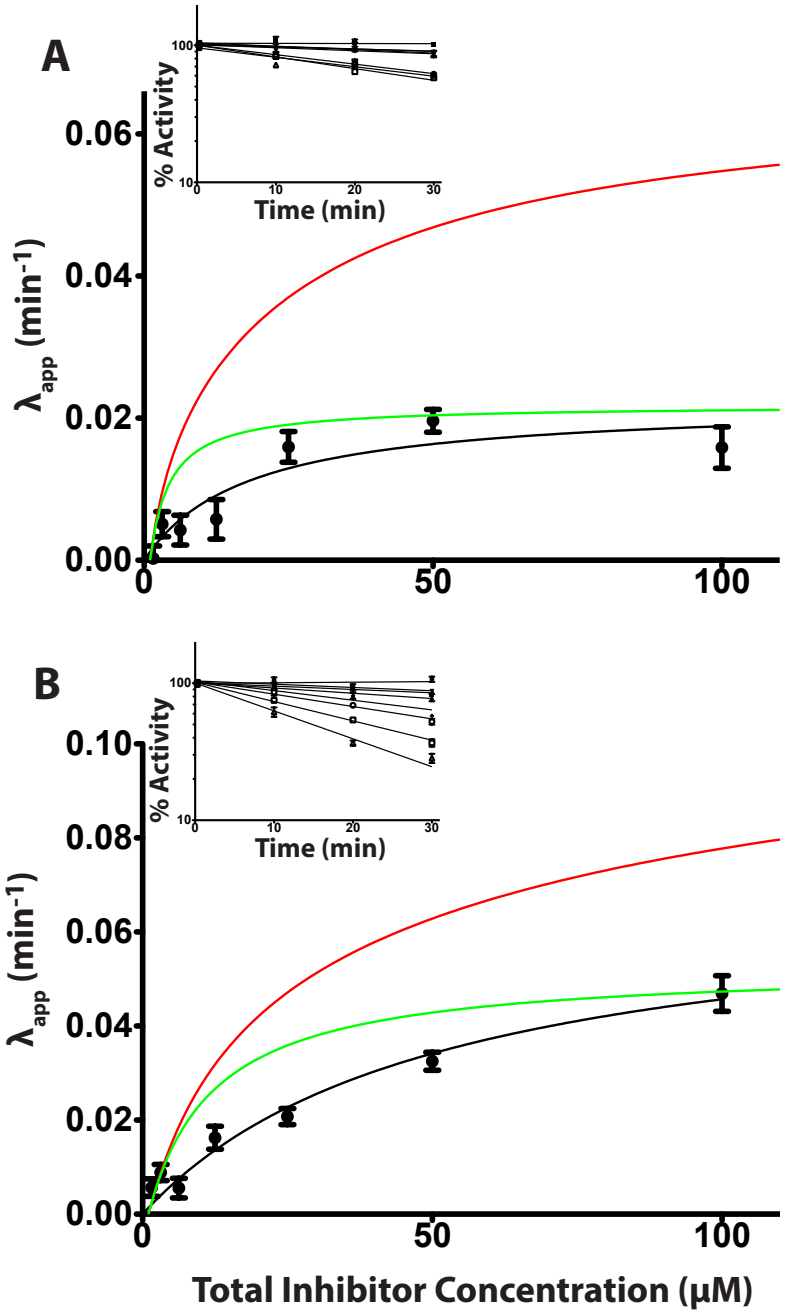

Figure 3.6. Comparison of simulated and experimentally determined time-dependent inhibition rates of CYP2C19 by a 1:1 fluoxetine:norfluoxetine mixture in pooled HLMs. The time-dependent inhibition of CYP2C19 by a 1:1 mixture of (R)-fluoxetine:(R)-norfluoxetine (panel A) and (S)-fluoxetine:(S)-norfluoxetine (Panel B) is depicted. The insets show the percent of CYP2C19 activity versus time at each total inhibitor concentration. The error bars are the standard deviation of three replicate experiments. The black lines show the best fit to the experimentally determined time-dependent inhibition data, the red lines show the simulated time-dependent inhibition curve using the additive model (Equation 3.4) and the green lines show the simulated time-dependent inhibition curve using the inhibitor-inhibitor interaction model (Equation 3.5). Simulations were performed by predicting 1:1 fluoxetine:norfluoxetine time-dependent inhibition from the individual enantiomer values.

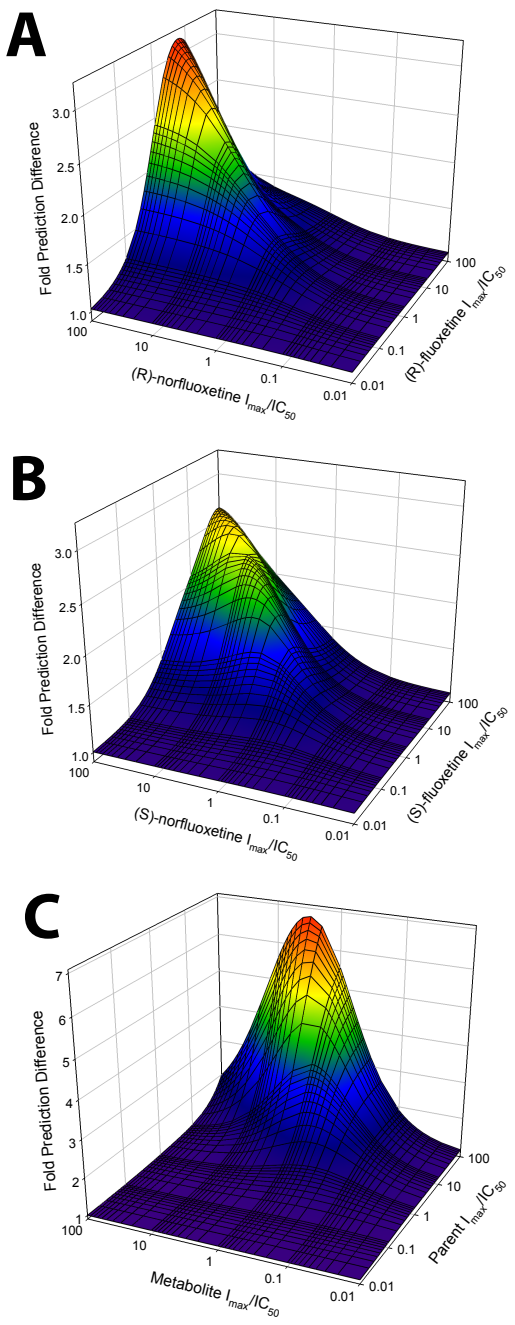

Figure 3.7. Simulation of the fold difference in prediction magnitude that would occur using the additive model instead of the inhibitor-inhibitor interaction model as a function of *in vivo* inhibitor potency. The simulations were for (R)-fluoxetine with (R)-norfluoxetine (Panel A) and (S)-fluoxetine with (S)-norfluoxetine (Panel B) inhibitor pairs and an example parent-metabolite pair where the $k_{inact,app}$ for the parent is 10-fold greater than the metabolite (Panel C).

Table 3.1. *In vitro* reversible (IC_{50}) and time-dependent (K_I and $k_{inact,app}$) inhibition constants for the enantiomers of fluoxetine and norfluoxetine in HLMs. N.D. indicates that the value was not determined. All inhibition values are expressed as mean and standard error.

		IC_{50} (μM)	K_I (μM)	$k_{inact,app}$ (min^{-1})	$k_{inact,app}/K_I$ (L/min/μmol)
CYP2C19	(R)-fluoxetine	2 ± 1	2 ± 1	0.017 ± 0.001	9.4
	(S)-fluoxetine	34 ± 5	55 ± 17	0.055 ± 0.006	1.0
	(R)-norfluoxetine	15 ± 1	15 ± 3	0.050 ± 0.010	3.3
	(S)-norfluoxetine	4 ± 1	7 ± 1	0.059 ± 0.002	8.4
CYP3A4	(R)-fluoxetine	80 ± 9	N.D.	N.D.	N.D.
	(S)-fluoxetine	47 ± 5	21 ± 19	0.009 ± 0.003	0.5
	(R)-norfluoxetine	5 ± 1	8 ± 3	0.011 ± 0.001	1.4
	(S)-norfluoxetine	11 ± 1	N.D.	N.D.	N.D.

Table 3.2. The unbound fractions (f_u) for the enantiomers of fluoxetine and norfluoxetine in pooled HLMs at 0.1 mg/mL and 1.0 mg/mL microsomal protein and in plasma.

	$f_{u,HLM}$		$f_{u,plasma}$
	0.1 mg/mL	1.0 mg/mL	
(R)-fluoxetine	0.48	0.09	0.22
(S)-fluoxetine	0.52	0.10	0.14
(R)-norfluoxetine	0.42	0.07	0.20
(S)-norfluoxetine	0.47	0.07	0.13

Table 3.3. Stereospecific risk assessment of the inhibition of CYP2C19 and CYP3A4 after fluoxetine coadministration. The predicted values for the change in *in vivo* enzyme activity from before to after fluoxetine coadministration due to reversible (I_{max}/IC_{50}) and time-dependent (λ/k_{deg}) inhibition are shown. N.A. indicates that the value is not applicable.

	CYP2C19		CYP3A4	
	I_{max}/IC_{50}	λ/k_{deg}	I_{max}/IC_{50}	λ/k_{deg}
(R)-fluoxetine	0.03	5.8	< 0.01	N.A.
(S)-fluoxetine	< 0.01	1.2	< 0.01	0.5
(R)-norfluoxetine	< 0.01	2.9	0.01	1.1
(S)-norfluoxetine	0.02	9.4	< 0.01	N.A.

Table 3.4. Predicted magnitude of *in vivo* P450 inhibition (Cl_i/Cl_i') by different combinations of fluoxetine and norfluoxetine enantiomers using the additive (Equation 3.8) and the inhibitor-inhibitor interaction (Equation 3.9) models.

	CYP2C19		CYP3A4	
	Additive	Inhibitor-inhibitor interaction	Additive	Inhibitor-inhibitor interaction
(R)- and (S)-fluoxetine	8	8	1.5	1.5
(R)- and (S)-norfluoxetine	13	13	2.1	2.1
(R)-enantiomers	10	10	2.1	2.1
(S)-enantiomers	12	12	1.5	1.5
All enantiomers	20	20	2.6	2.5

Chapter 4

In vitro prediction and *in vivo* determination of the complex metabolite-dependent drug-drug interactions precipitated by fluoxetine: a strong inhibitor of CYP2D6 and CYP2C19

4.1 Abstract

Fluoxetine and its metabolite norfluoxetine represent a complex multiple inhibitor system that inhibits CYP2D6, CYP3A4, and CYP2C19 *in vitro* via reversible or time-dependent mechanisms. Fluoxetine is predicted to inhibit all three enzymes *in vivo*. Its effect on CYP2D6, CYP2C19 and CYP3A4 activity was determined in healthy volunteers following two week dosing of fluoxetine. Fluoxetine increased dextromethorphan AUC by 51-fold and omeprazole AUC by 7.5-fold but had no effect on the midazolam and lovastatin AUC. Based on plasma concentrations, the interaction with CYP2D6 was under-predicted, CYP2C19 accurately predicted and CYP3A4 over-predicted. Multiple linear regression analysis indicated that (S)-norfluoxetine was solely responsible for *in vivo* CYP2D6 inhibition and (S)-norfluoxetine unbound *in vivo* K_i for CYP2D6 was 16-fold lower than *in vitro,* suggesting significant hepatic partitioning. The application of (S)-norfluoxetine hepatocyte partitioning afforded accurate predictions of all *in vivo* interactions. This study suggests a major role of (S)-norfluoxetine in P450 inhibition and gives insight into analysis of complex drug-drug interactions.

4.2 Introduction

Complex drug-drug interactions (DDIs) can arise from several scenarios: coadmininstration of multiple inhibitors (including racemic mixtures) of the same enzyme (Kharasch *et al.*, 2009; Schmitt *et al.*, 2009), presence of inhibitory metabolites (Reese *et al.*, 2008; Templeton *et al.*, 2010), multiple inhibition mechanisms (Fahmi *et al.*, 2009) and inhibition of multiple enzymes and/or transporters (Isoherranen *et al.*, 2012). Such complex DDIs present significant challenges to identification, prediction and rationalization of clinically important DDIs. Fluoxetine is a complex inhibitor. It is a mixture of four inhibitors, the two stereoisomers of fluoxetine and its metabolite norfluoxetine, with nonlinear and stereoselective pharmacokinetics (Peyton *et al.*, 1991; Jannuzzi *et al.*, 2002; Scordo *et al.*, 2005). Fluoxetine and norfluoxetine

enantiomers also inhibit multiple P450s *in vitro* via reversible and time-dependent inhibition mechanisms (Stevens and Wrighton, 1993; Mayhew *et al.*, 2000; Stresser *et al.*, 2009). It is not known whether accurate *in vitro*-to-*in vivo* prediction of DDIs can be obtained for inhibitors as complex as fluoxetine. The aim of this study was to comprehensively analyze fluoxetine *in vitro*-to-*in vivo* predictions as a model of complex DDI scenarios.

Based on *in vitro* data for (R)-fluoxetine, (S)-fluoxetine, (R)-norfluoxetine and (S)-norfluoxetine from Chapter 3 and Stevens and Wrighton (1993), fluoxetine is predicted to cause strong inhibition (AUC increase > 5-fold) of CYP2D6 and CYP2C19 and at least moderate inhibition (AUC increase > 2-fold) of CYP3A4 *in vivo*. However, existing *in vivo* data shows a striking discrepancy with these predictions. *In vivo,* fluoxetine is a strong CYP2D6 inhibitor (7.8-fold increase in desipramine AUC) (Bergstrom *et al.*, 1992) but only a moderate CYP2C19 inhibitor (2.9-fold increase in lansoprazole AUC) (Vlase *et al.*, 2011). Classification of *in vivo* CYP3A4 inhibition is unclear. Multiple dose fluoxetine (for 7 - 12 days) increased alprazolam and carbamazepine AUC 1.3-fold (Grimsley *et al.*, 1991; Greenblatt *et al.*, 1992) but had no effect on midazolam AUC (Lam *et al.*, 2003). Overall, prediction accuracy of fluoxetine DDIs appears to be P450- and probe-dependent. This could be due to different dosing regimens and nonlinear pharmacokinetics of fluoxetine (Altamura *et al.*, 1994) resulting in different fluoxetine and norfluoxetine exposures between studies. Alternatively, this could be due to different inhibition mechanisms or effective inhibitors for each enzyme. The aim of this study was to simultaneously determine the magnitude of *in vivo* inhibition of CYP2D6, CYP2C19 and CYP3A4 by fluoxetine and establish the role of individual inhibitors in the DDIs that result from this complex multiple inhibitor system. In addition, two CYP3A4 probes with different intestinal CYP3A4 inhibition sensitivity (midazolam and lovastatin) (Olkkola *et al.*, 1994; Neuvonen and Jalava, 1996) were studied. This study shows that the major inhibitor in a complex multiple inhibitor system can be identified and complex DDIs can be predicted.

4.3 Materials and Methods

4.3.1 *In vitro* CYP2D6 inhibition determination

Reversible CYP2D6 inhibition constants (K_i) of fluoxetine and norfluoxetine enantiomers (0 μM to 2.0 μM) were determined in pooled human liver microsomes (HLMs) from 6 donors confirmed to be CYP2D6*1/*1, CYP2D6*1/*2 or CYP2D6*2/*2 as well as CYP2C19*1/*1 and CYP3A5*3/*3 genotypes. Dextromethorphan (1.7 μM, 5 μM and 25 μM) O-demethylation was used as a probe as previously described (VandenBrink *et al.*, 2012). Reversible competitive inhibition affinity constants (K_i) were determined via the method of Segel *et al.* (Segel, 1993) using nonlinear regression and visual inspection of Lineweaver-Burke plots. The IC_{50}, K_I and $k_{inact,app}$ values against CYP2C19 and CYP3A4 as well as the f_u values for all compounds were previously determined (Chapter 3).

4.3.2 Clinical protocol

The University of Washington Institutional Review Board approved this protocol and the study was registered at www.clinicaltrials.gov (NCT01361217). Ten subjects (5 women and 5 men) were enrolled in the study after giving their written informed consent. Eight subjects were Caucasian, one Chicano and one Hispanic. The subjects were 30 ± 10 yr of age, 172 ± 11 cm high and 72 ± 14 kg on average. None of the subjects had a history of systemic disease and all had normal laboratory renal and hepatic function values. Tobacco users or subjects with history of allergy to any of the study medications or related medications were excluded. Each subject was genotyped as previously described (Templeton *et al.*, 2010) for CYP2D6, CYP2C19 and CYP3A5. Subjects with a CYP2D6 copy number other than 2 or CYP2D6*3, CYP2D6*4, CYP2D6*10, CYP2C19*2 or CYP3A5*1 single nucleotide polymorphism where excluded from the study. From 2 weeks before to 3 weeks after the study, subjects were asked to abstain from

over-the-counter medications, prescription medications and grapefruit products. Subjects also abstained from caffeine (1 day before) and alcohol products (2 days before) through the end of each sample collection period. Each subject participated in two control and two treatment sessions. On control day 1 and treatment day 12, subjects received a validated cocktail (Ryu *et al.*, 2007) of: 100 mg caffeine, 2 mg midazolam, 30 mg dextromethorphan and 20 mg omeprazole (delayed release formulation) orally with 250 mL of water (Ryu *et al.*, 2007). On control day 3 and treatment day 14, subjects received 20 mg of lovastatin with 250 mL of water. Subjects took 20 mg of fluoxetine orally on treatment day 1 then increased to 60 mg daily for 13 days. The probes were administered 1 hour after fluoxetine. Blood samples were collected over 12 hours (control days 1 and 3) and 24 hours (treatment days 12 and 14) after probe administration. Plasma was isolated from blood by centrifugation and stored at -80°C until analysis. Urine was collected from 0 - 12 hr and 12 - 24 hr after each probe administration. Total urine volume for each collection was recorded and aliquots were stored at -20°C until analysis.

4.3.3 Quantification of study drugs and metabolites

Concentrations of omeprazole, 5-hydroxyomeprazole, dextromethorphan, dextrorphan, dextrorphan-O-glucuronide, midazolam and caffeine in plasma and urine were analyzed using a Shimadzu Prominence UHPLC (Tokyo, Japan) coupled to an AB Sciex API3200 MS/MS (Framingham, MA) as described previously in Chapter 2, Hanson *et al.* (2010) and Shirasaka *et al* (2013). Cortisol, cortisone, 6β-hydroxycortisol, 6β-hydroxycortisone, lovastatin and hydroxylovastatin acid were analyzed using an Agilent 1290 UHPLC (Santa Clara, CA) coupled to an AB Sciex API5500 MS/MS. Analytes were separated using a Thermo Hypersil Gold 100x2.1 mm, 1.9 µm column (West Palm Peach, FL) with a gradient elution from 90% water with 0.1% formic acid:10% acetonitrile (0.5 min), to 90% acetonitrile by 3.5 minutes, held until 5 min, then allowed to re-equilibrate to initial conditions until 7 minutes. The (R)- and (S)-

enantiomers of fluoxetine and norfluoxetine were separated using an Astec Chirobiotic V 250x2.1 mm, 5 µm (St. Louis, MO) column and isocratic elution with 10% water and 90% methanol with 10 mM ammonium formate. All analytes were detected using positive electrospray ionization except for dextrorphan-O-glucuronide, 6β-hydroxycortisol, 6β-hydroxycortisone and hydroxylovastatin acid, which were detected using negative electrospray ionization. Not previously described MRM transitions (m/z) used were 432→256 (dextrorphan-O-glucuronide), 195→138 (caffeine), 363→121 (cortisol), 361→163 (cortisone), 423→347 (6β-hydroxycortisol), 421→345 (6β-hydroxycortisone), 427→325 (lovastatin) and 421→319 (hydroxylovastatin acid). The injection volume for all assays was 10 µL. The lower limits of quantitation were less than 1 nM for all analytes, except for caffeine (15 nM). Inter-day percent coefficient of variation for all analytes at 1 nM (30 nM for caffeine) was less than 15%. All samples were protein precipitated with 1:2 sample:acetonitrile, except omeprazole and 5-hydroxyomeprazole (2:3:1 sample:acetonitrile:methanol), centrifuged at 3000 g for 15 min and the supernatant was used for analysis. The organic solvent contained 100 nM of d_3-omeprazole, d_4-midazolam, d_6-fluoxetine or simvastatin as internal standards. Cortisol, cortisone, 6β-hydroxycortisol and 6β-hydroxycortisone were extracted from the 6 hr plasma sample and the 0-12 hr urine sample from control day 3 and study day 14 using a previously described liquid-liquid extraction method (Peng *et al.*, 2011) with the addition of a second extraction and using the internal standard of 100 nM 16β-methylprednisolone.

4.3.4 *In vitro*-to-*in vivo* predictions

In vivo DDIs were predicted using static and time-dependent (dynamic) models. All static predictions were made individually for each study subject using the average inhibitor plasma concentrations (I) over 24 hrs after 12 days of fluoxetine administration. Initial risk assessment for reversible inhibition was determined using I divided by either K_i or IC_{50} (Lutz and

Isoherranen, 2012b) and for time-dependent inhibition by the *in vivo* time-dependent inhibition rate (λ) divided by the *in vivo* P450 degradation rate constant (k_{deg}) as previously described (Fujioka *et al.*, 2012). The change in intrinsic clearance (Cl_i) after 12 days of fluoxetine administration (Cl_i') was predicted as previously described (Fahmi *et al.*, 2009; Zhang *et al.*, 2009b) using unbound inhibition constants and concentrations for reversible and time-dependent inhibition, respectively:

$$\frac{Cl_i}{Cl_i'} = 1 + \sum_{a=1}^{n} \frac{I_a}{K_{i,a}} \qquad (4.1)$$

$$\frac{Cl_i}{Cl_i'} = \left(1 + \sum_{a=1}^{n} \frac{I_a}{IC_{50,a}}\right) * \left(1 + \sum_{a=1}^{n} \frac{k_{inact,app,a} I_a}{k_{deg}\left(K_{I,a}\left(1 + \sum_{b\neq a}^{n-1} \frac{I_b}{IC_{50,b}}\right) + I_a\right)}\right) \qquad (4.2)$$

where the k_{deg} for CYP2C19 and CYP3A4 were 4.5 x 10^{-4} min^{-1} and 4.8 x 10^{-4} min^{-1}, respectively (Ghanbari *et al.*, 2006; Obach *et al.*, 2007). All Cl_i/Cl_i' values were transformed to percent activity remaining (100*Cl_i'/Cl_i). The change in the fraction of probe drug (midazolam and lovastatin) that escapes first pass CYP3A4 gut metabolism (F_g) after fluoxetine administration (F_g') was predicted as previously described (Wang *et al.*, 2004). The F_g used for midazolam and lovastatin were 0.51 and 0.07, respectively (Obach *et al.*, 2007). The change in the area under the plasma concentration-time curve (AUC) after fluoxetine administration (AUC') was predicted by combining the effect on Cl_i and F_g (Wang *et al.*, 2004). The fraction of probe drug eliminated by the inhibited P450 (f_m) was 0.99 for dextromethorphan (CYP2D6) and 0.93 for omeprazole (CYP2C19) (calculated from genetic polymorphism studies (Isoherranen *et al.*, 2012)) as well as 0.94 for midazolam and 0.90 for lovastatin (Furuta *et al.*, 1999; Shi *et al.*, 2010; Brunton *et al.*, 2011; Chiba *et al.*, 2012). P450 inhibition and increase in probe drug AUC were also predicted via semi-physiologically-based pharmacokinetic (dynamic) modeling with SimCYP v.12 (Certara, Sheffield, UK) using the default healthy population with the same gender proportion,

age range and genotype as the study. To reflect probe control session exposure and P450 f_m, several modifications were made to the default dextromethorphan, omeprazole and midazolam models. For dextromethorphan, previously described modifications were used (Ke *et al.*, 2013) with the addition of a smaller steady-state volume (V_{ss}) of 7.2 L/kg, slower absorption rate constant (k_a) of 0.41 hr^{-1}, and addition of secondary compartment distribution (k_{out}) and redistribution (k_{in}) rate constants of 0.39 hr^{-1} and 0.04 hr^{-1}, respectively. For omeprazole, k_a was decreased to 1.7 hr^{-1}, an absorption lag time (t_{lag}) of 0.68 hr was added and CYP2C19-mediated 5-hydroxyomeprazole formation was increased by 4-fold. For midazolam, k_{out} and k_{in} of 1.18 hr^{-1} and 0.47 hr^{-1} were added, respectively. Additionally, CYP3A4-mediated midazolam clearance was increased by 1.5-fold to yield a plasma clearance of 29 L/hr and V_{ss} was decreased to 0.78 L/kg, as determined *in vivo* after intravenous administration (Thummel *et al.*, 1994). The *rac*-fluoxetine dosage regimen simulated was identical to the dosage regimen in the *in vivo* study and the default *rac*-fluoxetine model was used for each enantiomer, after incorporating *in vitro* stereoselective norfluoxetine formation (Margolis *et al.*, 2000). Systemic clearance was added for (R)-fluoxetine (11 L/hr), (S)-fluoxetine (2.7 L/hr), (R)-norfluoxetine (500 mL/hr) and (S)-norfluoxetine (100 mL/hr) to obtain exposures reflective of the study values. Distribution parameters for all four inhibitors were predicted using LogP and pKa values. The *in vitro* inhibition and protein binding values were the same as the static model and only CYP2D6 and CYP2C19 inhibition was incorporated for dextromethorphan and omeprazole predictions.

4.3.5 Pharmacokinetic calculations

Noncompartmental pharmacokinetic analysis was performed using Phoenix (Pharsight, Mountainview, CA). For lovastatin, the ring closed lactone and ring opened hydroxylovastatin acid were measured separately and summed for pharmacokinetic analysis. The metabolite/parent AUC ratios (AUC_m/AUC_p) were calculated using $AUC_{0-\infty}$ for dextromethorphan

and dextrorphan and $AUC_{0\text{-}12}$ for omeprazole and 5-hydroxyomeprazole. The metabolite/parent urinary molar amount excreted over 24 hr ratio (U_m/U_p) was measured for dextrorphan plus dextrorphan-O-glucuronide then divided by dextromethorphan. Based on literature values, the cutoff for categorizing subject phenotype between extensive metabolizer (EM) and poor metabolizer (PM) was EM > 3.3 > PM for dextrorphan/dextromethorphan U_m/U_p and EM > 0.11 > PM for 5-hydroxyomeprazole/omeprazole AUC_m/AUC_p (Basci *et al.*, 1998; Furuta *et al.*, 1999). The metabolite/parent plasma concentration ratio (C_m/C_p) for 6β-hydroxycortisol/cortisol and 6β-hydroxycortisone/cortisone was calculated at 6 hr after probe administration. The formation clearance (Cl_f) of 6β-hydroxycortisol and 6β-hydroxycortisone was calculated from the amount of metabolite excreted in urine from 0 - 12 hr divided by the 6 hr plasma concentration of parent as described (Peng *et al.*, 2011). The renal clearance (Cl_r) was calculated from the amount excreted in urine from 0 - 12 hr divided by the plasma concentration at 6 hr. For (S)-norfluoxetine CYP2D6 inhibition, *in vivo* unbound reversible inhibition constant ($K_{i,u,IV}$) was determined using the equation (Yao *et al.*, 2001):

$$\frac{AUC'}{AUC} = 1 + \frac{I_u}{K_{i,u,IV}} \qquad (4.3)$$

where I_u is the unbound plasma inhibitor concentration.

4.3.6 Statistical analysis

The arithmetic mean and standard deviation are reported for $AUC_{0\text{-}12}$ and $AUC_{0\text{-}\infty}$. The geometric mean and range are reported for Cl, Cl_r, Cl_i, Cl_f, $t_{1/2}$, AUC_m/AUC_p, AUC'/AUC, C_m/C_p, U_m/U_p, % activity remaining and treatment/control ratios. Two-sided paired t-tests were used to evaluate the significance of change in *in vivo* parameters between control and treatment days. *Post hoc* power analysis was performed assuming a paired, two-sided hypothesis, α = 0.05 and β = 0.20. All statistical analyses were performed using Excel (Microsoft Office 2011, Redmond,

WA), except for stepwise multiple linear regression (MLR) analysis of dextromethorphan or omeprazole AUC'/AUC versus (R)-fluoxetine, (S)-fluoxetine, (R)-norfluoxetine and (S)-norfluoxetine, which was performed using StatPlus:mac LE (AnalystSoft Inc., www.analystsoft.com). The regression equation used was:

$$\frac{AUC'}{AUC} = B + \sum M * I_u \qquad (4.4)$$

where M and B are the regression slope and y-intercept. Only positive slopes were considered for M. A p-value of < 0.05 was considered statistically significant for all tests.

4.4 Results

(R)- and (S)-fluoxetine as well as (R)- and (S)-norfluoxetine were high affinity reversible inhibitors of CYP2D6 (Table 4.1) with the (S)-enantiomers being approximately 10-fold more potent than the (R)-enantiomers. Stereospecific *in vitro* inhibition data was used to predict the *in vivo* change in CYP2D6, CYP2C19 and CYP3A4 activity (Figure 4.1 and Table 4.1). Based on I/K_i values, (S)-fluoxetine and (S)-norfluoxetine were predicted to contribute the most to *in vivo* CYP2D6 inhibition. λ/k_{deg} values predict (R)-fluoxetine and (S)-norfluoxetine to contribute the most to *in vivo* CYP2C19 inhibition and (S)-fluoxetine and (R)-norfluoxetine the most to *in vivo* CYP3A4 inhibition. I/IC_{50} values predict little reversible inhibition of CYP2C19 and CYP3A4 *in vivo.* For dynamic modeling, the concentration-versus time curves for fluoxetine and norfluoxetine enantiomers at day 12 of fluoxetine administration and control session dextromethorphan, omeprazole and midazolam were simulated and compared to observed (Figure 4.2). When combining all four inhibitors, the static and dynamic models predicted a mean 87 - 92% decrease in CYP2D6 activity, 97 - 98% decrease in CYP2C19 activity, 84 - 87% decrease in hepatic CYP3A4 activity and 84 - 92% decrease in intestinal CYP3A4 activity after 12 days of fluoxetine (Figure 4.1 and Table 4.1). Static modeling predicted an AUC'/AUC of 11

(7 - 15) for dextromethorphan, 11 (11 - 12) for omeprazole, 8 (6 - 11) for midazolam and 18 (11 - 31) for lovastatin. Dynamic modeling predicted an AUC'/AUC of 9 (4 - 19) for dextromethorphan, 9 (4 - 21) for omeprazole and 16 (6 - 32) for midazolam. Overall, both the static and dynamic models predict strong *in vivo* inhibition of all three P450s by fluoxetine.

Inhibition of CYP2D6, CYP2C19 and CYP3A4 *in vivo* and the validity of the *in vitro*-to-*in vivo* predictions were determined in a cocktail study after multiple dose fluoxetine administration. The average plasma concentrations on day 12 were 280 ± 90 nM for (R)-fluoxetine, 770 ± 270 nM for (S)-fluoxetine, 200 ± 70 nM for (R)-norfluoxetine and 320 ± 110 nM for (S)-norfluoxetine (Figure 4.2). The fluctuation in these plasma concentrations was < 2-fold over the dosing interval.

Fluoxetine significantly decreased CYP2D6 activity based on a 98% (81 - 99%) decrease in oral Cl of dextromethorphan (Table 4.2). Dextromethorphan $AUC_{0-\infty}$ increased by 51-fold, from 58 nmol*hr/L to 1600 nmol*hr/L (Table 4.2 and Figure 4.3). Plasma dextrorphan/dextromethorphan AUC_m/AUC_p decreased by 98% (90 - 99%), but dextrorphan $AUC_{0-\infty}$ was unchanged ($P > 0.05$). The dextrorphan/dextromethorphan U_m/U_p decreased by 99% (95 - > 99%) after fluoxetine administration, resulting in EM to PM phenotype conversion in all subjects except one, whose U_m/U_p decreased by 95% after fluoxetine administration but was < 3.3 on control day. Based on MLR, the majority of the interaction is explained by (S)-norfluoxetine plasma concentrations ($R^2 = 0.83$ and $p < 0.001$) with no other circulating inhibitor resulting in significant regression (Figure 4.3). (S)-Norfluoxetine *in vivo* $K_{i,u,IV}$ was calculated to be 1.1 nM, 16-fold lower than the *in vitro* unbound K_i (18 nM).

Fluoxetine decreased oral Cl of omeprazole by 86% (77 - 95%), from 55 L/hr in the control day to 7.5 L/hr (Table 4.2). One subject was excluded from the omeprazole analysis as an outlier (Grubb's outlier test, $p < 0.01$). This individual's omeprazole concentrations were < 4

nM on the fluoxetine administration day (compared to mean 2800 ± 1200 nM in the other subjects) except for 34 nM at the 12-hour sample. The $AUC_{0\text{-}12}$ of omeprazole was increased by 7.5-fold following fluoxetine administration (Table 4.2 and Figure 4.4). No change in $AUC_{0\text{-}12}$ for the CYP2C19-formed metabolite, 5-hydroxyomeprazole, was observed ($p > 0.05$), but the plasma AUC_m/AUC_p of 5-hydroxyomeprazole/omeprazole decreased by 87% (80 - 94%) ($p < 0.01$) (Table 4.2 and Figure 4.4). Based on the decrease in AUC_m/AUC_p, 5 of the 9 subjects converted from EM to PM phenotype. Stepwise MLR analysis demonstrated that no inhibitors significantly regressed with omeprazole AUC'/AUC ($p<0.05$).

Fluoxetine did not affect the $AUC_{0\text{-}\infty}$ (43 ± 22 μmol*hr/L versus 43 ± 15 μmol*hr/L), oral Cl (13 L/hr versus 12 L/hr) or $t_{1/2}$ (4.3 hr versus 4.5 hr) of caffeine ($p > 0.05$), a CYP1A2 probe (Figure 4.5). Based on *post hoc* power analysis ($\beta = 0.20$ and $n = 10$) the study had sufficient power to detect a ≥ 19% change from control in caffeine $AUC_{0\text{-}\infty}$. Following 12 days of fluoxetine administration, midazolam $AUC_{0\text{-}\infty}$, oral Cl and $t_{1/2}$ were unchanged ($p > 0.05$) (Table 4.3 and Figure 4.5). Following 14 days of fluoxetine administration, lovastatin $AUC_{0\text{-}\infty}$, oral Cl and $t_{1/2}$ ($n = 7$) were also unchanged ($p > 0.05$) (Table 4.3 and Figure 4.5). Based on a *post hoc* analysis ($\beta = 0.20$), the study had sufficient power to detect a ≥ 34% increase in midazolam $AUC_{0\text{-}\infty}$ ($n = 10$) and a ≥ 24% in lovastatin $AUC_{0\text{-}\infty}$ ($n = 7$) (Table 4.3). Fluoxetine had no effect on endogenous (6β-hydroxycortisol or 6β-hydroxycortisone) urine or plasma measures of hepatic CYP3A4 activity (Table 4.3), which is in agreement with the lack of effect on midazolam and lovastatin. The 6β-hydroxycortisol/cortisone U_m/U_p, 6β-hydroxycortisone/cortisone U_m/U_p, 6β-hydroxycortisol Cl_f and 6β-hydroxycortisone Cl_f were highly variable between subjects. The variability in 6β-hydroxycortisol/cortisol C_m/C_p and 6β-hydroxycortisone/cortisone C_m/C_p was much less. Based on a *post hoc* power analysis ($\beta = 0.20$, $n = 10$), the 6β-hydroxycortisol and 6β-hydroxycortisone C_m/C_p measures had sufficient power to detect approximately a ≥ 30%

change from control. Fluoxetine administration did not affect the Cl_r of cortisol, cortisone, 6β-hydroxycortisol or 6β-hydroxycortisone ($p > 0.05$).

4.5 Discussion

Fluoxetine, together with its metabolite norfluoxetine, was studied as a model complex inhibitor system. Several attributes of this system present significant challenges in DDI prediction, including stereoselective P450 inhibition with stereoselective pharmacokinetics and multiple enzyme inhibition by reversible and time-dependent mechanisms. In addition, partitioning into hepatocytes has been proposed (Greenblatt *et al.*, 1996). *In vitro* data for all four inhibitors predicted a 97 - 98% decrease in hepatic CYP2C19, 87 - 92% in CYP2D6 and 84 - 87% in CYP3A4 activity, resulting in a predicted inhibition magnitude rank order of CYP2C19 > CYP2D6 ≈ CYP3A4. When probe-specific pharmacokinetics was incorporated, a 9 - 11 fold increase in dextromethorphan, 9 - 11 in omeprazole and 8 - 16 in midazolam AUC was predicted, suggesting an interaction with all probes. Additionally, static modeling predicted a lovastatin AUC'/AUC = 18. The observed DDI with dextromethorphan (AUC'/AUC = 51) was under-predicted whereas omeprazole (AUC'/AUC = 7.5) was accurately predicted. No change in midazolam or lovastatin AUC indicates that CYP3A4 inhibition was over-predicted. These data clearly show an enzyme- and mechanism-dependent *in vitro*-to-*in vivo* prediction discrepancy.

The discrepancy between predicted and observed P450 inhibition may be explained via identification of contributing inhibitors to DDIs. In this study, MLR analysis was used to determine the relative *in vivo* importance of the individual inhibitors in this system. This was possible because inhibitor plasma concentrations varied 2.7 - 3.6 fold between subjects and dextromethorphan AUC'/AUC varied 35-fold between subjects. Smaller variability in omeprazole AUC'/AUC (5-fold) between subjects is likely due to attenuation by CYP2C19 f_m (Furuta *et al.*, 1999), decreasing AUC'/AUC dynamic range (Ito *et al.*, 2005) and ultimately precluding *in vivo*

determination of inhibitor contribution to CYP2C19 inhibition. MLR analysis did suggest that variability in (S)-norfluoxetine concentrations alone explains CYP2D6 inhibition, accounting for 60% of observed variability in dextromethorphan AUC'/AUC. Based on *in vitro* data, (S)-norfluoxetine is predicted to contribute approximately 40% of CYP2D6 inhibition, but (S)-fluoxetine is predicted to contribute approximately 50% to *in vivo* CYP2D6 inhibition. It is possible that the role of (S)-fluoxetine in the CYP2D6 DDI was not detected by MLR because (S)-norfluoxetine concentrations correlate with (S)-fluoxetine (R^2 = 0.56 and p = 0.01) (data not shown). However, individual regression analysis showed no correlation with (S)-fluoxetine and dextromethorphan AUC'/AUC (p > 0.05). Hence, none of the *in vivo* analysis supported a significant role of (S)-fluoxetine in *in vivo* CYP2D6 inhibition. A study with administration of (S)-norfluoxetine alone would be required to confirm the predominant role of (S)-norfluoxetine in CYP2D6 inhibition and to resolve the *in vitro*-to-*in vivo* discrepancy. Overall, the *in vitro* and *in vivo* data emphasizes the potential importance of metabolites to *in vivo* DDIs and supports the conclusion that (S)-norfluoxetine is mainly responsible for the CYP2D6 DDI.

The *in vivo* DDI with CYP2D6 was under-predicted from *in vitro* data. *In vivo* $K_{i,u}$ ($K_{i,u,IV}$) has been used to assess *in vitro*-to-*in vivo* prediction discrepancies (Yao *et al.*, 2001; Neal *et al.*, 2003; Yao *et al.*, 2003; Templeton *et al.*, 2010). $K_{i,u}$ may be different *in vitro* versus *in vivo* due to 1) inhibitor hepatic partitioning, 2) unaccounted inhibitory metabolite(s), 3) different inhibitory potency or 4) inhibition mechanism *in vitro* versus *in vivo* (Yao *et al.*, 2001). Metabolite formation within the hepatocyte could also result in a concentration gradient between the hepatocyte and plasma. $K_{i,u,IV}$ could only be determined for (S)-norfluoxetine reversible inhibition of CYP2D6 (1.1 nM) and was 16-fold lower than the *in vitro* $K_{i,u}$, most likely due to hepatocyte partitioning. Hepatic partitioning of fluoxetine and norfluoxetine has been observed in mice and suggested to be required for accurate inhibition prediction (Greenblatt *et al.*, 1996). Due to the cocktail approach employed here, (S)-norfluoxetine partitioning can be used to refine the

CYP2C19 and CYP3A4 predictions, since all P450s are affected by identical hepatocyte concentrations. Assuming (S)-norfluoxetine is the only effective inhibitor *in vivo* and incorporating 16-fold hepatocyte partitioning, the *in vivo* DDIs observed with dextromethorphan and omeprazole can be accurately predicted (AUC'/AUC of 42 and 13, respectively) using static modeling. Furthermore, under these assumptions only a 1.2-fold increase in midazolam or lovastatin AUC is predicted. This is in good agreement with the lack of CYP3A4 inhibition observed, but this observed negative DDI could also be due to simultaneous *in vivo* CYP3A4 induction. Fluoxetine has been shown to be a weak inducer (maximum 2-fold induction) of CYP3A4 *in vitro* (Fahmi *et al.*, 2009), but it is unknown if norfluoxetine also induces CYP3A4. The finding that (S)-norfluoxetine may partition into the hepatocyte and can alone predict *in vivo* CYP2D6 and CYP2C19 inhibition is interesting and future *in vitro* hepatocyte studies are warranted to obtain better mechanistic understanding and validate the *in vivo* findings.

In addition to the complexity of multiple possible inhibitors of a single enzyme, this system also possesses challenges in DDI prediction due to simultaneous inhibition of multiple enzymes. Simultaneous inhibition of more than one P450 by a single inhibitor is recognized as a risk factor in clinical DDIs (Isoherranen *et al.*, 2012). To date, fluvoxamine is the only inhibitor known to strongly inhibit more than one P450 (CYP1A2 and CYP2C19) *in vivo* (Isoherranen *et al.*, 2012). This study shows that fluoxetine is also a strong inhibitor of two enzymes (CYP2D6 and CYP2C19). This could result in clinically significant interactions with drugs not commonly considered sensitive to DDIs or significantly stronger DDIs than expected from single enzyme inhibition. Atomoxetine is used to treat attention deficit hyperactivity disorder and coadministration with fluoxetine is likely. *In vivo*, atomoxetine is eliminated via CYP2D6, demonstrating a 7.1-fold increase in AUC'/AUC after paroxetine administration (Belle *et al.*, 2002). Remaining atomoxetine elimination is mostly due to CYP2C19 (Ring *et al.*, 2002).

Simultaneous strong inhibition of both P450s due to fluoxetine coadministration could result in a greater increase in atomoxetine exposure than with paroxetine.

Strong inhibition of CYP2C19 alone by fluoxetine has clinical implications. The 7.5-fold increase in omeprazole AUC due to fluoxetine is comparable to the 6.3-fold increase in omeprazole AUC after fluconazole (Kang *et al.*, 2002) and 9.8-fold increase in (S)-mephenytoin AUC after fluvoxamine administration (Yao *et al.*, 2003) suggesting that caution should be exercised when fluoxetine is administered with CYP2C19 substrates. The clinically plausible coadministration of fluoxetine with diazepam, a CYP2C19 substrate, could cause increased diazepam concentrations, resulting in increased sedation and other adverse effects (Ishizaki *et al.*, 1995; Jung *et al.*, 1997). In contrast, CYP2C19 is principally responsible for the formation of the active metabolite of clopidogrel (Gilard *et al.*, 2008; Farid *et al.*, 2010) and fluoxetine is likely to inhibit the formation of this metabolite, leading to decreased anti-platelet activity.

In conclusion, this study shows that multiple dose fluoxetine strongly inhibits CYP2D6 and CYP2C19 activity *in vivo*, without affecting CYP3A4 or CYP1A2 activity. The results suggest that caution should be taken when coadministering fluoxetine with drugs that are metabolized by CYP2D6, CYP2C19 or both. Significant *in vitro*-to-*in vivo* discrepancies in P450 inhibition were observed using standard DDI prediction methodologies, suggesting that challenges remain in extrapolation of drug-drug interaction predictions for complex multiple inhibitor systems across P450s. *In vitro* and *in vivo* data indicates that (S)-norfluoxetine is solely responsible for observed P450 inhibition and the prediction discrepancies can be completely resolved by assigning (S)-norfluoxetine as the main *in vivo* inhibitor and incorporating a 16-fold hepatocyte uptake of (S)-norfluoxetine. These results suggest that further research is needed to accurately predict metabolite contribution and appropriately identify necessary *in vivo* DDI studies during early drug development.

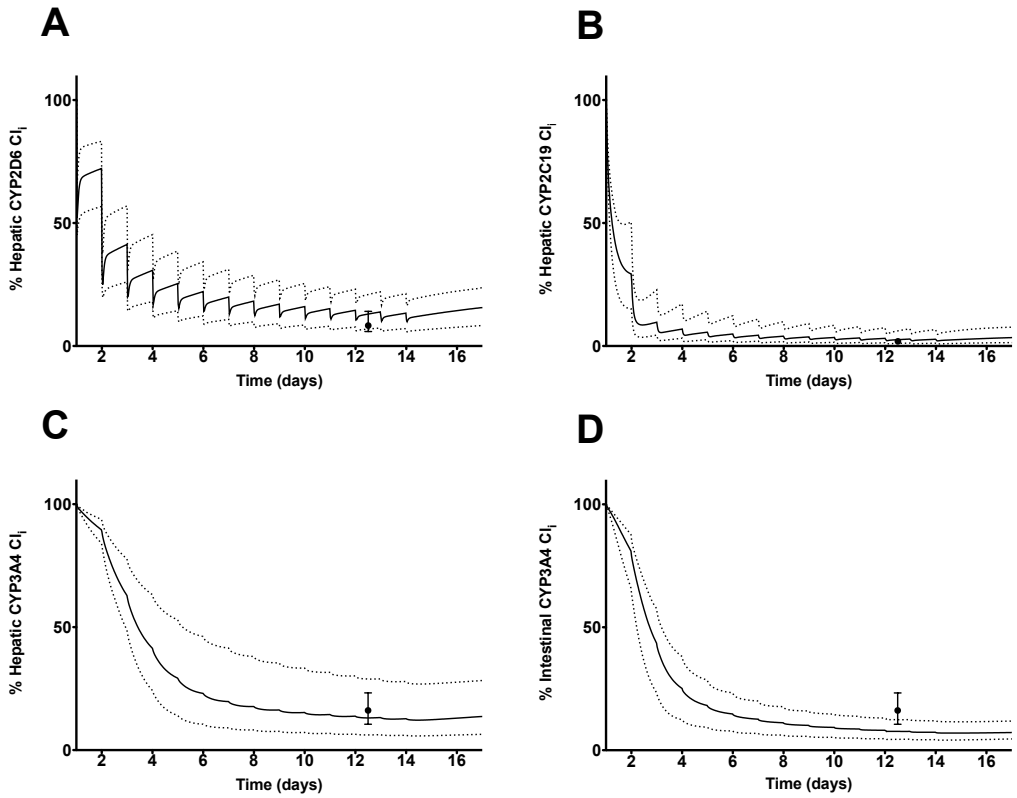

Figure 4.1. Predicted decrease in P450 activity after multiple dose fluoxetine administration. Shown is the static (geometric mean and range are denoted as solid circle as error bars, respectively) and dynamic (geometric mean and range are denoted as solid and dotted lines, respectively) model predicted decrease in % P450 Cl_i for hepatic CYP2D6 (A), CYP2C19 (B) and CYP3A4 (C) as well as intestinal CYP3A4 (D).

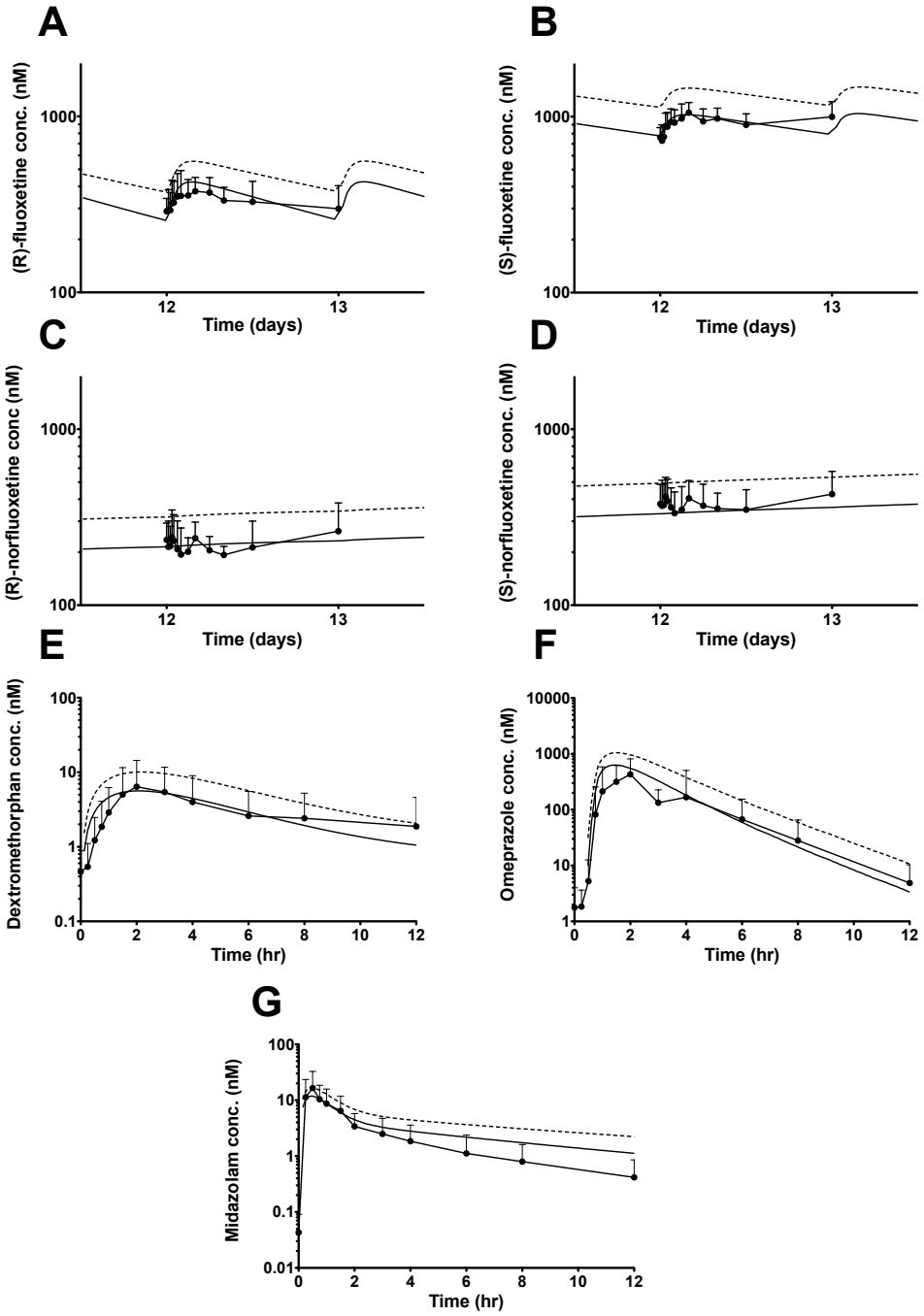

Figure 4.2. Observed and simulated plasma concentration versus time profiles. Shown are the enantiomers of fluoxetine (A and B) and norfluoxetine (C and D) after 12 daily doses of fluoxetine. Also shown is dextromethorphan (E), omeprazole (F) and midazolam (G) in the control session. Closed circles and solid black line represent averaged values. The error bars and dashed lines represent observed and simulated standard deviation.

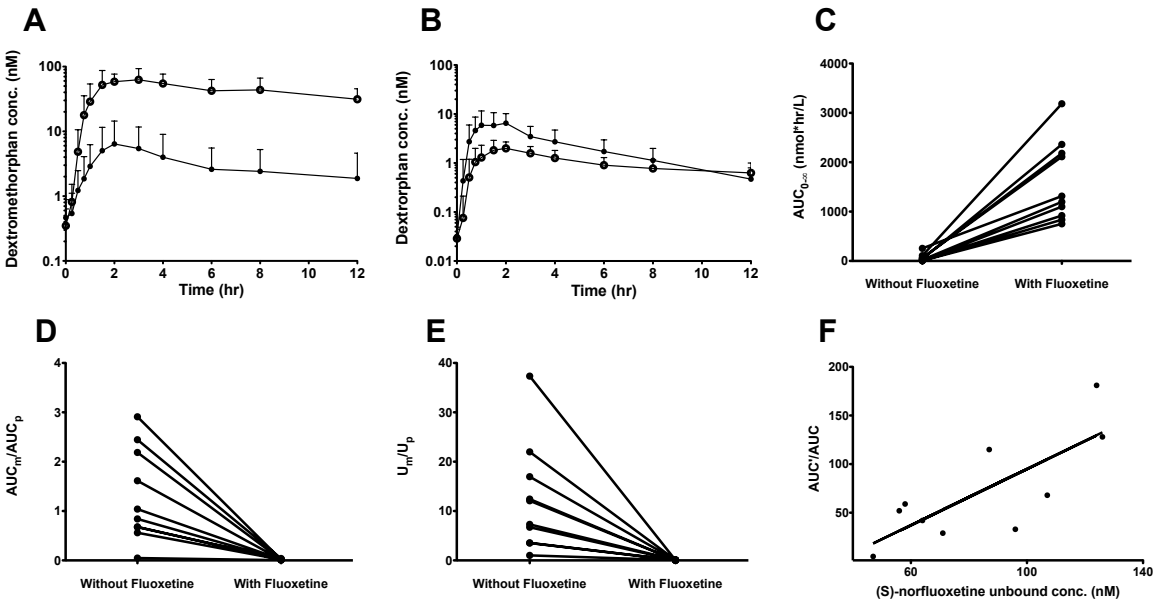

Figure 4.3. Effect of fluoxetine on dextromethorphan and dextrorphan. The mean plasma concentration versus time curves for dextromethorphan in the presence (open circles) and absence (closed circles) of fluoxetine administration (n = 10) are shown in panel A. Panel B shows the effect of fluoxetine on dextromethorphan $AUC_{0-\infty}$ in individual subjects. Dextrorphan AUC without (closed circles) and with (open circles) fluoxetine administration is shown in panel C. The decrease in dextrorphan/dextromethorphan AUC_m/AUC_p in each subject is depicted in panel D. The decrease in dextrorphan/dextromethorphan U_m/U_p in each subject is depicted in panel E. The error bars show the standard deviation. Also, the linear regression between dextromethorphan AUC'/AUC and (S)-norfluoxetine (F) is shown.

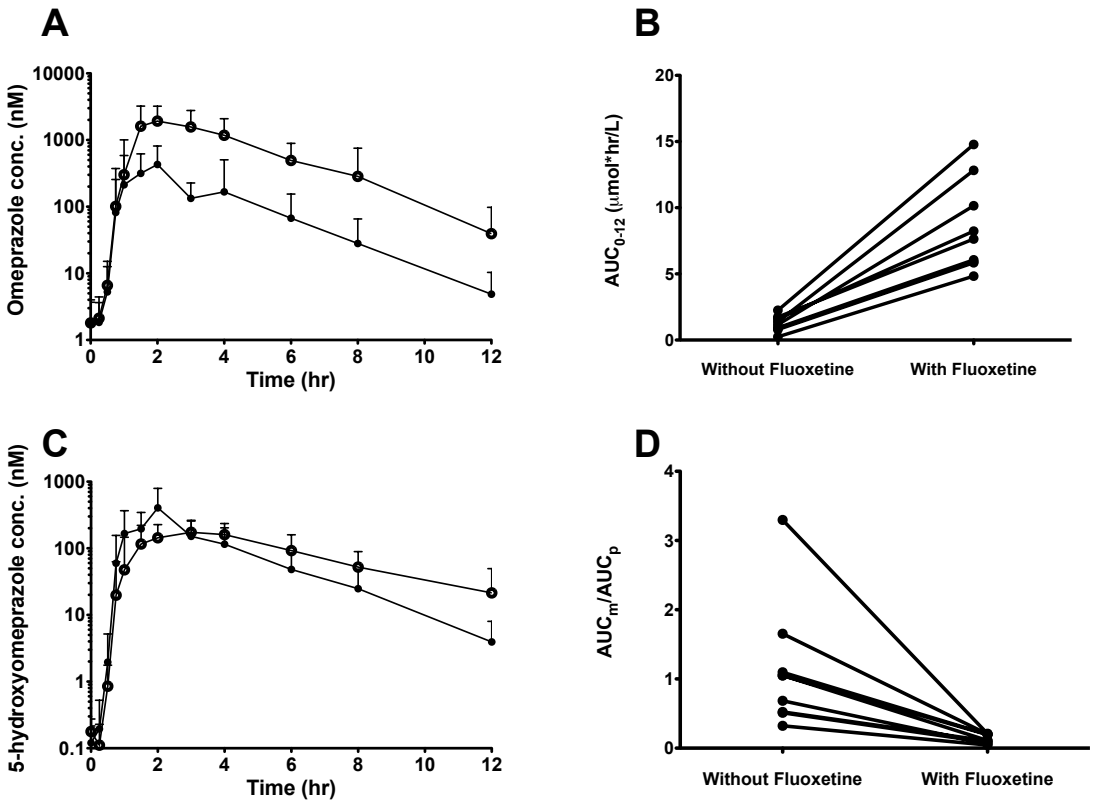

Figure 4.4. Effect of fluoxetine on omeprazole and 5-hydroxyomeprazole disposition. The mean plasma concentration versus time curves for omeprazole in the presence (open circles) and absence (closed circles) of fluoxetine administration (n = 9) are shown in panel A. Panel B shows the effect of fluoxetine on omeprazole $AUC_{0\text{-}12}$ in individual subjects. 5-hydroxyomeprazole AUC without (closed circles) and with (open circles) fluoxetine administration is shown in panel C. The decrease in 5-hydroxyomeprazole/omeprazole AUC_m/AUC_p in individual subjects is shown in panel D. The error bars depict the standard deviation.

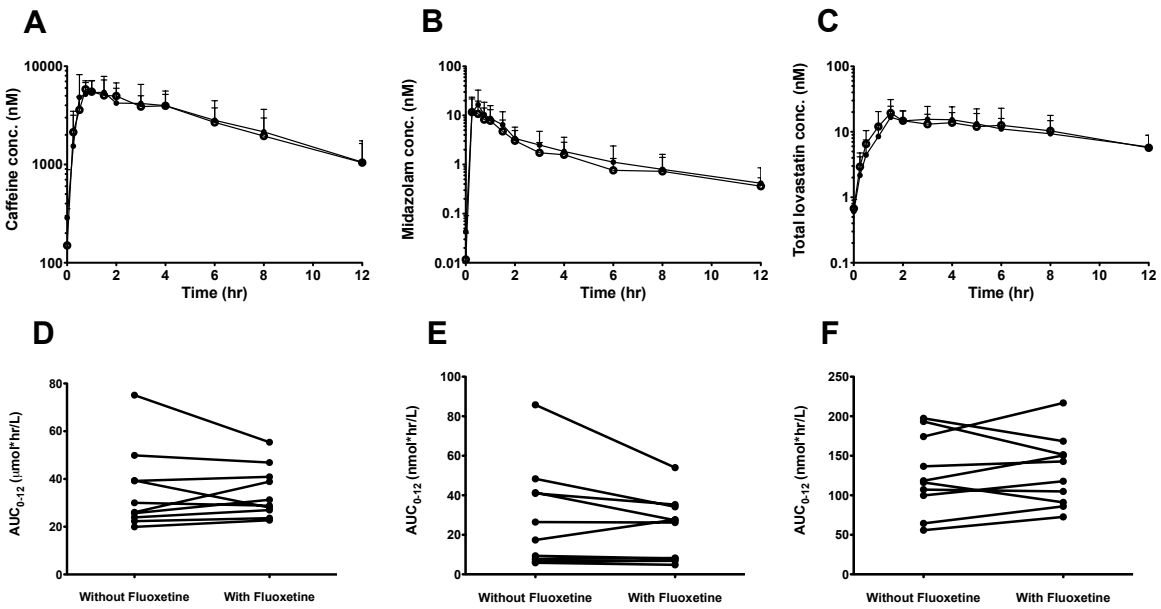

Figure 4.5. Disposition of caffeine, midazolam and lovastatin in the presence and absence of fluoxetine. The plasma concentration versus time curves and individual subject $AUC_{0\text{-}12}$ changes for caffeine (Panels A and D), midazolam (Panels B and E) and lovastatin (Panels C and F) are displayed in the presence (open circles) and absence (closed circles) of fluoxetine. The error bars depict the standard deviation in the 10 subjects.

Table 4.1. *In vitro* fluoxetine and norfluoxetine P450 inhibition and protein binding (f_u) values as well as predicted % P450 activity remaining at day 12 of fluoxetine administration. All I/K_i, I/IC_{50}, λ/k_{deg} and % P450 activity remaining values are listed as geometric mean and range. All K_i, K_I and $k_{inact,app}$ values are listed as arithmetic mean and standard deviation of triplicate experiments.

	(R)-fluoxetine	(S)-fluoxetine	(R)-norfluoxetine	(S)-norfluoxetine
CYP2D6				
K_i (nM)	860 ± 10	68 ± 1	500 ± 10	38 ± 1
I/K_i	0.3 (0.2 - 0.5)	5.8 (2.5 - 9.0)	0.4 (0.3 - 0.7)	4.5 (2.6 - 7.1)
% Hepatic Activity Remaining	Static Model: 8 (6 - 14) and Dynamic Model: 13 (7 - 21)			
CYP2C19				
IC_{50} (μM)*	2 ± 1	34 ± 5	15 ± 1	4 ± 1
I/IC_{50}	0.11 (0.07 - 0.18)	0.01 (< 0.01 - 0.02)	0.01 (< 0.01 - 0.02)	0.04 (0.02 - 0.07)
K_I (μM)*	2 ± 1	55 ± 17	15 ± 3	7 ± 1
$k_{inact,app}$ (min^{-1})*	0.017 ± 0.001	0.055 ± 0.006	0.050 ± 0.010	0.059 ± 0.002
λ/k_{deg}	15 (12 - 20)	4 (2 - 6)	7 (5 - 12)	17 (11 - 25)
% Hepatic Activity Remaining	Static Model: 2 (1 - 3) and Dynamic Model: 3 (1 - 6)			
CYP3A4				
IC_{50} (μM)*	80 ± 9	47 ± 5	5 ± 1	11 ± 1
I/IC_{50}	< 0.01 (< 0.01 - 0.01)	0.01 (< 0.01 - 0.01)	0.04 (0.02 - 0.07)	0.02 (0.01 - 0.02)
K_I (μM)*	N.A.	21 ± 19	8 ± 3	N.A.
$k_{inact,app}$ (min^{-1})*	N.A.	0.009 ± 0.003	0.011 ± 0.001	N.A.
λ/k_{deg}	N.A.	1.7 (0.8 - 2.5)	3.0 (2.1 - 5.1)	N.A.
% Intestinal Activity Remaining	Static Model: 16 (11 - 23) and Dynamic Model: 8 (4 - 12)			
% Hepatic Activity Remaining	Static Model: 16 (11 - 23) and Dynamic Model: 13 (6 - 29)			
f_u				
HLM at 0.1 mg/mL*	0.48	0.52	0.42	0.47
HLM at 1.0 mg/mL*	0.09	0.1	0.07	0.07
Plasma*	0.2	0.14	0.2	0.13

*Data from Chapter 3. N.A. indicates a value that is not applicable

Table 4.2. The effect of fluoxetine on dextromethorphan, dextrorphan, omeprazole and 5-hydroxyomeprazole pharmacokinetics. Values are given as before (control) and after (treatment) daily fluoxetine administration. All values are listed as geometric mean and range except for AUC, which is given as arithmetic mean and standard deviation. Values are calculated for n = 10 and n = 9 subjects for dextromethorphan and omeprazole, respectively. *, ** and *** indicate a p-value of < 0.01, < 0.001 and < 0.0001, respectively

	Control	Treatment	Treatment/Control
Dextromethorphan			
$AUC_{0\text{-}12}$ (nmol*hr/L)	37 ± 42	510 ± 220***	24 (2.2 - 94)
$AUC_{0\text{-}\infty}$ (nmol*hr/L)	58 ± 77	1600 ± 800***	51 (5.1 - 180)
Dextrorphan			
$AUC_{0\text{-}12}$ (nmol*hr/L)	27 ± 17	12 ± 5*	0.48 (0.27 - 0.89)
$AUC_{0\text{-}\infty}$ (nmol*hr/L)	29 ± 18	28 ± 17	0.91 (0.47 - 1.4)
AUC_m/AUC_p	0.88 (0.047 - 2.9)	0.016 (0.0043 - 0.038)**	0.018 (0.0062 - 0.091)
U_m/U_p	8.2 (1.0 - 37)	0.058 (0.026 - 0.10)*	0.0068 (0.0014 - 0.051)
Omeprazole			
$AUC_{0\text{-}12}$ (µmol*hr/L)	1.2 ± 0.6	8.5 ± 3.4***	7.5 (4.4 - 20)
$AUC_{0\text{-}\infty}$ (µmol*hr/L)	1.2 ± 0.6	8.5 ± 3.6**	7.4 (4.4 - 20)
5-Hydroxyomeprazole			
$AUC_{0\text{-}12}$ (µmol*hr/L)	1.0 ± 0.4	0.97 ± 0.30	0.99 (0.68 - 1.5)
$AUC_{0\text{-}\infty}$ (µmol*hr/L)	1.0 ± 0.4	1.1 ± 0.3	1.0 (0.69 - 1.7)
AUC_m/AUC_p	0.90 (0.32 - 3.3)	0.12 (0.045 - 0.21)*	0.13 (0.063 - 0.20)

Table 4.3. The disposition of CYP3A4 probes in the presence (treatment) and absence (control) of fluoxetine. None of the values were significantly different ($p > 0.05$) between control and treatment. The calculated minimum % detectable change from control to treatment for each measure is listed assuming a $\beta = 0.20$. All values are listed as geometric mean and range except for AUC and concentration (C_p and C_m), which are arithmetic means with standard deviations.

	Control	Treatment	Minimum % Change
Midazolam			
$AUC_{0\text{-}12}$ (nmol*hr/L)	29 ± 26	23 ± 16	32%
$AUC_{0\text{-}\infty}$ (nmol*hr/L)	30 ± 27	24 ± 17	34%
Cl (L/hr)	300 (67 - 1000)	340 (110 - 1300)	N.D.
$t_{1/2}$ (hr)	2.2 (1.6 - 3.5)	2.3 (1.4 - 4.0)	N.D.
Lovastatin			
$AUC_{0\text{-}12}$ (nmol*hr/L)	130 ± 50	130 ± 40	18%
$AUC_{0\text{-}\infty}$ (nmol*hr/L)*	180 ± 90	170 ± 70	24%
Cl (L/hr)*	300 (130 - 780)	320 (160 - 620)	N.D.
$t_{1/2}$ (hr)*	5.1 (3.3 - 10)	4.4 (2.8 - 8.9)	N.D.
Cortisol			
C_p (nM)	140 ± 60	160 ± 80	N.D.
Cl_r (mL/hr)	36 (9.0 - 77)	35 (16 - 80)	N.D.
Cortisone			
C_p (nM)	27 ± 9	23 ± 5	N.D.
Cl_r (L/hr)	0.43 (0.14 - 1.2)	0.48 (0.14 - 0.91)	N.D.
6β-hydroxycortisol			
C_m (nM)	1.3 ± 0.5	1.6 ± 1.2	N.D.
Cl_r (L/hr)	4.2 (0.85 - 30)	3.4 (0.43 - 13)	N.D.
Cl_f (mL/hr)	40 (5.8 - 340)	28 (6.8 - 130)	160%
U_m/U_p	1.1 (0.25 - 5.8)	0.79 (0.17 - 3.0)	110%
C_m/C_p	0.010 (0.0069 - 0.014)	0.0083 (0.0037 - 0.017)	31 %
6β-hydroxycortisone			
C_m (nM)	0.11 ± 0.04	0.11 ± 0.05	N.D.
Cl_r (L/hr)	25 (13 - 68)	19 (7.1 - 30)	N.D.
Cl_f (mL/hr)	100 (38 - 390)	87 (39 - 190)	73%
U_m/U_p	0.24 (0.10 - 0.56)	0.18 (0.082 - 0.91)	87%
C_m/C_p	0.0041 (0.0025 - 0.0063)	0.0046 (0.0023 - 0.0075)	23 %

Values are calculated for n = 10, except for the lovastatin parameters marked with an asterisk, which were determined for an n = 7. N.D. indicates a value that was not determined.

Chapter 5

Overall Discussion

The work presented in this chapter was, in part, previously published

in

Expert Opinion in Drug Metabolism and Toxicology 6(9):1095-1109 (2010).

5.1 Importance of predicting metabolite disposition and metabolite-dependent DDIs

Due to recent FDA and EMA guidance, interest in better understanding drug metabolites during new drug development has increased. This thesis study was conducted to improve the understanding of metabolite disposition and develop methods that can be incorporated to understand the role that drug metabolites play in drug toxicity and DDIs. The focus was toward improving predictions of *in vivo* metabolite disposition and metabolite-dependent DDIs from *in vitro* data. The results presented in this thesis will improve assessment of metabolite safety and DDI liability during new drug development. Additionally, these results will improve the ability to rationalize disproportionate *in vivo* metabolite exposure predicted from *in vitro* metabolite formation clearance and *in vivo* DDIs inaccurately predicted from parent *in vitro* inhibition.

5.2 *In vitro*-to-*in vivo* prediction of metabolite disposition

5.2.1 Accuracy and limitations of the proposed model

An *in vitro*-to-*in vivo* model was developed to predict *in vivo* AUC_m/AUC_p from *in vitro* metabolite formation and elimination data. An important finding of this model is that characterization of metabolite formation clearance is necessary for understanding *in vitro* metabolite disposition. The model was validated using two model systems, dextromethorphan with dextrorphan and omeprazole with 5-hydroxyomeprazole and omeprazole sulfone. The *in vivo* dextrorphan/dextromethorphan, 5-hydroxyomeprazole/omeprazole and omeprazole sulfone/omeprazole AUC_m/AUC_p values were well predicted from *in vitro* data (Table 2.2). It is unlikely that any inaccuracies in the AUC_m/AUC_p predictions are a result of *in vitro*-to-*in vivo* scaling because, when utilizing a ratio as the primary predicted measure, any systematic error made in the scaling of *in vitro*-to-*in vivo* clearance (Cl) is negated, although random error in the

prediction will propagate in the AUC_m/AUC_p. An interesting outcome of this thesis study is that in comparison to parent Cl predictions, the AUC_m/AUC_p predicts with similar accuracy (Obach, 1999; Ito and Houston, 2004) suggesting that important human metabolites can be quantitatively predicted using *in vitro* data.

Although accurate prediction of AUC_m/AUC_p is obtainable, several limitations to the model exist. One obvious limitation to this model is that it can only address the disposition of primary metabolites formed after parent administration. Theoretically, the same necessity of predicting both formation and elimination are relevant for subsequent downstream metabolites making quantitative predictions of downstream metabolites very challenging. However, if primary metabolites are used in *in vitro* incubation experiments, the likelihood of qualitatively identifying downstream metabolites is greatly increased. Renal clearance (Cl_r) as well as biliary excretion and gut metabolism are often important elimination pathways for xenobiotics, especially metabolites. These pathways were not considered for either the parent or metabolite in this thesis study and it is likely that, to be fully applicable in new drug development, prediction of the total Cl of the metabolite (sum of predicted Cl_h and Cl_r) will be necessary. Unfortunately *in vitro*-to-*in vivo* prediction models for prediction of Cl_r, transport and gut metabolism are currently not as well established as Cl_h predictions. Nonetheless, the preliminary success of the predictions indicates that *in vitro*-to-*in vivo* prediction of AUC_m/AUC_p, after further development and validation, could prove to be a useful tool in addressing metabolite-related concerns in new drug development.

The *in vitro*-to-*in vivo* prediction model developed in Chapter 1 and validated in Chapter 2 was designed to predict the outcome of AUC_m/AUC_p. Oftentimes, the pharmacologic or toxicologic effect is a function of the maximum concentration (C_{max}) rather than total body exposure. Predictions of metabolite C_{max} would require additional parametric information about the input and disposition rates of both the parent and the metabolite, obtainable only after *in*

vivo administration of the compounds. Based on available pharmacokinetic theory, the AUC_m/AUC_p is the most appropriate value to be used as the relevant outcome measure of metabolite exposure in *in vitro*-to-*in vivo* prediction. Since this value does not depend on dose or the F_a of the parent drug (assuming linear pharmacokinetics), it is a more robust and generally applicable measure of metabolite exposure than the dose-dependent measure of absolute AUC_m. Predicting absolute AUC_m would require knowledge of the clinical dose of the parent drug and prediction of its F_a. Additionally, the predicted AUC_m/AUC_p, when multiplied by the expected clinically effective average steady-state parent concentration, can be used to determine prior to human studies the approximate absolute concentration of the metabolite.

5.2.2 Importance of understanding *in vitro* and *in vivo* metabolite clearance

This thesis study shows that, as predicted by original metabolite kinetic theory, for any quantitative or semi-quantitative prediction of metabolite abundance or relative importance *in vivo*, the *in vivo* elimination clearance of the metabolite (Cl_m) has to be predicted or rationalized in addition to basic metabolite profiling *in vitro*. This is shown by the fact that scaling of *in vitro* metabolite elimination was necessary for accurate prediction of *in vivo* AUC_m/AUC_p and further bolstered by the fact that the *in vivo* abundance of metabolites of a given drug are no more likely to rank order correctly based on *in vitro* formation clearance (Cl_f) values than when left to random probability (Table 1.1). Although the equally important role of metabolite elimination and metabolite formation in metabolite disposition *in vivo* is generally known, this concept was never applied to *in vitro*-to-*in vivo* prediction in preclinical new drug development prior to this thesis study. Inclusion of Cl_m and Cl_f values in predictions allows prediction of *in vivo* AUC_m/AUC_p or, if AUC_p is known, the absolute AUC_m from *in vitro* data. It is interesting that the early metabolite kinetic theory has not been thoroughly reexamined in light of modern experimental approaches. It is likely that better understanding of metabolite disposition can be obtained by further testing

in vitro-to-*in vivo* prediction models applied to metabolites, even by using a relatively simplistic model detailed in this thesis study. It would also be beneficial if such models would be further developed and validated. This is important not only to address the MIST guidance, but also to improve our current understanding of the *in vivo* pharmacokinetics of probe metabolic ratios that are used in DDI studies as well as in pharmacogenetic studies.

Metabolite/parent ratios are increasingly being utilized as specific *in vivo* P450 measures (Streetman *et al.*, 2000). When a metabolite is considered pharmacokinetically relevant, the enzymes responsible for the elimination of that metabolite should be identified for proper interpretation of DDI and genetic polymorphism studies. When a metabolite is considered pharmacologically relevant, again, these secondary metabolic pathways should be identified in order to understand the therapeutic impact of said DDI or genetic polymorphism. There is a dearth of literature on *in vitro* metabolite Cl_i values, and this thesis study suggests that there is a great need to generate more metabolite relevant *in vitro* kinetic data. Even metabolite/parent pairs that are commonly utilized as *in vivo* P450 probes possess metabolite elimination pathways that are not kinetically characterized. For example, the urinary or plasma ratio of dextrorphan and dextromethorphan is a common probe for phenotyping CYP2D6 (Figure 2.1), yet the major elimination pathway of dextrorphan is via glucuronidation, a pathway that was not previously kinetically characterized *in vitro* prior to this thesis study (Chládek *et al.*, 2000). Additionally, the plasma ratios of 5-hydroxyomeprazole and omeprazole or omeprazole sulfone and omeprazole are often used as probes for CYP2C19 and CYP3A4 drug interactions (Figure 2.2), respectively, yet neither the kinetics of 5-hydroxyomeprazole nor omeprazole sulfone metabolism were characterized *in vitro* prior to this thesis study (Abelo *et al.*, 2000; Yang *et al.*, 2009). This raises some concerns of the validity of these ratios, as genetic factors, physiological changes or DDIs affecting the unknown elimination pathways of the metabolite could result in skewed data. This phenomenon was illustrated via pharmacokinetic simulation (Figure 2.6). It

can be concluded that unaccounted effects on metabolite elimination due to *in vivo* study treatment can confound interpretation of the primary study outcome (AUC_m/AUC_p). For example, sufficient inhibition of Cl_m due to inhibitor co-administration can elicit apparent induction of metabolite Cl_f (as estimated by change in AUC_m/AUC_p) despite the fact that no intrinsic change in Cl_f exists. Inadequate accounting for these possibilities could lead to improper study outcome interpretation.

5.2.3 Advantages of the proposed model

The developed model and future models that address the same primary outcome may be useful in new drug development, allowing early attention on potential quantitatively important metabolites. Since chemical synthesis of metabolites can be time consuming, expensive and difficult, it is likely that predictions of Cl_m need to be obtained from minimal amounts of primary metabolites generated in *in vitro* systems and isolated using chromatographic methods to justify investment of resources to synthesis of reference materials. However, the obtained predictions can be used to guide prioritization of synthetic efforts of metabolite standards. It is noteworthy, that intrinsic Cl_m of a metabolite can be predicted from a substrate depletion experiment conducted at a concentration below K_m of the metabolite (Mohutsky *et al.*, 2006; Nath and Atkins, 2006). Additionally, pre-clinical animal studies can be utilized not only to determine the absolute abundance of a metabolite after parent administration, but also to examine the overall pharmacokinetics of the metabolite after administration of the metabolite or the parent. This data can be leveraged for *in vivo* human metabolite kinetic prediction and may provide further confidence in the *in vivo* predictions of Cl_m and AUC_m/AUC_p from *in vitro* data.

5.2.4 Prediction of metabolite disposition: conclusions

In conclusion, the *in vivo* AUC_m/AUC_p can be predicted from *in vitro* Cl_f and Cl_m data, but the developed *in vitro*-to-*in vivo* prediction method has significant limitations (i.e. the need for validated metabolite standards) and warrants further research. Additionally, treatment effects on *in vivo* metabolite elimination clearance can cause misinterpretation of AUC_m/AUC_p when used as a P450 probe measure, indicating the need for better understanding of metabolite elimination *in vitro* and *in vivo*, prior to probe measure validation. The results of this thesis study will prove useful for better prediction of *in vivo* metabolite disposition during new drug development and proper interpretation of *in vivo* AUC_m/AUC_p probe measures in DDI and genetic polymorphism studies.

5.3 *In vitro*-to-*in vivo* prediction of metabolite-dependent DDIs

5.3.1 Challenges of studying the role of inhibitory metabolites

In vivo P450 inhibition due to inhibitory metabolites is of increasing concern and recent FDA and EMA guidance state that better characterization of inhibitory metabolites during new drug development is important (http://www.fda.gov/downloads/Drugs/GuidanceComplianceRegulatoryInformation/Guidances/ucm292362.pdf and http://www.ema.europa.eu/docs/en_GB/document_library/Scientific_guideline/2012/07/WC500129606.pdf). Despite this fact, only a handful of studies have investigated whether or not inclusion of metabolite *in vitro* inhibition improves *in vivo* DDI prediction accuracy (Reese *et al.*, 2008; Zhang *et al.*, 2009b; Templeton *et al.*, 2010) and there is no consensus on how to appropriately incorporate multiple (i.e. parent and metabolite) *in vitro* reversible or time-dependent inhibitors into *in vivo* DDI prediction models. This thesis study aimed to better understand the role of inhibitory metabolites in *in vivo* DDIs and determine prudent methods for predicting *in vivo* metabolite-dependent DDIs.

Fluoxetine was chosen as the model system for the study of metabolite-dependent DDIs because it is a secondary alkylamine MIC-forming TDI with a circulating N-dealkylated metabolite, norfluoxetine. This system demonstrates challenges for DDI prediction because of 1) *in vitro* stereoselective P450 inhibition and stereoselective *in vivo* disposition, 2) multiple P450 inhibition and 3) both reversible as well as time-dependent inhibition mechanism involvement by parent and metabolite. The advantages of using fluoxetine as a model system are that it allows for the study of norfluoxetine in DDI prediction of both *in vitro* reversible and time-dependent inhibition, depending on which P450 is examined (reversible inhibition with CYP2D6 and time-dependent inhibition with CYP2C19 or CYP3A4). Additionally, this system allows for the simultaneous determination of fluoxetine and norfluoxetine *in vivo* CYP2D6, CYP2C19 and CYP3A4 inhibition when using a probe cocktail approach, eliminating many inter-subject, inter-day and inter-study confounding variables that could occur when determining *in vivo* P450 inhibition separately.

For both *in vitro* reversible and time-dependent inhibition, conflicting models for incorporating inhibitory metabolites into DDI prediction have been presented in the literature. For reversible inhibition, it was believed that a different prediction model would have to be employed if parent and metabolite inhibited the P450 via different reversible inhibition mechanisms (competitive, non-competitive, etc.) (Equation 1.12) as opposed to an identical competitive mechanism (Equation 1.13) (Rostami-Hodjegan and Tucker, 2004). This was mathematically determined to be a false assumption and the inhibitory effect of multiple inhibitors can be summed during DDI prediction (irrespective of reversible inhibition mechanism) when object drug circulates at *in vivo* unbound concentrations well below its *in vitro* P450 K_m (Equation 1.19). Similarly, two competing models for DDI prediction of parent and metabolite time-dependent inhibition exist (Zhang *et al.*, 2009b; Rowland Yeo *et al.*, 2010), differing as to whether or not time-dependent inhibition is attenuated by mutual reversible inhibition (Equations

1.23 versus 1.24). The results of this thesis study demonstrate that the inhibitor-inhibitor interaction model (Equation 1.24) is more kinetically accurate, but both models yield identical predictions when both parent and metabolite TDIs circulate at *in vivo* unbound concentrations below *in vitro* K_I or IC_{50} values (Table 3.3 and Figure 3.7). The validation and simplification of parent and metabolite inhibition DDI prediction models allows for the application of predicting reversible and time-dependent inhibition by fluoxetine and norfluoxetine. Additionally, these models can be applied to prediction of *in vivo* DDIs that result from administration of racemic mixtures of inhibitor stereoisomers or multiple coadministered inhibitors, two multiple-inhibitor systems that can occur *in vivo* and may result in unanticipated DDIs when predicted using inappropriate single inhibitor models.

5.3.2 Assessment of metabolite-dependent DDI prediction accuracy

Based on I/K_i values, (S)-norfluoxetine and (S)-fluoxetine are predicted to contribute the most to observed *in vivo* CYP2D6 inhibition, providing initial evidence that accounting for (S)-norfluoxetine inhibition is crucial for accurate prediction of *in vivo* CYP2D6 inhibition. Indeed, 12 daily doses of oral fluoxetine increased dextromethorphan AUC by 51-fold (Figure 4.3 and Table 4.2), indicating that fluoxetine is a strong *in vivo* inhibitor (AUC'/AUC > 5) of CYP2D6, but this DDI was ultimately under-predicted from *in vitro* inhibition data. Using reversible CYP2D6 inhibition constants for the enantiomers of fluoxetine and norfluoxetine, dextromethorphan AUC'/AUC of 9 - 11 (Chapter 4) was predicted. If norfluoxetine enantiomers are not considered in the prediction, a dextromethorphan AUC'/AUC of 5 - 7 is predicted, indicating significant improvement in prediction accuracy when incorporating metabolite reversible inhibition, despite overall under-prediction. Based on multiple linear regression analysis and the discrepancy between *in vivo* and *in vitro* $K_{i,u}$ values for (S)-norfluoxetine reversible inhibition of CYP2D6, the under-prediction is most likely due to accumulation of (S)-norfluoxetine in the hepatocyte.

(S)-Norfluoxetine and (R)-fluoxetine were predicted to contribute the most to *in vivo* CYP2C19 inhibition, based on λ/k_{deg} values (Tables 3.1 and 4.1), providing initial evidence of the importance of norfluoxetine in *in vivo* CYP2C19 inhibition. *In vivo*, 12 daily doses of fluoxetine increased omeprazole AUC by 7.5-fold, indicating strong *in vivo* CYP2C19 inhibition (Figure 4.4 and Table 4.2). Predicting this DDI based on stereospecific time-dependent *in vitro* inhibition values for fluoxetine and norfluoxetine yielded an accurate (0.5 < predicted/observed AUC'/AUC < 2) prediction (AUC'/AUC of 9 – 11), but this DDI is only predicted accurately due to attenuation of AUC'/AUC because of the omeprazole f_m by CYP2C19 (f_m = 0.93). To elaborate, CYP2C19 polymorphism studies demonstrate an increase in omeprazole AUC by 14 (Furuta *et al.*, 1999) indicating the maximum possible predicted AUC'/AUC and hence, predicted AUC'/AUC due to fluoxetine and norfluoxetine inhibition mathematically cannot be greater than a 2-fold over-prediction of the observed AUC'/AUC (7.5-fold). In fact, *in vivo* CYP2C19 Cl_i/Cl_i' is predicted to be 33-50, indicating significant AUC'/AUC attenuation due to f_m. Interestingly, if norfluoxetine enantiomer time-dependent inhibition is not incorporated into the static DDI prediction, a more accurate AUC'/AUC of 7 - 9 is predicted. This finding suggests that incorporation of norfluoxetine time-dependent inhibition worsens prediction accuracy, a result in stark contrast to that observed with reversible CYP2D6 inhibition. Other confounding variables, such as specific inhibitor hepatocyte partitioning, could explain this P450 and/or mechanism-dependent prediction discrepancy, indicating that this explanation may not suffice. Therefore, further investigation into the *in vivo* contribution of each inhibitor to not only positive CYP2D6 and CYP2C19 inhibition but also negative CYP3A4 inhibition is warranted.

In the studies reported in this thesis, (R)-norfluoxetine is predicted to contribute the most to any observed *in vivo* CYP3A4 inhibition, based on λ/k_{deg} values (Tables 3.1 and 4.1). Significant intestinal and hepatic CYP3A4 inhibition is predicted to occur *in vivo* (Figure 4.1), but no change in midazolam AUC after 12 days of fluoxetine administration and no change in

lovastatin AUC after 14 days of fluoxetine administration was observed *in vivo*. This false-positive prediction is difficult to rationalize, but can be better understood when put into context of how well DDI liability is predicted for TDIs in general. Figure 5.1 depicts the unbound λ/k_{deg} versus *in vivo* probe drug AUC'/AUC for 21 *in vitro* TDIs predicted from literature data (adapted from Fujioka *et al.* (2012)). Also shown are the predicted and observed fluoxetine DDIs with midazolam and omeprazole from this thesis study. The green areas are true predictions, whereas the red areas indicate false-positive (lower right) and false-negative (upper left) predictions. What can be concluded is that most TDIs predict true, i.e. a DDI is predicted to be likely and is also observed *in vivo*. No false-negative predictions were determined in this dataset, but several false-positive predictions existed. Except for dasatinib and fluoxetine (towards CYP3A4), all false-positive predictions can be rationalized by the fact that either a low sensitivity probe drug was used or simultaneous P450 induction occurred *in vivo* (Fujioka *et al.*, 2012). Midazolam and lovastatin are both highly sensitive CYP3A4 probe drugs, but it is possible that fluoxetine- and/or norfluoxetine-mediated CYP3A4 induction is occurring *in vivo*, masking the true decrease in CYP3A4 activity. Fluoxetine was previously determined to be a weak CYP3A4 inducer *in vitro* (maximum 2-fold induction) (Fahmi *et al.*, 2009), but norfluoxetine induction potential is not known. A total *in vivo* CYP3A4 induction of approximately 6- to 12-fold would be required to negate the predicted effects of *in vivo* CYP3A4 inhibition. Further *in vitro* research is warranted to determine if CYP3A4 induction is responsible for the observation of false-positive CYP3A4 DDI prediction from fluoxetine and norfluoxetine *in vitro* inhibition data.

The false-positive CYP3A4 DDI prediction observed in this thesis study may be further rationalized by the realization that negative-to-weak DDI prediction accuracy is highly dependent on accurate *in vitro* TDI characterization and *in vivo* P450 k_{deg} determination. Figure 5.2 is a conceptual diagram of DDI prediction accuracy sensitivity as a function of DDI magnitude. The green and red lines represent the change in prediction accuracy sensitivity due

to inhibitor-specific (K_I and k_{inact}) or P450-specific (k_{deg}) values and probe-specific (f_m and F_g) values, respectively. Prediction of strong DDIs is highly dependent on accurate determination of *in vivo* probe values (i.e. the predicted fluoxetine-omeprazole DDI is highly dependent on omeprazole f_m). Pertaining to false-positive CYP3A4 prediction, determination of *in vivo* k_{deg} is challenging and many different estimates for CYP3A4 have been reported (Venkatakrishnan and Obach, 2007). Due to experimental limitations in weak (S)-fluoxetine and (R)-norfluoxetine time-dependent CYP3A4 inhibition characterization in HLMs, the K_I values for both inhibitors are not well characterized (Figure 3.2 ad Table 3.1), possibly decreasing DDI prediction accuracy. Hepatocytes allow for longer incubation times and decreased yet quantifiable k_{inact} values compared to HLMs (Kirby *et al.*, 2011), resulting in more precise and possibly more *in vivo* representative *in vitro* TDI determination. Future studies should entail time-dependent inhibition characterization of fluoxetine and norfluoxetine enantiomers in human hepatocytes to determine if a CYP3A4 DDI is still predicted to occur *in vivo.* Furthermore, hepatocytes may decrease the occurrence of false-positive DDI prediction of *in vitro* TDIs, decreasing the need to conduct unnecessary negative *in vivo* DDI studies during new drug development.

5.3.3 Advantages of using an *in vivo* probe cocktail approach and rationalization of prediction inaccuracies

One of the most commonly cited reasons for DDI prediction failure is use of incorrect inhibitor plasma concentrations to drive the predicted interaction (Galetin *et al.*, 2007; Obach *et al.*, 2007; Venkatakrishnan and Obach, 2007; Obach, 2009). The advantage of using an *in vivo* probe cocktail approach to determine *in vivo* P450 inhibition after fluoxetine administration is that all P450s were subject to identical unbound inhibitor concentrations. Despite this fact, under-prediction of reversible CYP2D6 inhibition, accurate prediction of time-dependent CYP2C19 inhibition and over-prediction of time-dependent CYP3A4 inhibition was initially

observed (Chapter 4). As previously stated, (S)-norfluoxetine is predicted to play an important role in both CYP2D6 and CYP2C19 *in vivo* inhibition, but little role in CYP3A4 *in vivo* inhibition. Furthermore, stepwise multiple linear regression analysis of dextromethorphan AUC'/AUC indicates that the majority of *in vivo* CYP2D6 inhibition is explained by (S)-norfluoxetine concentrations (Figure 4.3) and a lower $K_{i,u,IV}$ compared to *in vitro* $K_{i,u}$ suggests that (S)-norfluoxetine partitions considerably into the hepatocyte. If an approximate 16-fold increase in hepatic (S)-norfluoxetine concentrations versus plasma and no inhibition by the other inhibitors is assumed, (S)-norfluoxetine *in vitro* data accurately predicts observed *in vivo* CYP2D6 and CYP2C19 *in vivo* inhibition. Additionally, no clinically significant CYP3A4 inhibition is predicted and the observed P450 inhibition magnitude rank order is predicted correctly (CYP2D6 > CYP2C19 >> CYP3A4). Further *in vitro* data is necessary to confirm the apparent result of (S)-norfluoxetine partitioning and its role as the primary inhibitory species *in vivo*. Until this result is confirmed, the initial determined inaccurate predictions cannot be disregarded and it should be concluded that time-dependent inhibition is systematically over-predicted, based on the fact that false-positive prediction of *in vivo* CYP3A4 inhibition occurs and CYP2C19 inhibition prediction accuracy may be driven by CYP2C19 f_m of omeprazole. As previously stated, this over-prediction may be due to the use of HLMs in *in vitro* inhibition determination. An alternative hypothesis is that systematic inaccuracy in DDI prediction of TDIs is due to unaccounted for metabolic complexity in both *in vitro* TDI characterization and *in vivo* DDI prediction. This hypothesis may be particularly applicable to alkylamine metabolic-intermediate complex (MIC) forming TDIs such as fluoxetine.

5.3.4 Metabolic complexity of time-dependent inhibition

Fluoxetine and norfluoxetine are secondary and primary alkylamines, respectively. It has been determined that both species can undergo hydroxylation and ultimate convergent

metabolism to the nitrosoalkane species that complexes with the heme (Figure 1.2) (Mansuy *et al.*, 1977; Kalgutkar *et al.*, 2007; Hanson *et al.*, 2010; Barbara *et al.*, 2013). Formation of the nitrosoalkane from the alkylamine requires three metabolic conversions. In theory, the nitrosoalkane does not dissociate from the P450 active site prior to complexation (Silverman, 1988), but the primary and secondary hydroxylamines may dissociate and circulate *in vivo*. *In vitro* determination of time-dependent inhibition with alkylamine TDIs is generally performed by incubating the alkylamine at varying concentrations and monitoring the ultimate decrease in P450 activity due to MIC-formation. This methodology determines an apparent time-dependent inhibition rate at a specific inhibitor concentration, ignoring downstream metabolic complexity. Furthermore, DDI prediction is performed using the apparent *in vitro* time-dependent inhibition constants and *in vivo* determined or anticipated alkylamine inhibitor plasma concentrations, once again, ignoring downstream metabolic complexity. This practice intrinsically relies on the assumption that formation of nitrosoalkane, and ultimately MIC, is linear and constant relative to alkylamine concentration both *in vitro* and *in vivo*. It is reasonable to think that this assumption may not be valid due to differences in P450 conformation and environment between *in vitro* and *in vivo*. It is hypothesized that DDI prediction utilizing *in vitro* characterization of primary and secondary hydroxylamine time-dependent inhibition and *in vivo* quantitation of primary and secondary hydroxylamine plasma concentrations will improve prediction accuracy of MIC-forming TDIs compared to predictions relying on the respective upstream primary and secondary alkylamines. Yet, this hypothesis has not been examined.

5.3.5 Prediction of metabolite-dependent DDIs: conclusions

In conclusion, inhibitory metabolites are predicted to play a significant role in *in vivo* P450 inhibition. Although significant challenges and uncertainties still exist in the quantitative prediction of *in vivo* DDIs from *in vitro* inhibition data, adequate risk assessment of *in vivo* DDI

liability using existing models can be obtained. Often, time-dependent inhibition is the result of a complex metabolite-dependent process and this complexity should be accounted for if better prediction of DDIs due to parent and/or metabolite time-dependent inhibition is to be obtained. The results of this thesis study are useful in better predicting the contribution of inhibitory metabolites in *in vivo* DDIs during new drug development.

5.4 Mass spectrometry and hepatocytes as tools for better prediction of metabolite disposition and metabolite-dependent DDIs

5.4.1 Advancements in reference-free metabolite quantitation

One of the biggest limitations in predicting *in vivo* metabolite disposition and metabolite-dependent DDIs from *in vitro* data during new drug development is the availability of validated metabolite chemical standards. Prediction of AUC_m/AUC_p requires metabolic incubation with the primary metabolite as substrate of interest to determine depletion clearance. Furthermore, prediction of metabolite-dependent DDIs requires metabolic incubation with the metabolite(s) as inhibitor(s) to determine the magnitude of reversible and/or time-dependent P450 inhibition. Neither methodology can be applied without a metabolite standard.

Metabolite identification and structural characterization via mass spectrometry (MS) is commonplace. MS is also a highly sensitive method-of-choice for quantifying metabolites *in vitro* and *in vivo* (Ramanathan *et al.*, 2010). Often, differences in analyte MS response can be significant, even between similar chemical entities such as a parent and metabolite, (Ramanathan *et al.*, 2007), necessitating validated analyte standards for response normalization. Recently, advances in metabolite quantitation in the absence of validated standards have been developed. Coupling MS with radiometric (Ramanathan *et al.*, 2007) or UV spectroscopic (Yang *et al.*, 2011) analyses allows for MS response normalization, but

requires radiolabeled parent or the knowledge that the chromophore remains intact during metabolic transformation, respectively. Quantitative ^{1}H-NMR analysis of *in situ* generated metabolite allows for MS response normalization (Espina *et al.*, 2009), but requires generation of microgram quantities of metabolite. Coupling MS with charged aerosol detection (CAD) provides for near universal response normalization regardless of chemical structure (Cai *et al.*, 2010), but similar to UV and ^{1}H-NMR spectroscopy, this method has limited sensitivity. Methods for reducing the effect of solvent environment on MS response between parent and metabolite have been developed (captive spray ionization, post-column solvent normalization, etc.), but these methods cannot universally normalize MS response (Ramanathan *et al.*, 2007; Raghavan *et al.*, 2010). Although each method has its caveats, advancements in MS response normalization provide the ability to quantify metabolites in the absence of validated standards, *in vitro* and *in vivo*.

5.4.2 Predicting metabolite disposition without validated chemical standards

Prediction of *in vivo* AUC_m/AUC_p from *in vitro* data requires metabolic incubation with the metabolite as substrate and plated human hepatocytes yielded more accurate prediction of AUC_m/AUC_p than HLMs (Table 2.2). One additional advantage of plated human hepatocytes compared to HLMs is that longer incubation times can be employed, in the range of hours rather than minutes. Furthermore, development of plated hepatocytes co-cultured with non-parenchymal cells allows for metabolic incubations to occur over days rather than hours (Khetani and Bhatia, 2008; Wang *et al.*, 2010). It is hypothesized that the *in vitro* AUC_m/AUC_p determined (after incubation of parent drug as substrate) in plated human hepatocytes after monitoring decline of parent as well as accumulation and declination of primary metabolite will be predictive of *in vivo* AUC_m/AUC_p. The predictive ability of this methodology has never been

examined. Since primary and secondary metabolism would have to sufficiently progress in order to accurately characterize *in vitro* AUC_m/AUC_p, significant method development prior to prediction accuracy evaluation is anticipated. Additionally, this method would be hindered by similar limitations to the AUC_m/AUC_p prediction model proposed in this thesis study (i.e. metabolite must be primarily formed and eliminated via hepatic metabolism *in vivo*). When coupled with MS response normalization methods, this method could allow for prediction of *in vivo* AUC_m/AUC_p in the absence of validated metabolite standards and warrants further research.

5.4.3 Predicting metabolite-dependent TDIs without validated chemical standards

As previously discussed, time-dependent inhibition by alkylamine MIC-formers is a complex metabolite-dependent system of several metabolic steps to nitrosoalkane-heme complexation. It was earlier hypothesized that more accurate *in vitro*-to-*in vivo* DDI prediction will be obtained when the predictions are based on hydroxylamine versus alkylamine time-dependent inhibition. To address this hypothesis, sophisticated analytical methods are required. Using high-resolution MS methods, a recent study identified many of the *in vitro* downstream metabolites of lapatinib, a secondary alkylamine CYP3A4 time-dependent inhibitor, including secondary hydroxylamine, primary alkylamine and nitrosoalkane (Barbara *et al.*, 2013). This study suggests that, when coupled to MS response normalization, many of the analytical technologies to characterize the metabolic complexity of TDIs, both *in vitro* and *in vivo*, are already established. Time-dependent inhibition is traditionally characterized *in vitro* via the "two-step" methodology as used in this thesis study. *In vitro* TDI characterization via "progress curve" methodology has demonstrated significant promise for accurate DDI prediction (Burt *et al.*, 2012). This method utilizes simultaneous determination of substrate metabolite, inhibitor

and inhibitor metabolite concentrations as well as global non-linear regression to determine relevant *in vitro* time-dependent inhibition constants after incubation with substrate and parent inhibitor. When coupled with MS response normalization, *in situ* generated inhibitory metabolites can be characterized in the absence of validated metabolite standards, and these metabolites (such as hydroxylamines) could be used to drive more accurate DDI prediction. Failing that, the critical assumption of identical nitrosoalkane formation relative to alkylamine concentration *in vitro* and *in vivo,* that is employed in traditional prediction of alkylamine TDIs, could be further examined to determine its validity.

5.5 Final Thoughts

Since its inception, *in vivo* pharmacokinetic study has proven integral to understanding drug disposition, allowing for the characterization of drug concentration over time and the extrapolation of pharmacokinetic parameters between studies. *In vitro*-to-*in vivo* prediction is a powerful method to anticipate or rationalize *in vivo* pharmacokinetics, but many factors can complicate these predictions. Metabolites are not only of concern in drug safety and efficacy evaluation, but represent an aspect of *in vivo* pharmacokinetics that *in vitro-to-in vivo* prediction science has mostly neglected. The work presented in this thesis study advances the ability to predict metabolite disposition and metabolite-dependent DDIs, but many aspects still remain unexplored. Although often chemically similar to the parent drug, metabolites can have very different clearance, distribution and P450 inhibition. Recognition and characterization of the pharmacokinetic challenges that metabolites pose is imperative for the development of more accurate *in vitro*-to-*in vivo* prediction methodologies. More sophisticated MS analysis and physiologically-relevant enzyme systems will be integral in better *in vitro* and *in vivo* characterization of metabolites, but advancements in these areas must be supported by prediction models that account for metabolite complexity. Ultimately, the marriage of new

analytical, enzymatic and pharmacokinetic techniques will provide the necessary information for better anticipation and rationalization of the role of metabolites in *in vivo* pharmacology/toxicity and DDIs, improving patient safety of newly developed drugs and clinical management of existing drug therapies.

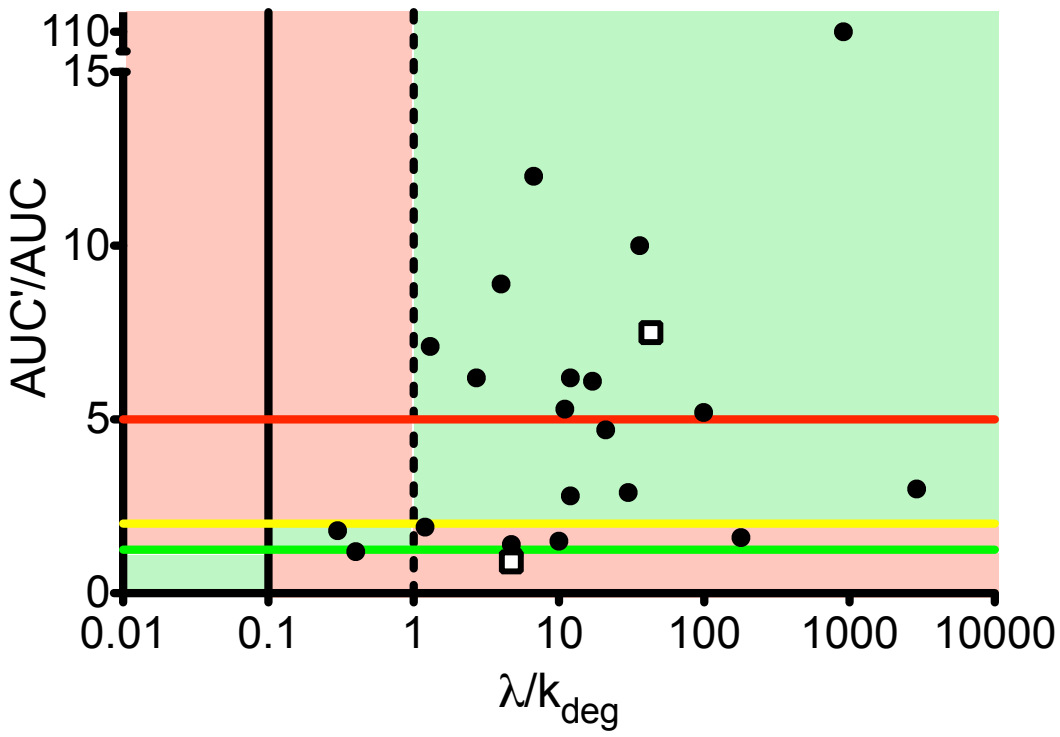

Figure 5.1. Accuracy of *in vivo* DDI risk assessment for *in vitro* TDIs. Shown are the unbound λ/k_{deg} values versus *in vivo* probe AUC'/AUC for 21 *in vitro* TDIs (adapted from Fujioka *et al.* (2012)) (black circles) as well as for the fluoxetine and midazolam (below green line) or omeprazole (above red line) DDIs as determined in this thesis study (white squares). The horizontal green, yellow and red lines indicate a probe AUC'/AUC of 1.25-, 2- and 5-fold, respectively. The vertical solid and dashed lines indicate an unbound λ/k_{deg} of 0.1 and 1, respectively. The light red and light green areas indicate false and true predictions, respectively.

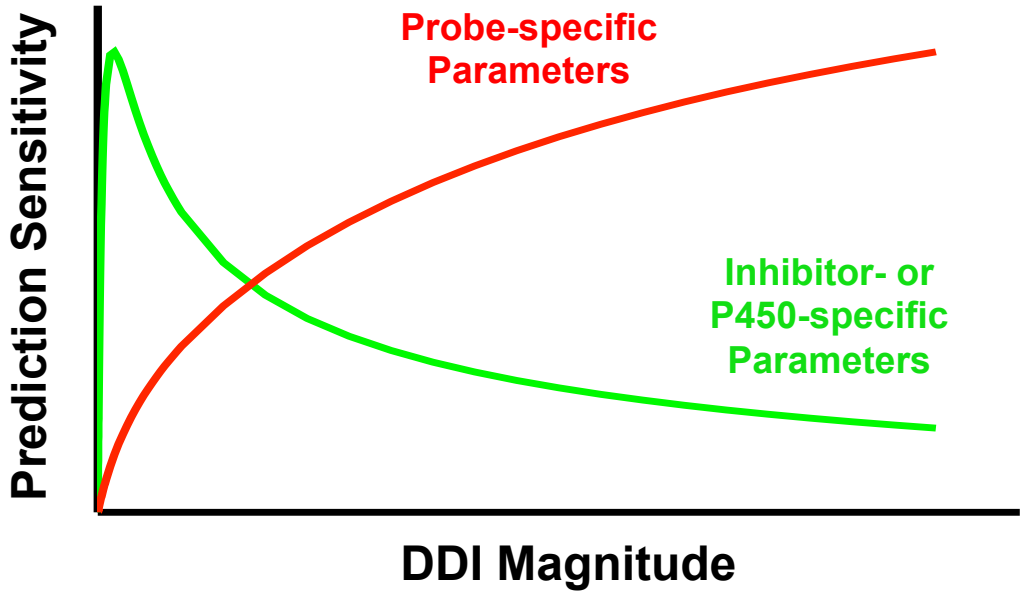

Figure 5.2. Conceptual diagram of DDI prediction accuracy sensitivity as a function of DDI magnitude. The green and red lines represent the change in prediction accuracy sensitivity due to inhibitor-specific (K_I and k_{inact}) or P450-specific (k_{deg}) values and probe-specific (f_m and F_g) values, respectively.

References

Abdul-Manap R, Wright CE, Gregory A, Rostami-Hodjegan A, Meller ST, Kelm GR, Lennard MS, Tucker GT, and Morice AH (1999) The antitussive effect of dextromethorphan in relation to CYP2D6 activity. *Br J Clin Pharmacol* **48:**382-387.

Abduljalil K, Frank D, Gaedigk A, Klaassen T, Tomalik-Scharte D, Jetter A, Jaehde U, Kirchheiner J, and Fuhr U (2010) Assessment of activity levels for CYP2D6*1, CYP2D6*2, and CYP2D6*41 genes by population pharmacokinetics of dextromethorphan. *Clin Pharmacol Ther* **88:**643-651.

Abelo A, Andersson TB, Antonsson M, Knuts-Naudot A, Skanberg I, and Weidolf L (2000) Stereoselective metabolism of omeprazole by human cytochrome P450 enzymes. *Drug Metab Dispos* **28:**966-972.

Akinyinka OO, Sowunmi A, Honeywell R, and Renwick AG (2000) The effects of acute falciparum malaria on the disposition of caffeine and the comparison of saliva and plasma-derived pharmacokinetic parameters in adult Nigerians. *Eur J Clin Pharmacol* **56:**159-165.

Akiyoshi J, Isogawa K, Yamada K, Nagayama H, and Fujii I (1996) Effects of antidepressants on intracellular Ca2+ mobilization in CHO cells transfected with the human 5-HT2C receptors. *Biol Psychiatry* **39:**1000-1008.

Altamura AC, Moro AR, and Percudani M (1994) Clinical pharmacokinetics of fluoxetine. *Clin Pharmacokinet* **26:**201-214.

Anderson S, Luffer-Atlas D, and Knadler MP (2009) Predicting human circulating metabolites: how good are we? *Chem Res Tox* **22:**243-256.

Andersson T, Miners JO, Veronese ME, and Birkett DJ (1994) Identification of human liver cytochrome P450 isoforms mediating secondary omeprazole metabolism. *Br J Clin Pharmacol* **37:**597-604.

Andersson T, Miners JO, Veronese ME, Tassaneeyakul W, Tassaneeyakul W, Meyer UA, and Birkett DJ (1993) Identification of human liver cytochrome P450 isoforms mediating omeprazole metabolism. *Br J Clin Pharmacol* **36:**521-530.

Angiolillo DJ, Gibson CM, Cheng S, Ollier C, Nicolas O, Bergougnan L, Perrin L, LaCreta FP, Hurbin F, and Dubar M (2010) Differential effects of omeprazole and pantoprazole on the pharmacodynamics and pharmacokinetics of clopidogrel in healthy subjects: randomized, placebo-controlled, crossover comparison studies. *Clin Pharmacol Ther* **89:**65-74.

Barbara JE, Kazmi F, Parkinson A, and Buckley DB (2013) Metabolism-dependent inhibition (MDI) of CYP3A4 by lapatinib: evidence for formation of a metabolic intermediate (MI) complex with a nitroso/oxime metabolite formed via a nitrone intermediate. *Drug Metab Dispos*.

Basci NE, Bozkurt A, Kayaalp SO, Sayal A, and Isimer A (1998) Omission of the deconjugation step in urine analysis and the unaltered outcome of CYP2D6 phenotyping with dextromethorphan. *Eur J Drug Metab Pharmacokinet* **23:**1-5.

Bauman JN, Frederick KS, Sawant A, Walsky RL, Cox LM, Obach RS, and Kalgutkar AS (2008) Comparison of the bioactivation potential of the antidepressant and hepatotoxin nefazodone with aripiprazole, a structural analog and marketed drug. *Drug Metab Dispos* **36:**1016-1029.

Belle DJ, Ernest CS, Sauer JM, Smith BP, Thomasson HR, and Witcher JW (2002) Effect of potent CYP2D6 inhibition by paroxetine on atomoxetine pharmacokinetics. *J Clin Pharmacol* **42:**1219-1227.

Bergstrom RF, Peyton AL, and Lemberger L (1992) Quantification and mechanism of the fluoxetine and tricyclic antidepressant interaction. *Clin Pharmacol Ther* **51:**239-248.

Bertilsson L, Tybrin G, Widén J, Chang M, and Tomson T (1997) Carbamazepine treatment induces the CYP3A4 catalysed sulphoxidation of omeprazole, but has no or less effect on hydroxylation via CYP2C19. *Br J Clin Pharmacol* **44:**186-189.

Böttiger Y, Tybring G, Götharson E, and Bertilsson L (1997) Inhibition of the sulfoxidation of omeprazole by ketoconazole in poor and extensive metabolizers of S-mephenytoin. *Clin Pharmacol Ther* **62:**384-391.

Brunton LL, Chabner BA, and Knollmann BC (2011) *Goodman & Gilman's The Pharmacological Basis of Therapeutics*. McGraw-Hill Company, Inc., Columbus, OH.

Buch AB, Van Harken DR, Seidehamel RJ, and Barbhaiya RH (1993) A study of pharmacokinetic interaction between buspirone and alprazolam at steady state. *J Clin Pharmacol* **33:**1104-1109.

Burt HJ, Pertinez H, Sall C, Collins C, Hyland R, Houston JB, and Galetin A (2012) Progress curve mechanistic modeling approach for assessing time-dependent inhibition of CYP3A4. *Drug Metab Dispos* **40:**1658-1667.

Cai H, Josephs J, Ramanathan R, Crafts C, Bailey B, and Humphreys W (Year) A novel detection technology: charged aerosol detection coupled with HPLC, UV and LTQ-orbitrap MS for drug metabolism studies, Presented at: *58th ASMS Conference on Mass Spectrometry and Allied Topics*, Salt Lake City, UT, USA.

Carlile DJ, Hakooz N, Bayliss MK, and Houston JB (1999) Microsomal prediction of *in vivo* clearance of CYP2C9 substrates in humans. *Br J Clin Pharmacol* **47:**625-635.

Chiba K, Kato M, Ito T, Suwa T, and Sugiyama Y (2012) Inter-individual variability of in vivo CYP2D6 activity in different genotypes. *Drug Metab Pharmacokinet* **27:**405-413.

Chládek J, Zimová G, Beránek M, and Martínková J (2000) *In-vivo* indices of CYP2D6 activity: comparison of dextromethorphan metabolic ratios in 4-h urine and 3-h plasma. *Eur J Clin Pharmacol* **56:**651-657.

Court MH, Krishnaswamy S, Hao Q, Duan SX, Patten CJ, von Moltke LL, and Greenblatt DJ (2003) Evaluation of 3'-azido-3'-deoxythymidine, morphine and codeine as probe substrates for UDP-glucuronosyltransferase 2B7 (UGT2B7) in human liver microsomes: specificity and influence of the UGT2B7*2 polymorphism. *Drug Metab Dispos* **31:**1125-1133.

Crabb DW, Matsumoto M, Chang D, and You M (2004) Overview of the role of alcohol dehydrogenase and aldehyde dehydrogenase and their variants in the genesis of alcohol-related pathology. *Proc Nutrition Soc* **63:**49-63.

Cummings AJ, Martin BK, and Pang KS (1967) Kinetic considerations relating to the accrual and elimination of drug metabolites. *Br J Pharmac Chemother* **29:**136-149.

Desta Z, Ward BA, Soukhova NV, and Flockhart DA (2004) Comprehensive evaluation of tamoxifen sequential biotransformation by the human cytochrome P450 system *in vitro*: prominent roles for CYP3A and CYP2D6. *J Pharmacol Exp Ther* **310:**1062-1075.

Dilger K, Greiner B, Fromm MF, Hofmann U, Kroemer HK, and Eichelbaum M (1999) Consequences of rifampicin treatment on propafenone disposition in extensive and poor metabolizers of CYP2D6. *Pharmacogenetics* **9:**551-559.

Duché JC, Quérol-Ferrer V, Barré J, Mésangeau M, and Tillement JP (1993) Dextromethorphan O-demethylation and dextrorphan glucuronidation in a French population. *Int J Clin Pharmacol Ther Toxicol* **31:**392-298.

Eliot L, Butler J, Devane J, and Loewen G (2002) Pharmacokinetic evaluation of a sprinkle-dose regimen of a once-daily, extended-release morphine formulation. *Clin Ther* **24:**260-268.

Ernest CS, 2nd, Hall SD, and Jones DR (2005) Mechanism-based inactivation of CYP3A by HIV protease inhibitors. *J Pharmacol Exp Ther* **312:**583-591.

Espina R, Yu L, Wang J, Tong Z, Vashishtha S, Talaat R, Scatina J, and Mutlib A (2009) Nuclear magnetic resonance spectroscopy as a quantitative tool to determine the concentrations of biologically produced metabolites: implications in metabolites in safety testing. *Chem Res Toxicol* **22:**299-310.

Fahmi OA, Hurst S, Plowchalk D, Cook J, Guo F, Youdim K, Dickins M, Phipps A, Darekar A, Hyland R, and Obach RS (2009) Comparison of different algorithms for predicting clinical drug-drug interactions, based on the use of CYP3A4 in vitro data: predictions of compounds as precipitants of interaction. *Drug Metab Dispos* **37:**1658-1666.

Farid NA, Kurihara A, and Wrighton SA (2010) Metabolism and disposition of the thienopyridine antiplatelet drugs ticlopidine, clopidogrel, and prasugrel in humans. *J Clin Pharmacol* **50:**126-142.

Fitzgerald LW, Burn TC, Brown BS, Patterson JP, Corjay MH, Valentine PA, Sun J-H, Link JR, Abbaszade I, Hollis JM, Largent BL, Hartig PR, Hollis GF, Meunier PC, Robichaud AJ, and Robertson DW (2000) Possible Role of Valvular Serotonin 5-HT2B Receptors in the Cardiopathy Associated with Fenfluramine. *Molecular Pharmacology* **57:**75-81.

Fujioka Y, Kunze KL, and Isoherranen N (2012) Risk assessment of mechanism-based inactivation in drug-drug interactions. *Drug Metab Dispos* **40:**1653-1657.

Furuta T, Ohashi K, Kobayashi K, Iida I, Yoshida H, Shirai N, Takashima M, Kosuge K, Hanai H, Chiba K, Ishizaki T, and Kaneko E (1999) Effects of clarithromycin on the metabolism of omeprazole in relation to CYP2C19 genotype status in humans. *Clin Pharmacol Ther* **66:**265-274.

Galetin A, Hinton LK, Burt H, Obach RS, and Houston JB (2007) Maximal inhibition of intestinal first-pass metabolism as a pragmatic indicator of intestinal contribution to the drug-drug interactions for CYP3A4 cleared drugs. *Curr Drug Metab* **8:**685-693.

Ghanbari F, Rowland-Yeo K, Bloomer JC, Clarke SE, Lennard MS, Tucker GT, and Rostami-Hodjegan A (2006) A critical evaluation of the experimental design of studies of mechanism based enzyme inhibition, with implications for in vitro-in vivo extrapolation. *Curr Drug Metab* **7:**315-334.

Gilard M, Arnaud B, Cornily JC, Le Gal G, Lacut K, Le Calvez G, Mansourati J, Mottier D, Abgrall JF, and Boschat J (2008) Influence of omeprazole on the antiplatelet action of clopidogrel associated with aspirin: the randomized, double-blind OCLA (Omeprazole Clopidogrel Aspirin) study. *J Am Coll Cardiol* **51:**256-260.

Greenblatt DJ, Preskorn SH, Cotreau MM, Horst WD, and Harmatz JS (1992) Fluoxetine impairs clearance of alprazolam but not of clonazepam. *Clin Pharmacol Ther* **52:**479-486.

Greenblatt DJ, Von Moltke LL, Schmider J, Harmatz JS, and Shader RI (1996) Inhibition of human cytochrome P450-3A isoforms by fluoxetine and norfluoxetine: *in vitro* and *in vivo* studies. *J Clin Pharmacol* **36:**792-798.

Greene DS, Salazar DE, Dockens RC, Kroboth P, and Barbhaiya RH (1995) Coadministration of nefazodone and benzodiazepines: III. A pharmacokinetic interaction study with alprazolam. *J Clin Psychopharmacol* **15:**399-408.

Grimm SW, Einolf HJ, Hall SD, He K, Lim HK, Ling KH, Lu C, Nomeir AA, Seibert E, Skordos KW, Tonn GR, Van Horn R, Wang RW, Wong YN, Yang TJ, and Obach RS (2009) The conduct of *in vitro* studies to address time-dependent inhibition of drug-metabolizing enzymes: a perspective of the pharmaceutical research and manufacturers of America. *Drug Metab Dispos* **37:**1355-1370.

Grimsley SR, Jann MW, Carter JG, D'Mello AP, and D'Souza MJ (1991) Increased carbamazepine plasma concentrations after fluoxetine coadministration. *Clin Pharmacol Ther* **50:**10-15.

Hanson KL, VandenBrink BM, Babu KN, Allen KE, Nelson WL, and Kunze KL (2010) Sequential metabolism of secondary alkyl amines to metabolic-intermediate complexes: opposing

roles for the secondary hydroxylamine and primary amine metabolites of desipramine, (s)-fluoxetine, and N-desmethyldiltiazem. *Drug Metab Dispos* **38:**963-972.

He M, Kunze KL, and Trager WF (1995) Inhibition of (S)-warfarin metabolism by sulfinpyrazone and its metabolites. *Drug Metab Dispos* **23:**659-663.

Hemeryck A, De Vriendt C, and Belpaire FM (2000) Effect of selective serotonin reuptake inhibitors on the oxidative metabolism of propafenone: *in vitro* studies using human liver microsomes. *J Clin Psychopharmacol* **20:**428-434.

Hinton L, Galetin A, and Houston J (2008) Multiple inhibition mechanisms and prediction of drug–drug interactions: status of metabolism and transporter models as exemplified by gemfibrozil–drug interactions. *Pharm Res* **25:**1063-1074.

Hirota N, Ito K, Iwatsubo T, Green CE, Tyson CA, Shimada N, Suzuki H, and Sugiyama Y (2001) *In vitro/in vivo* scaling of alprazolam metabolism by CYP3A4 and CYP3A5 in humans. *Biopharm Drug Dispos* **22:**53-71.

Ho PC, Abbott FS, Zanger UM, and Chang TKH (2003) Influence of CYP2C9 genotypes on the formation of a hepatotoxic metabolite of valproic acid in human liver microsomes. *Pharmacogen J* **3:**335-342.

Houston JB (1981) Drug metabolite kinetics. *Pharmacol Ther* **15:**521-552.

Houston JB and Taylor G (1984) Drug metabolite concentration-time profiles: influence of route of drug administration. *Br J Clin Pharmacol* **17:**385-394.

Hsu A, Granneman GR, Cao G, Carothers L, el-Shourbagy T, Baroldi P, Erdman K, Brown F, Sun E, and Leonard JM (1998) Pharmacokinetic interactions between two human immunodeficiency virus protease inhibitors, ritonavir and saquinavir. *Clin Pharmacol Ther* **63:**453-464.

Ieiri I, Kishimoto Y, Okochi H, Momiyama K, Morita T, Kitano M, Morisawa T, Fukushima Y, Nakagawa K, Hasegawa J, K O, and Ishizaki T (2001) Comparison of the kinetic disposition of and serum gastrin change by lansoprazole versus rabeprazole during an 8-day dosing scheme in relation to CYP2C19 polymorphism. *Eur J Clin Pharmacol* **56:**485-492.

Ishizaki T, Chiba K, Manabe K, Koyama E, Hayashi M, Yasuda S, Horai Y, Tomono Y, Yamato C, and Toyoki T (1995) Comparison of the interaction potential of a new proton pump inhibitor, E3810, versus omeprazole with diazepam in extensive and poor metabolizers of S-mephenytoin 4'-hydroxylation. *Clin Pharmacol Ther* **58:**155-164.

Isoherranen N, Hachad H, Yeung CK, and Levy RH (2009) Qualitative analysis of the role of metabolites in inhibitory drug-drug interactions: literature evaluation based on the metabolism and transport drug interaction database. *Chem Res Toxicol* **22:**294-298.

Isoherranen N, Kunze KL, Allen KE, Nelson WL, and Thummel KE (2004) Role of itraconazole metabolites in CYP3A4 inhibition. *Drug Metab Dispos* **32:**1121-1131.

Isoherranen N, Lutz JD, Chung S, Hachad H, Levy RH, and Ragueneau-Majlessi I (2012) Importance of multi-P450 inhibition in drug-drug interactions: evaluation of incidence, inhibition magnitude and prediction from in vitro data. *Chem Res Toxicol* **25:**2285-2300.

Ito K, Hallifax D, Obach RS, and Houston JB (2005) Impact of parallel pathways of drug elimination and multiple cytochrome P450 involvement on drug-drug interactions: CYP2D6 paradigm. *Drug Metab Dispos* **33:**837-844.

Ito K and Houston JB (2004) Comparison of the use of liver models for predicting drug clearance using *in vitro* kinetic data from hepatic microsomes and isolated hepatocytes. *Pharm Res* **21:**785-792.

Jannuzzi G, Gatti G, Magni P, Spina E, Pacifici R, Zuccaro P, Torta R, Guarneri L, and Perucca E (2002) Plasma concentrations of the enantiomers of fluoxetine and norfluoxetine: sources of variability and preliminary observations on relations with clinical response. *Ther Drug Monit* **24:**616-627.

Jones DR, Gorski JC, Haehner BD, O'Mara EM, and Hall SD (1996) Determination of cytochrome P450 3A4/5 activity *in vivo* with dextromethorphan N-demethylation. *Clin Pharmacol Ther* **60:**374-384.

Jonsson KH and Lindeke B (1992) Cytochrome P-455 nm complex formation in the metabolism of phenylalkylamines. XII. Enantioselectivity and temperature dependence in microsomes and reconstituted cytochrome P-450 systems from rat liver. *Chirality* **4:**469-477.

Jung F, Richardson TH, Raucy JL, and Johnson EF (1997) Diazepam metabolism by cDNA-expressed human 2C P450s: identification of P4502C18 and P4502C19 as low Km diazepam N-demethylases. *Drug Metab Dispos* **25:**133-139.

Kalgutkar AS, Obach RS, and Maurer TS (2007) Mechanism-based inactivation of cytochrome P450 enzymes: chemical mechanisms, structure-activity relationships and relationship to clinical drug-drug interactions and idiosyncratic adverse drug reactions. *Curr Drug Metab* **8:**407-447.

Kang BC, Yang CQ, Cho HK, Suh OK, and Shin WG (2002) Influence of fluconazole on the pharmacokinetics of omeprazole in healthy volunteers. *Biopharm Drug Dispos* **23:**77-81.

Kawashima O, Yamauchi M, Maezawa Y, and Toda G (1996) Effects of cimetidine on blood ethanol levels after alcohol ingestion and genetic polymorphisms of sigma-alcohol dehydrogenase in Japanese. *Alchol Clin Exp Res* **20:**36A-39A.

Ke AB, Nallani SC, Zhao P, Rostami-Hodjegan A, Isoherranen N, and Unadkat JD (2013) A physiologically based pharmacokinetic model to predict disposition of CYP2D6 and CYP1A2 metabolized drugs in pregnant women. *Drug Metab Dispos* **41:**801-813.

Kenny JR, Mukadam S, Zhang C, Tay S, Collins C, Galetin A, and Khojasteh SC (2012) Drug-drug interaction potential of marketed oncology drugs: in vitro assessment of time-dependent cytochrome P450 inhibition, reactive metabolite formation and drug-drug interaction prediction. *Pharm Res* **29:**1960-1976.

Kerry NL, Somogyi AA, Bochner F, and Mikus G (1994) The role of CYP2D6 in primary and secondary oxidative metabolism of dextromethorphan: *in vitro* studies using human liver microsomes. *Br J Clin Pharmacol* **38:**243-248.

Kharasch ED, Hoffer C, Whittington D, Walker A, and Bedynek PS (2009) Methadone pharmacokinetics are independent of cytochrome P4503A (CYP3A) activity and gastrointestinal drug transport: insights from methadone interactions with ritonavir/indinavir. *Anesthesiology* **110:**660-672.

Khetani SR and Bhatia SN (2008) Microscale culture of human liver cells for drug development. *Nat Biotechnol* **26:**120-126.

Kilford PJ, Stringer R, Sohal B, Houston JB, and Galetin A (2009) Prediction of drug clearance by glucuronidation from *in vitro* data: use of combined cytochrome P450 and UDP-glucuronosyltransferase cofactors in alamethicin-activated human liver microsomes. *Drug Metab Dispos* **37:**82-89.

Kim K-A, Kim M-J, Park J-Y, Shon J-H, Yoon Y-R, Lee S-S, Liu K-H, Chun J-H, Hyun M-H, and Shin J-G (2003) Stereoselective metabolism of lansoprazole by human liver cytochrome P450 enzymes. *Drug Metab Dispos* **31:**1227-1234.

Kirby BJ, Collier AC, Kharasch ED, Whittington D, Thummel KE, and Unadkat JD (2011) Complex drug interactions of HIV protease inhibitors 1: inactivation, induction, and inhibition of cytochrome P450 3A by ritonavir or nelfinavir. *Drug Metab Dispos* **39:**1070-1078.

Kobayashi K, Yamamoto T, Chiba K, Tani M, Ishizaki T, and Kuroiwa Y (1995) The effects of selective serotonin reuptake inhibitors and their metabolites on S-mephenytoin 4'-hydroxylase activity in human liver microsomes. *Br J Clin Pharmacol* **40:**481-485.

Koyama E, Sohn DR, Shin SG, Chiba K, Shin JG, Kim YH, Echizen H, and Ishizaki T (1994) Metabolic disposition of imipramine in oriental subjects: relation to metoprolol alpha-

hydroxylation and S-mephenytoin 4'-hydroxylation phenotypes. *J Pharmacol Exper Ther* **271:**860-867.

Kramer-Nielsen K, Flinois JP, Beaune P, and Brosen K (1996) The biotransformation of clomipramine *in vitro*, identification of the cytochrome P450s responsible for the separate metabolic pathways. *J Pharmacol Exper Ther* **277:**1659-1664.

Labedzki A, Buters J, Jabrane W, and Fuhr U (2002) Differences in caffeine and paraxanthine metabolism between human and murine CYP1A2. *Biochemical pharmacology* **63:**2159-2167.

Lam YW, Alfaro CL, Ereshefsky L, and Miller M (2003) Pharmacokinetic and pharmacodynamic interactions of oral midazolam with ketoconazole, fluoxetine, fluvoxamine, and nefazodone. *J Clin Pharmacol* **43:**1274-1282.

Leclercq L, Cuyckens F, Mannens GSJ, Vries Rd, Timmerman P, and Evans DC (2009) Which human metabolites have we MIST? Retrospective analysis, practical aspects, and perspectives for metabolite identification and quantification in pharmaceutical development. *Chem Res Tox* **22:**280-293.

Levy RH, Lane EA, Guyot M, Brachet-Liermain A, Cenraud B, and Loiseau P (1983) Analysis of parent drug-metabolite relationship in the presence of an inducer. Application to the carbamazepine-clobazam interaction in normal man. *Drug Metab Dispos* **11:**286-292.

Lien EA, Anker G, Lonning PE, Solheim E, and Ueland PM (1990) Decreased serum concentrations of tamoxifen and its metabolites induced by aminoglutethimide. *Cancer Res* **50:**5851-5857.

Linnoila M, Insel T, Kilts C, Potter WZ, and Murphy DL (1982) Plasma steady state concentrations of hydroxylated metabolites of clomipramine. *Clin Pharmacol Ther* **32:**208-211.

Liu KH, Kim MJ, Shon JH, Moon YS, Seol SY, Kang W, Cha IJ, and Shin JG (2005) Stereoselective inhibition of cytochrome P450 forms by lansoprazole and omeprazole in vitro. *Xenobiotica* **35:**27-38.

Loi CM, Smith DA, and Dalvie D (2013) Which metabolites circulate? *Drug Metab Dispos* **41:**933-951.

Luo G, Lin J, Fiske WD, Dai R, Yang TJ, Kim S, Sinz M, LeCluyse E, Solon E, Brennan JM, Benedek IH, Jolley S, Gilbert D, Wang L, Lee FW, and Gan LS (2003) Concurrent induction and mechanism-based inactivation of CYP3A4 by an L-valinamide derivative. *Drug Metab Dispos* **31:**1170-1175.

Lutz JD, Fujioka Y, and Isoherranen N (2010) Rationalization and prediction of *in vivo* metabolite exposures: the role of metabolite kinetics, clearance predictions and *in vitro* parameters. *Expert Opin Drug Metab Toxicol* **6:**1095-1109.

Lutz JD and Isoherranen N (2012a) *In vitro*-to-*in vivo* predictions of drug-drug interactions involving multiple reversible inhibitors. *Expert Opin Drug Metab Toxicol* **8:**449-466.

Lutz JD and Isoherranen N (2012b) Prediction of relative *in vivo* metabolite exposure from *in vitro* data using two model drugs: dextromethorphan and omeprazole. *Drug Metab Dispos* **40:**159-168.

Mansuy D, Gans P, Chottard JC, and Bartoli JF (1977) Nitrosoalkanes as Fe(II) ligands in the 455-nm-absorbing cytochrome P-450 complexes formed from nitroalkanes in reducing conditions. *Eur J Biochem* **76:**607-615.

Mao J, Johnson TR, Shen Z, and Yamazaki S (2013) Prediction of Crizotinib-Midazolam Interaction Using the Simcyp Population-Based Simulator: Comparison of CYP3A Time-Dependent Inhibition between Human Liver Microsomes versus Hepatocytes. *Drug Metab Dispos* **41:**343-352.

Margolis JM, O'Donnell JP, Mankowski DC, Ekins S, and Obach RS (2000) (R)-, (S)-, and racemic fluoxetine N-demethylation by human cytochrome P450 enzymes. *Drug Metab Dispos* **28:**1187-1191.

Margolis JM and Obach RS (2003) Impact of nonspecific binding to microsomes and phospholipid on the inhibition of cytochrome P4502D6: implications for relating *in vitro* inhibition data to *in vivo* drug interactions. *Drug Metab Dispos* **31:**606-611.

Mayhew BS, Jones DR, and Hall SD (2000) An *in vitro* model for predicting *in vivo* inhibition of cytochrome P450 3A4 by metabolic intermediate complex formation. *Drug Metab Dispos* **28:**1031-1037.

McGinnity DF, Soars MG, Urbanowicz RA, and Riley RJ (2004) Evaluation of fresh and cryopreserved hepatocytes as *in vitro* drug metabolism tools for the prediction of metabolic clearance. *Drug Metab Dispos* **32:**1247-1253.

Mohutsky MA, Chien JY, Ring BJ, and Wrighton SA (2006) Predictions of the *in vivo* clearance of drugs from rate of loss using human liver microsomes for phase I and phase II biotransformations. *Pharm Res* **23:**654-662.

Morrish GA, Foster DJR, and Somogyi AA (2006) Differential *in vitro* inhibition of M3G and M6G formation from morphine by (R)- and (S)-methadone and structurally related opioids. *Br J Clin Pharmacol* **61:**326-335.

Murray M and Murray K (2003) Mechanism-based inhibition of CYP activities in rat liver by fluoxetine and structurally similar alkylamines. *Xenobiotica* **33:**973-987.

Nakamura A, Nakajima M, Yamanaka H, Fujiwara R, and Yokoi T (2008) Expression of UGT1A and UGT2B mRNA in Human Normal Tissues and Various Cell Lines. *Drug Metab Dispos* **36:**1461-1464.

Nakashima D, Takama H, Ogasawara Y, Kawakami T, Nishitoba T, Hoshi S, Uchida E, and Tanaka H (2007) Effect of cinacalcet hydrochloride, a new calcimimetic agent, on the pharmacokinetics of dextromethorphan: *in vitro* and clinical studies. *J Clin Pharmacol* **47:**1311-1319.

Nath A and Atkins WM (2006) A theoretical validation of the substrate depletion approach to determining kinetic parameters. *Drug Metab Dispos* **34:**1433-1435.

Neal JM, Kunze KL, Levy RH, O'Reilly RA, and Trager WF (2003) Kiiv, an in vivo parameter for predicting the magnitude of a drug interaction arising from competitive enzyme inhibition. *Drug Metab Dispos* **31:**1043-1048.

Neuvonen PJ and Jalava KM (1996) Itraconazole drastically increases plasma concentrations of lovastatin and lovastatin acid. *Clin Pharmacol Ther* **60:**54-61.

Nielsen TL, Rasmussen BB, Flinois JP, Beaune P, and Brosen K (1999) *In vitro* metabolism of quinidine: the (3S)-3-hydroxylation of quinidine is a specific marker reaction for cytochrome P-4503A4 activity in human liver microsomes. *J Pharmacol Exp Ther* **289:**31-37.

Novartis (2007) Tekturna New Drug Application, Switzerland, Basel.

Obach RS (1999) Prediction of human clearance of twenty-nine drugs from hepatic microsomal clearance data: and examination of *in vitro* half-life approach and nonspecific binding to microsomes. *Drug Metab Dispos* **27:**1350-1359.

Obach RS (2009) Predicting drug-drug interactions from *in vitro* drug metabolism data: challenges and recent advances. *Curr Opin Drug Discov Devel* **12:**81-89.

Obach RS (2013) Pharmacologically active drug metabolites: impact on drug discovery and pharmacotherapy. *Pharmacol Rev* **65:**578-640.

Obach RS, Baxter JG, Liston TE, Silber BM, Jones BC, Macintyre F, Rance DJ, and Wastall P (1997) The prediction of human pharmacokinetic parameters from preclinical and *in vitro* metabolism data. *J Pharmacol Exper Ther* **283:**46-58.

Obach RS, Walsky RL, and Venkatakrishnan K (2007) Mechanism-based inactivation of human cytochrome p450 enzymes and the prediction of drug-drug interactions. *Drug Metab Dispos* **35:**246-255.

Olkkola KT, Backman JT, and Neuvonen PJ (1994) Midazolam should be avoided in patients receiving the systemic antimycotics ketoconazole or itraconazole. *Clin Pharmacol Ther* **55:**481-485.

Ortiz de Montellano PE (2005) *Cytochrome P450: structure, mechanism and biochemistry*. Kluwer Academic/ Plenum Publishers, New York, NY.

Pang KS (1981) Metabolite pharmacokinetics: the area under the curve for the metabolite and the fractional rate of metabolism of a drug after different routes of administration for renally and hepatically cleared drugs and metabolites. *J Pharmacokinet Biopharm* **9:**477-487.

Pang KS and Gillette JR (1978) Theoretical relationship between area under the curve and route of administration of drugs and their precursors for evaluating sites and pathways of metabolism. *J Pharm Sci* **67:**703-704.

Pang KS and Gillette JR (1979) Sequential first pass metabolism of a metabolite derived from a precursor. *J Pharmacokinet Biopharm* **7:**275-290.

Pang KS and Kwan KC (1983) A commentary: methods and assumptions in the kinetic estimation of metabolite formation. *Drug Metab Dispos* **11:**79-84.

Park JE, Kim KB, Bae SK, Moon BS, Liu KH, and Shin JG (2008) Contribution of cytochrome P450 3A4 and 3A5 to the metabolism of atorvastatin. *Xenobiotica* **38:**1240-1251.

Patel IH, Levy RH, and Trager WF (1978) Pharmacokinetics of carbamazepine-10,11-epoxide before and after autoinduction in rhesus monkeys. *J Pharmacol Exper Ther* **206:**607-613.

Peng CC, Templeton I, Thummel KE, Davis C, Kunze KL, and Isoherranen N (2011) Evaluation of 6beta-hydroxycortisol, 6beta-hydroxycortisone, and a combination of the two as endogenous probes for inhibition of CYP3A4 in vivo. *Clin Pharmacol Ther* **89:**888-895.

Peyton AL, Carpenter R, and Rutkowski K (1991) The stereospecific determination of fluoxetine and norfluoxetine enantiomers in human plasma by high-pressure liquid chromatography (HPLC) with fluorescence detection. *Pharm Res* **8:**1528-1532.

Polk RE, Brophy DF, Israel DS, Patron R, Sadler BM, Chittick GE, Symonds WT, Lou Y, Kristoff D, and Stein DS (2001) Pharmacokinetic Interaction between amprenavir and rifabutin or rifampin in healthy males. *Antimicrob Agents Chemother* **45:**502-508.

Raghavan N, Ramanathan R, Comezoglu S, and Humphreys W (Year) LC–captivespray ionization-mass spectrometry for detection, characterization and quantification of circulating human metabolites, Presented at: *58th ASMS Conference on Mass Spectrometry and Allied Topics*, Salt Lake City, UT, USA.

Ramanathan R, Josephs JL, Jemal M, Arnold M, and Humphreys WG (2010) Novel MS solutions inspired by MIST. *Bioanalysis* **2:**1291-1313.

Ramanathan R, Zhong R, Blumenkrantz N, Chowdhury SK, and Alton KB (2007) Response normalized liquid chromatography nanospray ionization mass spectrometry. *J Am Soc Mass Spectrom* **18:**1891-1899.

Rambeck B, Sälke-Treumann A, May T, and Boenigk HE (1990) Valproic acid-induced carbamazepine-10,11-epoxide toxicity in children and adolescents. *Eur Neurol* **30:**79-83.

Rane A, Wilkinson GR, and Shand DG (1977) Prediction of hepatic extraction ratio from *in vitro* measurement of intrinsic clearance. *J Pharmacol Exper Ther* **200:**420-424.

Reese MJ, Wurm RM, Muir KT, Generaux GT, St John-Williams L, and McConn DJ (2008) An *in vitro* mechanistic study to elucidate the desipramine/bupropion clinical drug-drug interaction. *Drug Metab Dispos* **36:**1198-1201.

Renberg L, Simonsson R, and Hoffmann KJ (1989) Identification of two main urinary metabolites of [14C]-omeprazole in humans. *Drug Metab Dispos* **17:**69-76.

Ring BJ, Gillespie JS, Eckstein JA, and Wrighton SA (2002) Identification of the human cytochromes P450 responsible for atomoxetine metabolism. *Drug Metab Dispos* **30:**319-323.

Riss J, Cloyd J, Gates J, and S C (2008) Benzodiazepines in epilepsy: pharmacology and pharmacokinetics. *Acta neurologica Scandinavica* **118:**69-86.

Rodopoulos N and Norman A (1996) Assessment of dimethylxanthine formation from caffeine in healthy adults: comparison between plasma and saliva concentrations and urinary excretion of metabolites. *Scand J Clin Lab Invest* **56:**259 - 268.

Rostami-Hodjegan A and Tucker G (2004) '*In silico*' simulations to assess the '*in vivo*' consequences of '*in vitro*' metabolic drug-drug interactions. *Drug Discov Today Technol* **1:**441-448.

Rowland M and Matin SB (1973) Kinetics of drug-drug interactions. *J Pharmacokinet Biopharm* **1:**553-567.

Rowland M and Tozer TN (1995) *Clinical Pharmacokinetics: Concepts and Applications*. Lippincott, Williams and Wilkins, Philadelphia.

Rowland Yeo K, Jamei M, Yang J, Tucker GT, and Rostami-Hodjegan A (2010) Physiologically based mechanistic modelling to predict complex drug-drug interactions involving simultaneous competitive and time-dependent enzyme inhibition by parent compound and its metabolite in both liver and gut - the effect of diltiazem on the time-course of exposure to triazolam. *Eur J Pharm Sci* **39:**298-309.

Ryu JY, Song IS, Sunwoo YE, Shon JH, Liu KH, Cha IJ, and Shin JG (2007) Development of the "Inje cocktail" for high-throughput evaluation of five human cytochrome P450 isoforms *Clin Pharmacol Ther* **82:**531-540.

Schellens JH, Ghabrial H, van der Wart HH, Bakker EN, Wilkinson GR, and Breimer DD (1991) Differential effects of quinidine on the disposition of nifedipine, sparteine, and mephenytoin in humans. *Clin Pharmacol Ther* **50:**520-528.

Schmitt C, Hofmann C, Riek M, Patel A, and Zwanziger E (2009) Effect of saquinavir-ritonavir on cytochrome P450 3A4 activity in healthy volunteers using midazolam as a probe. *Pharmacotherapy* **29:**1175-1181.

Scordo MG, Spina E, Dahl ML, Gatti G, and Perucca E (2005) Influence of CYP2C9, 2C19 and 2D6 genetic polymorphisms on the steady-state plasma concentrations of the enantiomers of fluoxetine and norfluoxetine. *Basic Clin Pharmacol Toxicol* **97:**296-301.

Segel IH (1993) *Enzyme Kinetics: Behavior and Analysis of Rapid Equilibrium and Steady-State Enzyme Systems* John Wiley & Sons, Inc., New York, NY.

Shi S, Liu Y, Wu J, Li Z, Zhao Y, Zhong D, and Zeng F (2010) Comparative bioavailability and tolerability of a single 20-mg dose of two fluoxetine hydrochloride dispersible tablet formulations in fasting, healthy Chinese male volunteers: an open-label, randomized-sequence, two-period crossover study. *Clin Ther* **32:**1977-1986.

Shirai N, Furuta T, Moriyama Y, Okochi H, Kobayashi K, Takashima M, Xiao F, Kosuge K, Nakagawa K, Hanai H, Chiba K, Ohashi K, and Ishizaki T (2001) Effects of CYP2C19 genotypic differences in the metabolism of omeprazole and rabeprazole on intragastric pH. *Ailment Pharmacol Ther* **15:**1929-1937.

Shirasaka Y, Sager JE, Lutz JD, Davis C, and Isoherranen N (2013) Inhibition of CYP2C19 and CYP3A4 by omeprazole metabolites and their contribution to drug-drug interactions. *Drug Metab Dispos*.

Shu Y, Wang L-S, Xu Z-H, He N, Xiao W-M, Wang W, Huang S-L, and Zhou H-H (2000) 5-Hydroxylation of omeprazole by human liver microsomal fractions from chinese populations related to CYP2C19 gene dose and individual ethnicity. *J Pharmacol Exper Ther* **295:**844-851.

Silverman RB (1988) *Mechanism Based Enzyme Inactivation: Chemistry and Enzymology*. CRC Press, Inc., Boca Raton, FL.

Skelbo R and Brosen K (1992) Inhibitors of imipramine metabolism by human liver microsomes. *Br J Clin Pharmacol* **34:**256 - 261.

Smith DA and Obach RS (2009) Metabolites in safety testing (MIST): considerations of mechanism of toxicity with dose, abundance and duration of treatment. *Chem Res Tox* **22:**267-279.

Soars MG, Riley RJ, Findlay KAB, Coffey MJ, and Burchell B (2001) Evidence for Significant Differences in Microsomal Drug Glucuronidation by Canine and Human Liver and Kidney. *Drug Metab Dispos* **29:**121-126.

Stevens JC and Wrighton SA (1993) Interaction of the enantiomers of fluoxetine and norfluoxetine with human liver cytochromes P450. *J Pharmacol Exp Ther* **266:**964-971.

Streetman DS, Bertino JS, and Nafziger AN (2000) Phenotyping of drug-metabolizing enzymes in adults: a review of in-vivo cytochrome P450 phenotyping probes. *Pharmacogenetics* **10:**187-216.

Stresser DM, Mason AK, Perloff ES, Ho T, Crespi CL, Dandeneau AA, Morgan L, and Dehal SS (2009) Differential time- and NADPH-dependent inhibition of CYP2C19 by enantiomers of fluoxetine. *Drug Metab Dispos* **37:**695-698.

Takashima T, Murase S, Iwasaki K, and Shimada K (2005) Evaluation of dextromethorphan metabolism using hepatocytes from CYP2D6 poor and extensive metabolizers. *Drug Metab Pharmacokinet* **20:**177-182.

Tassaneeyakul W, Tassaneeyakul W, Vannaprasaht S, and Yamazoe Y (2000) Formation of omeprazole sulphone but not 5-hydroxyomeprazole is inhibited by grapefruit juice. *Br J Clin Pharmacol* **49:**139-144.

Templeton I, Peng CC, Thummel KE, Davis C, Kunze KL, and Isoherranen N (2010) Accurate prediction of dose-dependent CYP3A4 inhibition by itraconazole and its metabolites from *in vitro* inhibition data. *Clin Pharmacol Ther* **88:**499-505.

Templeton IE, Thummel KE, Kharasch ED, Kunze KL, Hoffer C, Nelson WL, and Isoherranen N (2007) Contribution of itraconazole metabolites to inhibition of CYP3A4 *in vivo*. *Clin Pharmacol Ther* **83:**77-85.

Thummel KE, Shen DD, Podoll TD, Kunze KL, Trager WF, Hartwell PS, Raisys VA, Marsh CL, McVicar JP, and Barr DM (1994) Use of midazolam as a human cytochrome P450 3A probe: I. *In vitro-in vivo* correlations in liver transplant patients. *J Pharmacol Exper Ther* **271:**549-556.

Tjia JF, Colbert J, and Back DJ (1996) Theophylline metabolism in human liver microsomes: inhibition studies. *J Pharmacol Exper Ther* **276:**912-917.

Tu JH, Hu DL, Dai LL, Sun Y, Fan L, Zhang M, Tan ZR, Chen Y, Li Z, and Zhou HH (2010) Effect of glycyrrhizin on CYP2C19 and CYP3A4 activity in healthy volunteers with different CYP2C19 genotypes. *Xenobiotica* **40:**393-399.

VandenBrink BM, Foti RS, Rock DA, Wienkers LC, and Wahlstrom JL (2012) Prediction of CYP2D6 drug interactions from in vitro data: evidence for substrate-dependent inhibition. *Drug Metab Dispos* **40:**47-53.

VandenBrink BM and Isoherranen N (2010) The role of metabolites in predicting drug-drug interactions: focus on irreversible cytochrome P450 inhibition. *Curr Opin Drug Discov Devel* **13:**66-77.

Venkatakrishnan K and Obach RS (2007) Drug-drug interactions via mechanism-based cytochrome P450 inactivation: points to consider for risk assessment from in vitro data and clinical pharmacologic evaluation. *Curr Drug Metab* **8:**449-462.

Venkatakrishnan K, von Moltke LL, Obach RS, and Greenblatt DJ (2003) Drug metabolism and drug interactions: application and clinical value of *in vitro* models. *Curr Drug Metab* **4:**423-459.

Vishwanathan K, Babalola K, Wang J, Espina R, Yu L, Adedoyin A, Talaat R, Mutlib A, and Scatina J (2009) Obtaining exposures of metabolites in preclinical species through plasma pooling and quantitative NMR: addressing metabolites in safety testing (MIST)

guidance without using radiolabeled compounds and chemically synthesized metabolite standards. *Chem Res Tox* **22:**311-322.

Vlase L, Popa A, Neag M, Muntean D, and Leucuta SE (2011) Effect of fluoxetine on the pharmacokinetics of lansoprazole: a two-treatment period study in healthy male subjects. *Clin Drug Investig* **31:**727-733.

Von Moltke LL, Greenblatt DJ, Granda BW, Grassi JM, Schmider J, Harmatz JS, and Shader RI (1999) Nefazodone, meta-chlorophenylpiperazine, and their metabolites *in vitro*: cytochromes mediating transformation, and P450-3A4 inhibitory actions. *Psychopharmacol* **145:**113-122.

von Moltke LL, Greenblatt DJ, Schmider J, Duan SX, Wright CE, Harmatz JS, and Shader RI (1996) Midazolam hydroxylation by human liver microsomes *in vitro*: inhibition by fluoxetine, norfluoxetine, and by azole antifungal agents. *J Clin Pharmacol* **36:**783-791.

Wang WW, Khetani SR, Krzyzewski S, Duignan DB, and Obach RS (2010) Assessment of a micropatterned hepatocyte coculture system to generate major human excretory and circulating drug metabolites. *Drug Metab Dispos* **38:**1900-1905.

Wang YH, Jones DR, and Hall SD (2004) Prediction of cytochrome P450 3A inhibition by verapamil enantiomers and their metabolites. *Drug Metab Dispos* **32:**259-266.

Wilkinson GR and Shand DG (1975) A physiologic approach to hepatic drug clearance. *Clin Pharmacol Ther* **18:**377-390.

Yang L-J, Fan L, Liu Z-Q, Mao Y-M, Guo D, Liu L-H, Tan Z-R, Peng L, Han C-T, Hu D-L, Wang D, and Zhou H-H (2009) Effects of allicin on CYP2C19 and CYP3A4 activity in healthy volunteers with different CYP2C19 genotypes. *Eur J Clin Pharmacol* **65:**601-608.

Yang Y, Grubb MF, Luk CE, Humphreys WG, and Josephs JL (2011) Quantitative estimation of circulating metabolites without synthetic standards by ultra-high-performance liquid chromatography/high resolution accurate mass spectrometry in combination with UV correction. *Rapid Commun Mass Spectrom* **25:**3245-3251.

Yao C, Kunze KL, Kharasch ED, Wang Y, Trager WF, Ragueneau I, and Levy RH (2001) Fluvoxamine-theophylline interaction: gap between *in vitro* and *in vivo* inhibition constants toward cytochrome P4501A2. *Clin Pharmacol Ther* **70:**415-424.

Yao C, Kunze KL, Trager WF, Kharasch ED, and Levy RH (2003) Comparison of in vitro and in vivo inhibition potencies of fluvoxamine toward CYP2C19. *Drug Metab Dispos* **31:**565-571.

Yeh GC, Tao PL, Ho HO, Lee YJ, Chen JY, and Sheu M-T (2003) Analysis of pharmacokinetic parameters for assessment of dextromethorphan metabolic phenotypes. *J Biomed Sci* **10:**552-564.

Yeung CK, Fujioka Y, Hachad H, Levy RH, and Isoherranen N (2011) Are circulating metabolites important in drug-drug interactions?: quantitative analysis of risk prediction and inhibitory potency. *Clin Pharmacol Ther* **89:**105-113.

Yu A and Haining R (2001) Comparative contribution to dextromethorphan metabolism by cytochrome P450 isoforms *in vitro*: can dextromethorphan be used as a dual probe for both CYP2D6 and CYP3A activities? *Drug Metab Dispos* **29:**1514-1520.

Yue QY, Hasselström J, Svensson JO, and Säwe J (1991a) Pharmacokinetics of codeine and its metabolites in Caucasian healthy volunteers: comparisons between extensive and poor hydroxylators of debrisoquine. *Br J Clin Pharmacol* **31:**635-642.

Yue QY, Svensson JO, Sjöqvist F, and Säwe J (1991b) A comparison of the pharmacokinetics of codeine and its metabolites in healthy Chinese and Caucasian extensive hydroxylators of debrisoquine. *Br J Clin Pharmacol* **31:**635-642.

Zhang X, Jones DR, and Hall SD (2009a) Prediction of the effect of erythromycin, diltiazem, and their metabolites, alone and in combination, on CYP3A4 inhibition. *Drug Metab Dispos* **37:**150-160.

Zhang X, Quinney SK, Gorski JC, Jones DR, and Hall SD (2009b) Semiphysiologically based pharmacokinetic models for the inhibition of midazolam clearance by diltiazem and its major metabolite. *Drug Metab Dispos* **37:**1587-1597.

VITÆ

Justin D. Lutz was born in Monroeville, PA, in 1983. In 2001, he graduated from Bradford Area High School in Bradford, PA. In 2007, Justin obtained his Doctor of Pharmacy at the University of Pittsburgh in Pittsburgh, PA. He then joined the Department of Pharmaceutics as a graduate student and in 2008 he joined Dr. Nina Isoherranen's lab. While in Dr. Isoherranen's lab his research focus has been to better understand the role that drug metabolites play in drug-drug interactions, either as *in vivo* P450 inhibitors or as *in vivo* measures of P450 activity. Throughout his graduate training, Justin maintained a part-time community pharmacy practice at Walgreens Pharmacy in Seattle, WA. Justin was the recipient of a University of Washington School of Pharmacy Bradley Fellowship.